FIGHTING CANCER WITH METALS: MAIN FOCUS ON RHENIUM(I) COMPLEXES

by

LUCY ELLEN KAPP

A dissertation submitted in the fulfilment of the requirements in respect of the Master's Degree

MAGISTER SCIENTIAE

in the

DEPARTMENT OF CHEMISTRY

In the

FACULTY OF NATURAL AND AGRICULTURAL SCIENCES

at the

UNIVERSITY OF THE FREE STATE

SUPERVISOR: DR MARIETJIE SCHUTTE-SMITH
CO-SUPERVISOR: PROFESSOR HENDRIK GIDEON VISSER

February 2019

For Jacinta, Barbara, Gary, Annatjie, Gerard, Jos, and Roko.

"Our greatest weakness lies in giving up. The most certain way to succeed is always to try just one more time." – Thomas Alva Edison

Acknowledgements

To the greater honour and glory of Almighty God.

Marietjie, for your support and guidance. Thank you for not only being my supervisor, but for being a dear friend. I am privileged to work with you and Deon.

Deon for your guidance and constant reminder that every day is an opportunity to learn something new.

To my fellow Masters candidates Andrea, Francois, George, Jani, Lisa, Ursula and Yuel, for your support and help during this year.

Professor Gilles Gasser and his group at Paristech in Paris, France for accomodating me at your laboratory, sharing your knowledge on PDT and *in vitro* cytotoxicity studies.

Dr Minas Papadopoulos and Dr Ioannis Pirmettis and your group at the National Centre for Scientific Research "Demokritos" in Athens, Greece. Thank you for sharing your knowledge on ^{99m}Tc radio labelling and allowing me to work in your laboratory. You treated me like family and I will always remember all of you with great fondness.

Professor Ted Kroon at the University of the Free State, Physics Department. Thank you for your assistance and the use of your laboratory during the photoluminescence studies. Professor Purcell and the analytical chemistry group at the University of the Free State Chemistry Department for elemental analysis and ICP-OES analysis.

To the Central Research Fund (CRF) of the University of the Free State for funding this research.

To my dear mother, Jacinta . I will never be able to express my gratitude, respect, and love for you. Being widowed at 35 with two young girls to bring up was not an easy

task. Thank you for every sacrifice and for all your support and love. To my father, Patrick, you are dearly missed. May your dear soul rest in peace.

To Father Stephen for your unfailing kindness and support throughout all the years I have had the pleasure of your acquaintance. I am privileged and blessed to know you.

To my grandmother, Luky, and my grandfather, Seán, for showing me the importance of hard work, honesty, and generosity. Granddad, may your dear soul rest in peace.

To Mary Anne for your support and love. Uncle Joe, thank you for the joy and amusement you bring. Janine and Jeaneme thank you for all your support and love always.

Tannie Chris-Mari and Oom Johann for your love and kindness and for accepting me into your family.

To my dearest Heinrich for your support, love, and patience. Your work ethic, kindness toward others and gentle heart are inspiring.

TABLE OF CONTENTS

Abbreviations

ATR	Attenuated total reflection
bpy	2,2'-bipyridine
CH_3OH	Methanol
CT	Charge transfer
DCM	Dichloromethane
DMSO	Dimethylsulfoxide
DNA	Deoxyribonucleic acid
fac	Facial
FDA	Food and Drug Administration
HEDP	Hydroxyethylidene Diphosphonic Acid
HPLC	High Performance Liquid Chromatography
IC_{50}	Half maximal inhibiting concentration
IR	Infrared
ISC	Intersystem crossing
K	Kelvin
LED	Light emitting diode
LF	Ligand field
MBq	Megabacquerel
MCi	Millicurie
MHz	Megahertz
MIBI	Methoxy Isobutyl Isonitrile
MLCT	Metal-to-ligand charge transfer
NH_4PF_6	Ammonium hexafluorophosphate
NIR	Near infrared region
NMR	Nuclear magnetic resonance
bid	Bidentate ligand
OCTs	Organic cation transporters
Pd	Palladium
PDT	Photodynamic therapy
Phen	1,10-phenanthroline
Phendione	1,10-phenanthroline-5,6-dione

PPh_3	Triphenylphosphine
Ps	Photosensitiser
Pt	Platinum
PTA	1,3,5-triaza-7-phosphaadamantane
QD	Quantum dots
QY	Quantum yield
Re	Rhenium
ReAA	$[NEt_4]_2[Re(CO)_3(Br)_3]$
R_t	Retention time
Ru	Ruthenium
S_0	Singlet state
SOC	Spin-orbit coupling
T_1	Triplet state
Tc	Technetium
UVA	Ultraviolet A
UV/Vis	Ultraviolet/Visible Spectroscopy
ν_{CO}	C=O stretching frequency
°	Degrees
$^{\cdot}O_2^-$	Oxygen radical
$^{\cdot}OH$	Hydroxide radical
Å	Angstrom
β	Beta
ε	Epsilon
γ	Gamma
λ	Lambda

Abstract

In recent years, photodynamic therapy (PDT) has aroused significant interest as a potential method of treatment for certain cancers. A non-intrusive treatment, PDT consequently overcomes various obstacles of currently available treatment methods, notably toxicity. However, PDT is not without its limitations. These include, although they are not limited to, low selectivity and an inability to penetrate deep tissues. To overcome such shortcomings, a range of rhenium(I) compounds of the type *fac*-$[Re(CO)_3(N,N'\text{-bid}(X)]^n$ and *cis-trans*-$[Re(CO)_2(N,N'\text{-bid})(X)_2]^n$ (n = 0, +1) were synthesised, most of which displayed good yields, ranging from 38.10 to 85.90 % for tricarbonyl and 12.80 to 80.30 % for dicarbonyl complexes, and characterised. Four bimetallic complexes $[(Cl_2)Pt(O,O'\text{-phen}O_2\text{-}N,N')\text{-}Re(CO)_3(Br)]$, $[(Cl_2)Pd(O,O'\text{-phen}O_2\text{-}N,N')\text{-}Re(CO)_3(Br)]$, $[(Cl_2)Pt(O,O'\text{-phen}O_2\text{-}N,N')\text{-}Ru(bpy)_2][PF_6]_2{\cdot}2H_2O$, and $[(Cl_2)Pd(O,O'\text{-phen}O_2\text{-}N,N')\text{-}Ru(bpy)_2][PF_6]_2 \cdot 2H_2O$ were synthesised and characterised. However, low yields ranging from 10.66 to 45.52 % were obtained. Two ^{99m}Tc complexes, *cis-trans*-$[^{99m}Tc(CO)_2(bpy)(PPh_3)_2]^+$ and *cis-trans*-$[^{99m}Tc(CO)_2(bpy)(PTA)_2]^+$ were synthesised and isolated with retention times of 16.928 and 11.385 minutes respectively.

The crystal structure of *fac*-$[Re(CO)_3(bpy)(Br)]$ was obtained and solved and is reported in this study. The rhenium to nitrogen bond distances (Re1-N1, Re1-N2) are reported as 2.171(4) Å and 2.170(4) Å with a bite-angle (N2-Re1-N1) of 74.95(16)°, while the rhenium to bromido bond distance was 2.6126(15) Å. The rhenium to carbonyl carbon bond distances range from 1.912(6) Å to 2.008(7) Å. A distortion of the octahedral sphere is confirmed by the angles N1-Re1-Br1, N2-Re1-Br1, and C1-Re1-Br1 which are 85.66(11)°, 83.50(11)° and 176.16(15)° respectively. A dihedral angle of 7.028(15)° was reported between the equatorial plane and the plane through the 2,2'-bipyridine system. A hydrogen bonding interaction is observed between H6 and Br1, while three π-interactions are observed in *fac*-$[Re(CO)_3(bpy)(Br)]$.

The photoluminescent properties of eleven rhenium(I) compounds were determined and emission wavelengths ranging from 604 to 650 nm were found for Re(I) tricarbonyl complexes and 610 to 670 nm in Re(I) dicarbonyl complexes. The highest

emission wavelength was obtained from the water soluble complex *cis-trans*-$[Re(CO)_2(bpy)(PTA)_2][NO_3]$ in CH_3OH solution. This emission was significantly higher than the same complex in aqueous solution, which displayed an emission wavelength of 642 nm. A second water soluble complex, *fac*-$[Re(CO)_3(bpy)(PTA)][NO_3]$, was studied in both CH_3OH and aqueous solution. This compound showed a similar trend to *cis-trans*-$[Re(CO)_2(bpy)(PTA)_2][NO_3]$, namely that the emission of these water soluble complexes is higher in CH_3OH than in aqueous solution.

1 General Background and Aim

1.1 Introduction

It is common cause among researchers and clinicians worldwide that the risk of cancer cases increases with life expectancy simply because the risk of cancer increases with age. Interestingly, and pertinent to this study, it appears that the global rise in cancer rates is not uniform across all social strata. In the United States, for example, cancer cases among the affluent are showing a rate of decrease, whereas cases among the less affluent reveal a degree of increase.[1] The effect of any increase in cases of cancer, be this great or small, will produce a concomitant burden on clinical, human and financial health care resources. South Africa is no exception to this acknowledged trend.

The histological diagnosis of cancer cases in South Africa for the year 2000 constitutes, 27 933 for males and 27 819 for females. In 2014 this figure increased to 37 787 for males and 36 790 for females.[2] In accordance with the Constitution of South Africa[3], Chapter 2, Bill of Rights, Section 27 (1) (a) 'Everyone has the right of access to health care and reproductive services' research into, and development of, clinically effective and cost-effective cancer diagnosis and treatments are pressing.

The designation 'cancer' describes a group of diseases that occur due to abnormal cell growth, which has the potential to spread from the original local site to other areas of the body. Currently available cancer treatments are extremely invasive and may result in unavoidable and excessively harmful side effects. Examples of such treatments currently in use include chemotherapy, radiation therapy, and surgery.

---

[1] American Cancer Society, https://www.cancer.org/content/dam/cancer-org/research/cancer-facts-and-statistics/annual-cancer-facts-and-figures/2018/cancer-facts-and-figures-2018.pdf (date accessed 09/01/2019).

[2] https://www.cansa.org.za/south-african-cancer-statistics/ (date accessed 25/05/2018).

[3] THE CONSTITUTION OF THE REPUBLIC OF SOUTH AFRICA 1996, 2017, 14th Edition, Juta and Company Ltd, Lansdown, South Africa.

Chemotherapy may be administered in respect of both curative and reductive treatment. Although chemotherapy has proven to result in significant tumour shrinkage, it also causes severe side effects such as inhibiting mitosis in healthy cells, resulting in hair loss and a reduced white blood cell count. Radiation therapy involves the treatment of a tumour externally by irradiation of the tumour site. This treatment frequently causes damage to the epithelial surface of the skin. Surgery may not only be too dangerous for certain types and stages of cancer, but also hold additional risks such as anaesthetics and possible infection. Some side effects of chemotherapy and radiation may even result in cancer, which is resistant to these types of treatment.

The risk of such adverse outcomes necessitates a need for less invasive and non-toxic interventions that will target cancerous cells only and not adversely affect or damage healthy cells. Ideally, such benign treatments should avoid the possibility of triggering additional cancers.

In addition to historical and existing clinical, human and financial constraints on the Department of Health's budget, a current major South African societal problem is that in rural and urban areas there are many households with inadequate finances to meet the burdensome costs of accessing diagnostic, clinical and medical treatment for any type of pathology, whether major or minor. Furthermore, in rural areas, many people are geographically remote from specialist medical and clinical facilities. Individuals in such restricted circumstances often discover their disease at a late stage when treatment may no longer be an option.

It is therefore a moral as well as a scientific imperative to research and develop cost-effective and easily deliverable diagnostic agents and cancer treatments to those who lack adequate finances and ready access to medical and clinical facilities; and to provide the same to those who can afford and enjoy easy access to such medical and clinical services.

1.2 Photodynamic Therapy

Photodynamic therapy (PDT) involves the treatment of a patient with a non-toxic photosensitiser (PS). Upon application of an artificial light source characterised by a long wavelength of red visible light (600 – 850 nm)[4,5], the photosensitiser causes the production of singlet oxygen which leads to destruction of the tumour site.

Since PDT displays specificity and selectivity, it therefore has the ability to control drug action spatially. It has been suggested that the type of resistance in cancer cells caused by mutations after exposure to chemotherapy is not necessarily observed after PDT treatment.[6] Repeated PDT treatments in respect of the same tumour site are therefore possible. Thus, PDT may be described as an attractive complement or alternative to conventional cancer treatment.

PDT can follow one of two possible pathways. Type I involves free radical formation, while type II concerns energy transfer from the photosensitiser to the oxygen molecule. Singlet oxygen has been reported as causing severe damage to cellular components, resulting in apoptosis or necrosis,[7,8] thus sparking great interest into the investigation of PDT as a possible treatment in respect of a range of cancers.

Structurally, photosensitisers were originally based on organic compounds, such as porphyrins and their derivatives. However, metal complexes have recently been investigated for this purpose, since they possess photochemical properties,[9,10.11] display structural diversity, have tuneable ligand exchange kinetics and also have

[4] Wähler, K.; Ludewig, A.; Szabo, P.; Harms, K.; Meggers, E., *Eur. J. Inorg. Chem*., 2014, 807-811.
[5] Robertson, C. A.; Hawkins Evans, D.; Abrahamse, H., *J. Photochem. Photobiol. B: Biology*, 96, 2009,1-8.
[6] Castano, A. P.; Demidova, T, N.; Hamblin, M. R., *Photodiag. Photodyn. Ther.*, 2005, 2, 1-23.
[7] Huang, Z., *Technol. Cancer Res. T.*, 2005, 4, 283-293.
[8] Tsay, J. M. ; Trzoss, M.; Shi, L.; Kong, X.; Selke, M.; Jung, M. E.; Weiss, S., *J. Am. Chem. Soc*., 2007, 129, 6865-6871.
[9] Schatzschneider, U., *Eur. J. Inorg. Chem.*, 2010, 1451-1467.
[10] Selke, M.; Karney, W. L.; Khan, S. I.; Foote, C. S., *Inorg. Chem.*, 1995, 34, 5715-5720.
[11] Zhou, C., -H.; Zhao, X., *J. Organomet. Chem.*, 2011, 696, 3322-3327.

radioisotopes available. The combination of these properties along with the photo-induced reactivity lend conviction to the potential success of such novel treatments.

Singlet oxygen has a short half-life and short diffusion distance, thus resulting in PDT treatment being considered to be highly selective in cancer treatment. PDT is considered to be a complex method since the outcome of this treatment may be altered by variants of cell type, incubation period, and illumination conditions.[12,13]

There are, however, several unresolved questions regarding PDT. These include, although they are not limited to, the vulnerability of cancer cells versus normal cells to PDT-induced cell death and the susceptibility of certain cellular components to undergo oxidation by singlet oxygen.

1.3 Aim of this Study

The key aim of this study is the synthesis and characterisation of a range of complexes and the investigation into their use as possible photosensitisers for photodynamic therapy.

The aims in serial order are:

- Synthesis of the organic ligand 1,10-phenanthroline-5,6-dione.
- Synthesis of complexes of the type *fac*-[Re(*N,N'*-bid)$(CO)_3X]^n$ (*N,N'*-bid = 2,2'-bipyridine and 1,10-phenanthroline-5,6-dione, X = MeOH, Br, PTA, PPh_3, n = 0, +1).
- Synthesis of the complexes of the type *cis*-[Re(*N,N'*-bid$)(CO)_2(X)_2]^{+1}$ (*N,N'*;-bid = 2,2'-bipyridine and 1,10-phenanthroline-5,6-dione, X = PTA and PPh_3).
- Synthesis of *cis*-[^{99m}Tc(*N,N'*-bid$)(CO)_2(X)_2]^{+1}$ (*N,N'*-bid = 2,2'-bipyridine, X = PTA and PPh_3).
- Synthesis of bimetallic complexes with the following combination of metals: Ru-Pt, Ru-Pd, Re-Pt, and Re-Pd.

[12] Castano, A. P.; Demidova, T. N.; Hamblin, M. R., *Photodiag. Photodyn. Ther.*, 2004, 1, 279-293.
[13] Castano, A. P.; Demidova, T. N.; Hamblin, M. R., *Photodiag. Photodyn. Ther.*, 2005, 2, 1-23.

- Characterisation of the ligand and complexes by single crystal X-ray crystallography, IR, ^{1}H NMR, ^{13}C NMR, and ^{31}P NMR. The ^{99m}Tc complexes will be characterised by HPLC (connected to a γ-detector) as well as characterisation of bimetallic complexes by ICP-OES analysis.
- Determination of photoluminescent properties of both *fac*-[Re(*N,N'*-bid)$(CO)_3X]^n$ and *cis*-[Re(*N,N'*-bid)$(CO)_2(X)_2]^n$ complexes and the determination of quantum yield.
- Cytotoxicity studies of bimetallic complexes.

2 Literature Study

2.1 Background

Cancer may be described as a group of diseases caused by abnormal cell growth that spread from one part of the body to another. Such tumours are termed malignant, whereas tumours that are unable to spread are termed benign. Cancer Research UK[1] asserts that 'worldwide, cancer cases will continue to increase, mostly because life expectancy continues to rise, and cancer risk increases significantly with age'.[1] If this assertion as well as the increase in life expectancy holds good for the Republic of South Africa, cancer cases and the rise in cancer risk will increase concomitantly. If such a scenario is realised in South Africa, an increased clinical and financial burden will be placed on currently stretched health service provisions.

For 2000, the number of histological diagnosis of cancer cases in South Africa constitutes male 27 933, and female 27 819. For 2014, the number of histological diagnosis of cancer cases is male 37 787, and female 36 790. Over fourteen years, this represents an increase of 18 825 for male and female cases combined.[2]

Currently available cancer treatments include chemotherapy, radiation therapy and surgery. Chemotherapy, which represents a major contributor to cancer treatment, may be administered with two types of intent, namely curative or reductive. The category of chemotherapy administered is determined by the type and stage of cancer. Although many varieties of chemotherapy have shown significant results in tumour shrinkage, these types of treatments are problematic as they cause severe side effects. One major issue with chemotherapy concerns the fact that it not only inhibits mitosis in cancer cells but also in healthy cells, for example, in hair and blood cells. For this reason, cancer patients often lose their hair and need to take supplements to increase their blood cell count.

---

[1]Cancer Research UK: 'Why more people are getting cancer'

http://scienceblog.cancerresearchuk.org/2015/02/04/why-are-cancer-rates-increasing/ date accessed 25/05/2018.

[2] https://www.cansa.org.za/south-african-cancer-statistics/ date accessed 25/05/2018.

Radiation therapy is normally targeted at one area of the body and may be described as therapy by irradiation. The malignant tumour site is identified and external radiation is administered to the tumour site. As in the case of chemotherapy, a problem, which exists in respect of radiation therapy, is that it causes acute side effects. Additionally, radiation therapy causes damage to the epithelial surface of the skin, commonly termed burning. Surgery may not always be an option, depending on the type and stage of the cancer. Surgery also entails possible side effects and may even cause death.

Side effects, both major and minor, are common to all the above treatments and some side effects may even cause more cancer. This creates a need for treatments that do not cause such severe or possibly catastrophic side effects; hence the necessity for research and development of cancer treatments that are non-toxic to healthy cells and specifically target only cancerous tumours. Moreover, such treatments should not adversely affect the rate of mitosis of healthy cells while avoiding the possibility of triggering additional types of cancer.

2.2 Photodynamic Therapy

Similar to radiotherapy, photodynamic therapy (PDT) makes use of chemicals to target affected cells. Upon exposure to electromagnetic radiation, these chemicals become cytotoxic. PDT involves the photosensitiser mediated by light-induced production of cytotoxic singlet oxygen ($^1O_2$) from various oxygen species. PDT is known to have several advantages, some of which include the possibility of repeated doses and spatial as well as temporal control.[3]

PDT has proven to be effective in the treatment of oncological disorders. The process of PDT involves effective localization of photosensitisers (PS) at tumour sites and the destruction of these sites, using an artificial light source, for example lasers. Some PS are known to possess heterocyclic ring structures. One of the first FDA-approved PS,

[3] Mari, C.; Pierroz, V.; Ferrari, S.; Gasser, G., *Chem. Sci*., 2015, 6, 2660-2686.

namely Photofrin® (Figure 2.1), which was produced by Dougherty[4] has been used to destroy tumours selectively.[5]

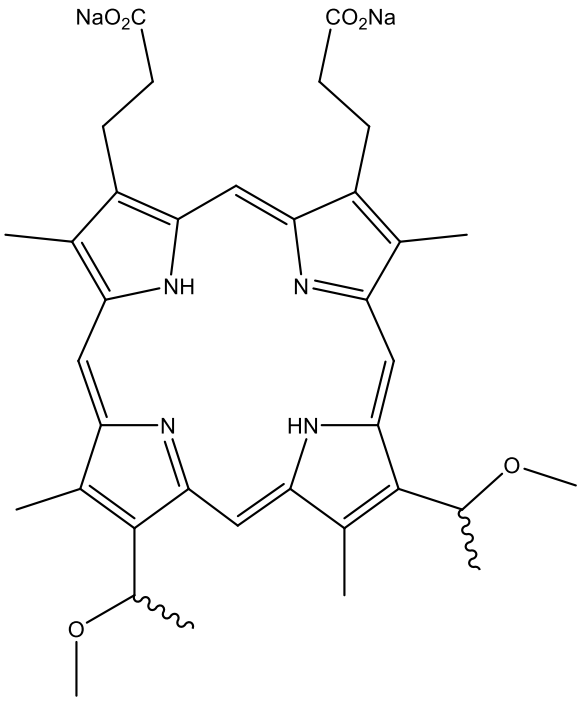

Figure 2.1: Chemical structure of Porfimer Sodium, the active component in Photofrin®.

PDT can follow two mechanistic pathways. Type I involves photosensitiser excitation resulting in free radical formation, such as ·OH and $\cdot O_2^-$. In this process biomolecules are oxidized by these free radicals, which promote the destruction of the tumour. Type II involves photosensitiser excitation resulting in a cross-over from its singlet to its triplet state and an energy transfer from this triplet state to oxygen molecules. In the process of converting triplet O_2 to singlet O_2, the singlet O_2 has been known to cause severe damage to cellular components as well as nucleic acids and enzymes leading to apoptosis or necrosis.[5,6] Gorman *et al*.[7] state that PDT should be considered as being a highly selective form of cancer treatment on account of the short half-life and short diffusion distance of the singlet oxygen.[7]

[4] Dougherty, T. J., *J. Photochem. Photobiol.*, 1987, 45, 879-889.
[5] Huang, Z., *Technol. Cancer Res. T.*, 2005, 4, 283-293.
[6] Tsay, J. M.; Trzoss, M.; Shi, L.; Kong, X.; Selke, M.; Jung, M. E.; Weiss, S., *J. Am. Chem. Soc*., 2007, 129, 6865-6871.
[7] Gorman, A.; Killoran, J.; O'Shea, C.; Kenna, T.; Gallagher, W. M.; O'Shea, D. F., *J. Am. Chem. Soc*., 2004, 126, 10619-10631.

Huang[5] asserts that chemists and clinicians have different ideals for PS. To clinicians, high selectivity and low toxicity may be important whereas chemists look for high quantum yields of singlet O_2 and high extinction coefficients. They do, however, agree that for PDT, PS must meet some criteria.[5] According to Bakalova *et al*.[8] for effective PDT, PS must target cancerous tumours, resist aggregation and in the absence of irradiation, PS should be non-toxic. Further, they must be easily flushed from the body, possess sufficient energy to transfer oxygen molecules and should be photo-stable.[8] Limitations of PS include low selectivity, instability, poor water solubility, skin phototoxicity and an inability to penetrate deep tissues.[9]

Various light sources have been applied in PDT, the first of which were non-coherent light sources. These are comparatively inexpensive and both safe and easy to use. They do, however, have several disadvantages, for instance, low light intensity. Light dosage is difficult to control and may cause thermal effects. Another PDT applied light source is a light-emitting diode (LED), which is known to generate various wavelengths of high-energy light. The most common PDT light source is a laser. Lasers produce specific wavelengths of high-energy monochromatic light, which are photosensitiser-specific and have narrow bandwidths.[5] The limitations of these light sources involve the diameter of the spot size and the depth of penetration. Marmur *et al*.[10] suggest that superior light sources and penetration enhancers need to be developed.[10]

Gorman *et al*.[7] suggest that the efficiency of a PDT agent is governed by three factors; the efficiency of an intersystem crossing (ISC), the location of the photosensitiser and the photosensitiser's extent of light activation.[7] The cytotoxic agent for PDT is singlet oxygen. Control over this component is important. The amount of singlet oxygen generated by the photosensitiser may be regulated by the spin-forbidden electronic transition (ISC) from singlet state to a triplet state. Heavy-atom introduction into a molecule is known as the heavy-atom effect and influences the rate of ISC. Spin-orbit

[8] Bakalova, R.; Ohba, H.; Zhelev, Z.; Nagase, T.; Jose, R.; Ishikawa, M.; Baba, Y., *Nano Lett*., 2004, 4, 1567-1573.
[9] Michalet, X.; Pinaud, F.; Bentolila, L. A.; Tsay, J. M.; Li, J. J.; Doose, S.; Weiss, S., *Science*, 2005, 307, 538-544.
[10] Marmur, E. S.; Schmults, C. D.; Goldberg, D. J., *Dermatol. Surg*., 2004, 30, 264-271.

perturbations are required for the transitions to occur between states that have different spin multiplicities. When a heavy-atom is attached directly to a molecule, it may enhance the spin-orbit perturbations and thus enhance the singlet oxygen production.

Gorman *et al*.[7] modulated the degree of spin-orbit coupling by three modes. Firstly, having a sensitiser with no heavy-atom, thereby relying on the molecules' inherent spin-orbit coupling. Secondly, the heavy-atoms were positioned directly onto the sensitiser. Thirdly, instead of positioning the heavy-atoms directly onto the sensitiser these were positioned onto the aryl rings, which gave rise to the intermediate level of singlet-oxygen generation. The second mode was found to be more favourable for singlet-oxygen production. The position of the heavy-atom within the sensitiser is critical because the introduction of heavy-atom substituents can cause non-radiative internal back conversion to the ground state, or inhibit the energy transfer from the photosensitiser triplet to ground-state oxygen. The position of the heavy-atom on the photosensitiser must affect the degree of spin-orbit coupling without giving rise to competing excited-state energy loss pathways.

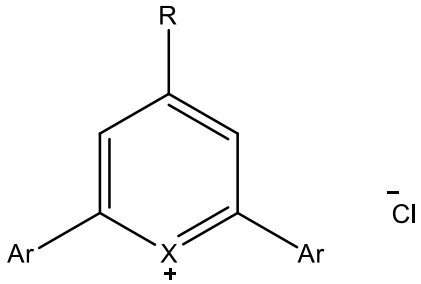

Figure 2.2: Illustration of the reported non-porphyrin PDT agent. [7]

The heavy-atom effect for the pyrylium class of PDT agents (Figure 2.2) was reported by Gorman *et al*.[7] The results of their study showed that by replacing the ring oxygen with the heavier tellurium atom, which did not increase the singlet-oxygen quantum yields, led to a decrease in the fluorescence quantum yield.[7] The substitution of two pyrrole nitrogen atoms of *meso*-tetraarylporphyrins with selenium by You *et al*.[11] showed similar results to that of Gorman *et al.*[7] as the singlet-oxygen quantum yields

were reduced when compared to the parent porphyrin.[11] Both Gorman *et al.*[7] and You *et al.*[11] explained this by the structural distortions of the pyrylium and porphyrin rings, due to the larger atomic radii of these heavy-atoms. This distortion causes a loss of sensitiser planarity, and promotes non-radiative decay to the ground-state. This distortion could also be caused by an internal heavy-atom effect, causing a shortening of the triplet lifetime.

2.3 Ruthenium Medicinal Applications

According to Allardyce and Dyson[12], ruthenium anti-cancer agents have shown promising activity to tumours that have been otherwise resistant to treatment. Similarly to other metal drugs, the activity of the ruthenium compound is dependent on the oxidation state and the type of ligand to which it is coordinated. Manipulation of these characteristics has succesfully led to anti-malarial, antibiotic and immuno-suppressive drugs.[12]

There are three properties of ruthenium compounds that suit them ideally for medicinal applications. These are the ligand exchange rate, the ability of ruthenium to change oxidation state and the iron-mimicking ability of ruthenium.[12] Ruthenium complexes are of interest in clinical application because Ru(II) and Ru(III) complexes have similar ligand exchange kinetics to those of Pt(II) complexes. Research reveals that only a few metal drugs are able to reach the biological target without modification. Thus, ligand exchange is important in biological activity. Some of the interactions with water, macromolecules and small S-donor compounds that bring about these modifications are necessary for the introduction of the desired therapeutic properties of these complexes.[12]

As opposed to the platinum group metals, ruthenium possesses the unique characteristic that several of its oxidation states (Ru(II), Ru(III), Ru(IV)) are accessible under physiological conditions.[12] Complexes in these oxidation states are generally found to have an octahedral geometry and the ruthenium center is hexa-coordinate. Ru(III) complexes have been found to be biologically inert compared to

[11] You, Y.; Gibson, S. L.; Hilf, R.; Davies, S. R.; Oseroff, A. R.; Roy, I.; Ohulchanskyy, T. Y.; Bergey, E. J.; Detty, M. R., *Med. Chem.* 2003, 46, 3734-3747.

their Ru(II) and Ru(IV) counterparts. Exploitation of the redox potential of the ruthenium compounds may improve drug effectiveness. The effect of cancer cells on biological tissue provides a strongly reducing environment, thereby facilitating redox reactions of these complexes. Cancer cells favour Ru(II) on account of the reductive environment of these cells. Therefore, biologically inactive Ru(III) should be used as a pro-drug which is activated by reduction upon reaching these cells. The iron-mimicking ability of ruthenium allows binding to many biomolecules; this is believed to result in the low toxicity of ruthenium drugs.[12] Ru(II) complexes have shown higher reactivity toward DNA than both Ru(III) and Ru(IV), thereby supporting the idea that the initial reduction of Ru(III) is involved in the anti-cancer activity of Ru(II) at the tumour site.[12]

Complexes of Ru(II) with 2,2'-bipyridine (bpy) have been widely studied as coordination compounds. This interest is largely due to the potential ability of the photo-excited state of these complexes to act as a redox catalyst.[12] Excited state-mediated oxidation and reduction processes are driven by the light energy absorbed by the complex resulting in possible photochemical applications. The highest wavelength electronic absorption of a Ru(II) polypyridine complex is known to correspond to the lowest-energy excited state of such a complex and is associated with an excited state metal-to-ligand charge transfer (MLCT).[12] This state may be described by the promotion of an electron from the Ru(II) d-orbital to the ligand π^*-orbital. The nature of the ligand has a great influence on the absorption properties of the complex. Ligands with delocalized π-systems and electronegative substituent bearing ligands are good electron acceptors which lead to longer wavelength absorptions and lower energy π^*-levels. However, the complex can become non-emissive if the π^*-energy level is lowered to an excessive degree, due to the low-lying states that compete for depopulation of the singlet MLCT state to such an extent that the lifetime of the excited state is drastically reduced.[13]

Ru(II) is commonly used in complexation reactions with different types of imidazo[4,5-f]-1,10-phenanthroline type ligands. These complexes were studied for

[12] Allardyce, C. S.; Dyson, P. J., *Platinum. Met. Rev*., 2001, 45, 62-69
[13] Chouai, A.; Wicke, S. E.; Turro, C.; Bacsa, J.; Dunbar, K. R.; Wang, D.; R. P. Thummel, R. P., *Inorg. Chem.,* 2005, 44, 5996-6003.

biological applications[14] and excited state properties.[15] Bai *et al*.[16] reported Ru(II) complexes with 3,4-dihydroxy-imidado[4,5-f][1,10]-phenanthroline ($dhipH_3$) (Figure 2.3) that show luminescence properties that are pH dependent.

[14] Nikolic, S.; Rangasamy, L.; Gligorijevic, N.; Arandelovic, S.; Radulovic, S.; Gasser, G.; Grguric-Sipka, S., *J. Inorg. Biochem.*, 2016, 160,156-165.
[15] Lu, Z. Z.; Peng, J. D.; Wu, A. K.; Lin, C. H.; Wu, C. G.; Ho, K. C.; Lin, Y. C.; Lu, K. L., *Eur. J. Inorg. Chem.*, 2016, 1214-1224.
[16] Bai, G. Y.; Wang, K. Z.; Duan, Z. M.; Goa, L. H., *J. Inorg. Biochem.*, 2004, 98, 1017-1022.

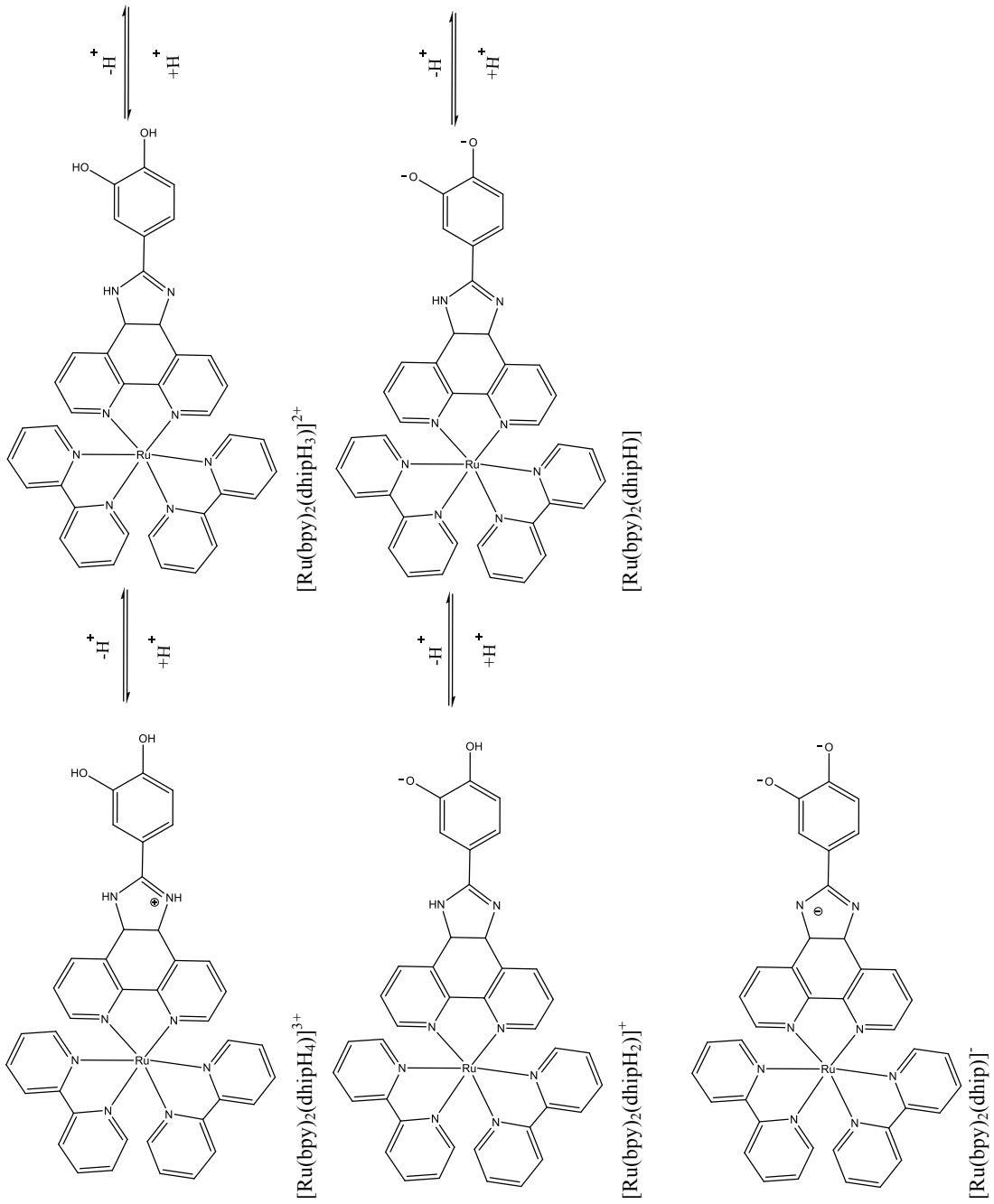

Figure 2.3: Molecular structure and protonation/ deprotonation of the Ru(II) complex.[16]

Wang *et al*.[17] used imidazo[4,5-f]-1,10-phenanthroline derived ligands (Figure 2.4) in chemosensor development for Co(II) ions. Efficient photo-generation of singlet oxygen with an Ir(II) core was developed by Sun *et al.*[18] in which a coumarin chromophore is in conjugation with the imidazo[4,5-f]-1,10-phenanthroline ligand.

[17] Wang, X.; Zheng, W.; Lin, H.; Liu, G.; Chen, Y.; Fang, J., *Tetrahedron. Lett.*, 50, 2009, 50, 1536-1538.
[18] Sun, J.; Zhao, J.; Guo, H.; Wu, W., *Chem. Commun.*, 2012, 48, 4169-4171.

Various metal complexes containing the imidazo[4,5-f]-1,10-phenanthroline type ligands have been used for cell imaging studies. These complexes have either an Ir(II) or Ru(II) metal core. The Ru(II) complexes established mitochondrial targeting behaviour[19] while the Ir(II) complexes revealed two-photon excitation as well as phosphorescence induced by aggregation.[20] Bonello *et al*.[21] report a one-pot synthesis for various Re-imidazo[4,5-f]-1,10-phenanthroline ligand based complexes and found that these ligands readily react with $ReBr(CO)_5$, thus forming *fac*-[$ReBr(CO)_3$(*N,N'*)] complexes. All of the complexes synthesised by Bonello *et al.*[21] were found to possess a MLCT emitting state and thereby gave visible luminescence at ambient temperature in a fluid medium.

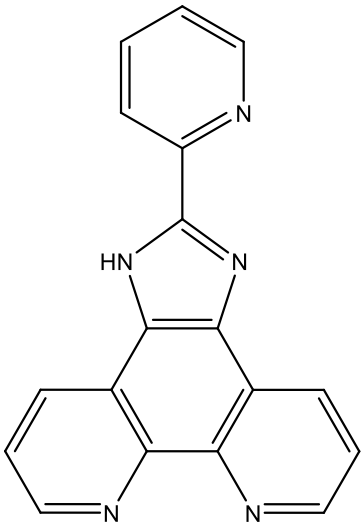

Figure 2.4 Illustration of 2-(2-pyridine)imidazo[4,5,f]-1,10-phenanthroline ligand synthesised by Wang *et al.*[17]

[19] Liu, J.; Chen, Y.; Li, G.; Zhang, P.; Jin, C.; Zeng, L.; Ji, L.; Chao, H., *Biomaterials*, 2015, 56,140-153.
[20] Jin, C.; Liu, J.; Chen, Y.; Zeng, L.; Guan, R.; Ouyang, C.; Ji, L.; Chao, H., *Chem. Eur. J.,*2015, 21, 12000-12010.
[21] Bonello, R.; Pitak, M. B.; Coles, S. J.; Hallett, A. J.; Fallis, I. A.; Pope, S. J. A., *J. Organomet. Chem.*, 2017, 841, 39-47.

2.4 Rhenium Medicinal Applications

Rhenium and technetium complexes that bear the *fac*-$[M(CO)_3]^+$ entity (M = Re(I), Tc(I)) have been a significant topic of interest as potential therapeutic as well as potential diagnostic radiopharmaceuticals. The application of these complexes for cancer treatment can largely be accredited to the work done by Alberto *et al.*[22,23,24,25,26,27]

A non-participant effect in antigen-negative neighbouring cells is applied by β-emissions, which have a path length which ranges from 1-10 mm in distance. Although γ-particles have a short path length, they exhibit a high rate of energy transfer, which contributes to their biological effectiveness and independence to dosage. γ-particles are used for diagnosis and β-particles are used for therapeutic purposes on account of their distance of penetration.[28] The radiation characteristics of rhenium as a β-emitting isotope suggest that a decrease in radiation dose to the patient will not cause a decrease in the dose deposition at the tumour site.[27] Characteristics of rhenium that contribute to the interest in rhenium as an agent of radiopharmacy include the compact size of the atom, low positive charge, coordination properties, d^6 low-spin configuration and the stability of the element.[29] Confirmation by Wagner *et al.*[30] shows that the yield of transmetallation reactions can be increased significantly by the use of 'cold' rhenium.

---

[22] Zobi, F.; Blacque, O.; Sigel, R. K. O.; Alberto, R., *Inorg. Chem.*, 2007, 46, 10458-10460.
[23] Alberto, R.; Schibli, R.; Waibel, R.; Abram, U.; Schubiger, A. P., *Coord. Chem. Rev*. 1999, 192, 901-919.
[24] Springler, B.; Mundwiler, S.; Ruiz-Sanchez, P.; van Staveren, D. R.; Alberto, R., *Eur. J. Inorg. Chem*. 2007, 18, 2641-2647.
[25] Alberto, R.; Herrmann, W. A.; Kiprof, P.; Baumgärtner, F., *Inorg. Chem*., 1992, 31, 895-899
[26] Alberto, R.; Schibli, R.; Schubiger, P. A.; Abram, U.; Kaden, T. A., *Polyhedron*, 1996, 15, 1079-1089.
[27] Abram, U.; Abram, S.; Alberto, R.; Schibli, R., *Inorg. Chim. Acta.*, 1996, 248, 193-202.
[28] Radiotherapy of Cancer. R.C. Bast; C.A. Kousparou; A.A. Epenetos; M.R. Zalutsky; R.J. Kreitman; E.A. Sausville; A.E. Frankel. Holland-Frei Cancer Medicine. 6th edtion.
[29] Schutte, M.; Roodt, A.; Visser, H.G. *Inorg. Chem.*, 2012, 51, 11996–12006.
[30] Wagner, T.; Zeglis, B.M.; Groveman, S.; Hille, C.H.; Pöthig, A.; Francesconi, L.C.; Hermann, W.A.; Kühn, F. E.; Reiner, T. *Radiopharm.* 2014, 57, 441-447.

Under mild conditions and in aqueous solution, Alberto *et al.* synthesised *fac*-[^{99m}Tc(CO)$_3$(H$_2$O)$_3$] showing that coordination to bidentate ligand chelators forms stable complexes. The primary reason of interest in the *fac*-[M(CO)$_3$(H$_2$O)$_3$]$^+$ synthon is the three labile sites occupied by the water molecules on the *fac*-metal tricarbonyl core.[31,32,33,34,35] These labile sites offer substitution possibilities. Strong coordination must occur between the entering ligand and the metal. This is important in receptor ligand labelling due to the possibility that free receptor sites may be saturated with unlabelled biomolecules, which may result in a decrease in radionucleotide accumulation in the target tissue.

Re(I) diimine tricarbonyls have been applied in biological labelling[36], solar-energy conversions[37] and sensor development[38] as these complexes show favourable photophysical properties, one of which is their ability to luminesce at room temperature[39] from tuneable low-lying metal-ligand charge transfer (MLCT) excited states. The lifetimes of these states are mostly controlled by non-radiative rate-constant values (K_{nr}) on account of 'energy-gap law' behaviour.[40,41] Excited-state resonance Raman spectroscopy[41] and spectral fitting[40] suggest that the radiationless decay process may be partially affected by a high-frequency CO stretching mode. This means that the formation of a dicarbonyl species by the removal of a carbonyl from a tricarbonyl species could possibly result in improved photophysical properties. Re(I) tricarbonyl complexes (*fac*-[Re(CO)$_3$(*N,N'*-bid)L]) (Figure 2.5) where an

[31] Mundwiler, S.; Kundig, M.; Ortner, K.; Alberto, R. *J. Chem. Soc., Dalton Trans*. 2004, 9, 1320-1328.
[32] Gorshkov, N.I.; Schibli, R.; Schubiger, A.P.; Lumpov, A.A.; Miroslavov, A.E.; Suglobov, D.N.J. *Organomet. Chem.* 2004, 689, 4757-4763.
[33] Riondato, M.; Camporese, D.; Martin, D.; Suades, J.; Alvarez-Lorena, A.; Mazzi, U. *Eur. J. Inorg. Chem.* 2005, 4048-4055.
[34] Agorastos, N.; Borsig, L.; Renard, A.; Antoni, P.; Viola, G.; Spingler, B.; Kruz, P.; Alberto, R. *Chem. Eur. J.* 2007, 13, 3842-3852.
[35] Gorshkov, N.I.; Lumpov, A.A.; Miroslavov, A.E.; Suglobov, D.N.; *Radiochemistry* 2005, 47, 45-49.
[36] Oriskovich, T. A.; White, P.S.; Thorp, H. H., *Inorg. Chem.* 1995, 34, 1629-1631.
[37] Takeda, H.; Ohashi, M.; Tani, T.; Ishitani, O.; Inagaki, S., *Inorg. Chem.*, 2010, 49, 4554-4559.
[38] Shen, Y.; Sullivan, B. P., *Inorg. Chem.*1995,34, 6235-6236.
[39] Wrighton, M.; Morse, D. L., *J. Am. Chem. Soc.* 1974, 96, 998-1003.
[40] Baiano, J. A.; Kessler, R. J.; Lumpkin, R. S.; Monley, M. J.; Murphy, W. R., Jr. *J. Phys. Chem.* 1995, 99, 17680-17690.
[41] Shen, Y.; Sullivan, B. P., *J. Chem. Educ.* 1997, 74, 685-689.

aromatic diimine is represented by *N,N'*-bid and L is a monodentate ligand, are known to show intense and long-lifetime luminescence in both the green and orange spectral regions. These emissions have been attributed to the charge transfer from the electronic transition of d(Re)→ $\pi*$ (diimine) [42,43,44,45,46] By substitution with various *N,N'*-bid and monodentate ligands, the excited-state lifetime as well as the emission energy can be altered to synthesise various different luminescent probes.

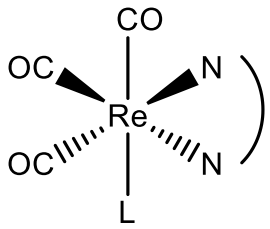

Figure 2.5: Illustration of the Re-diimine tricarbonyl moiety.

Black and Hightower[47] reported a series of meridionally-coordinated terpyridine Re(I) dicarbonyl complexes of the type *mer,cis*-$[Re(tpy\text{-}\kappa^3N)(CO)_2(L)]^+$. Luminescence studies of these complexes showed no steady-state luminescence at room temperature. Black and Hightower suggest this is due to the smaller than 90 ° bite-angles of the terpyridine tridentate ligand, causing it to be in a distorted octahedral geometry around the rhenium atom. Frenzel *et al.*[48] reported on a more expanded series of meridionally-coordinated terpyridine Re(I) dicarbonyl complexes of the type *mer,cis*-$[Re(tpy\text{-}\kappa^3N)(CO)_2(L)]^+$ and found that several of the complexes absorb light throughout a large section of the visible spectrum. Low temperature (196.15 °C) emission spectra were obtained for two of these compounds; *mer,cis*-[Re(tpy-

[42] Zalis, S.; Milne, C. J.; Nahhas, A. E.; Blanco-Rodriguez, A. M.; Van der Veen, R. M.; Vlcek Jr. A., *Inorg. Chem.*, 2013, 52, 5775-5785.
[43] Chu, W. K.; Ko, C. C.; Chan, K. C.; Yiu, S. M.; Wong, F. L.; Lee, C. S.; Roy, V. A. L., *Chem. Mater.*, 2014, 26, 2544-2550.
[44] Vaughan, J. G.; Reid, B. L.; Wright, P. J.; Ramchandani, S.; Skelton, B. W.; Raiteri, P.; Muzzioli, S.; Brown, D. H.; Stagni, S.; Massi, M., *Inorg. Chem.*, 2014, 53, 3629-3641.
[45] Czerwieniec, R.; Kapturkiewicz, A.; Lipkowski, J.; Nowacki, J., *Inorg. Chim. Acta.*, 2005, 358, 2701-2710.
[46] Caspar, J. V.; Meyer, T. J., *J. Phys. Chem.*, 1983, 87, 952-957.
[47] Black, D. R.; Hightower, S. E., *Inorg. Chem. Commun.*, 2012, 24, 16-19.
[48] Frenzel, B. A.; Schumaker, J. E.; Black, D. R.; Hightower, S. E., *Dalton Trans.*, 2013, 42, 12440-12451.

κ^3N)$(CO)_2$(Cl)] and *mer,cis*-[Re(tpy-κ^3N)$(CO)_2(P(OEt)_3)]^+$; these displayed metal-to-ligand charge transfer (^{3}MLCT) luminescence.

Marker *et al.*[49] reported the synthesis of two dicarbonyl rhenium photoproducts; $[Re(CO)_2(bpy)(DAPTA)(Cl)]$ (DAPTA-1A) and $[Re(CO)_2(bpy)(PTA)(Cl)]$ (PTA-3A) (Figure 2.6). The dicarbonyl complex was obtained by liberation of the axial CO ligand and subsequent substitution thereof with a chlorido ligand. The study of the anti-cancer activity of these compounds revealed that PTA-3A was non-toxic toward HeLA cells up to 200 μM in the dark, while DAPTA-1A revealed mild cytotoxicity at concentrations larger than 50 μM.

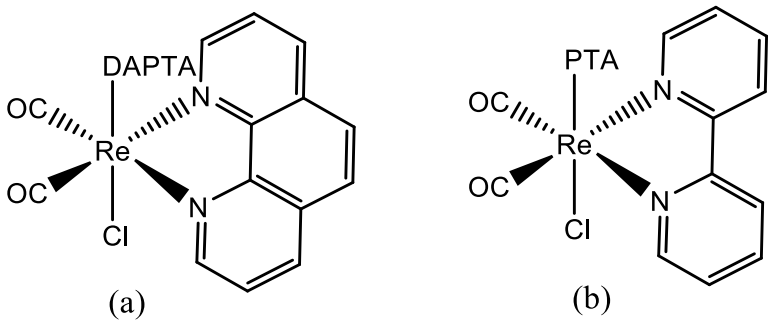

Figure 2.6: Illustration of the structure of the Re(I) dicarbonyl complexes, $[Re(CO)_2(bpy)(DAPTA)(Cl)]$ (a) $[Re(CO)_2(bpy)(PTA)(Cl)]$ (b), as synthesised by Marker *et al.*[49]

Smithback *et al.*[50] successfully prepared mixed-ligand rhenium(I) dicarbonyls with high quantum yields and long-lived excited state lifetimes. This group developed four synthetic routes that rely on combinations of chloride or triflate labilisation as well as the *trans*-effect of phosphines. Figure 2.7 shows two of the four synthetic routes developed by this group. From the four synthetic routes that were developed by Smithback *et al.,*[50] the *trans*-labilisation of carbonyls to yield *cis*-$[Re(CO)_2(P,P')(N,N')]^+$ creates room for various *N,N'* and *P,P'* (phosphine) ligands to be used while creating possibilities for various luminescent probes.

[49] Marker, S. C.; MacMillan, S. N.; Zipfel, W. R.; Li, Z.; Ford, P. C.; Wilson, J. J., *Inorg. Chem.*, 2018, 57, 1311-1331.
[50] Smithback, J. L.; Helms, J. B.; Schutte, E.; Woessner, S. M.; Sullivan, B. P., *Inorg. Chem.*, 2006, 45, 2163-2174.

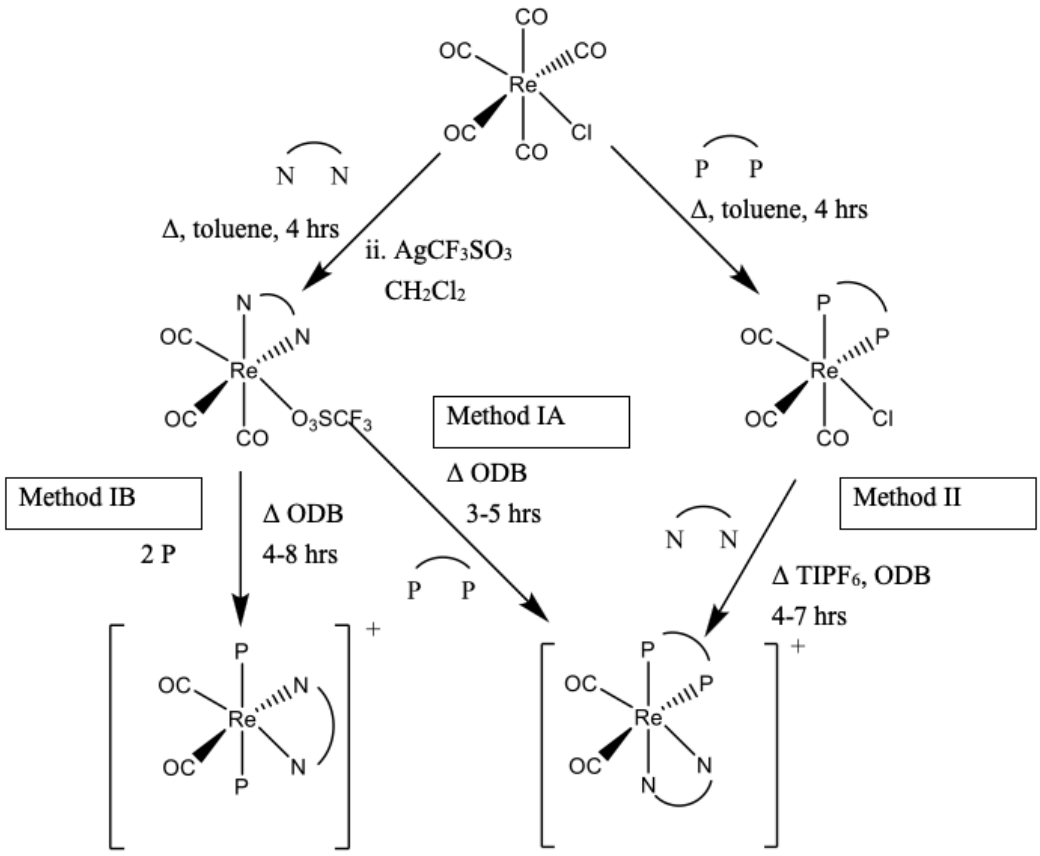

Figure 2.7: Preparation of mixed-ligand rhenium(I) dicarbonyl complexes. [50]

2.4.1 Rhenium Complexes for Photodynamic Therapy

Rhenium has photophysical and spectroscopic properties that are favourable for use in photodynamic therapy. Various rhenium(I) tricarbonyl complexes have been investigated for this purpose, many of which are clearly manifested as having potent *in vitro* phototoxic effects. These include rhenium(I) pyridocarbazole complexes by Wähler *et al.*[51] and *N,N'*-bis(quinolinoyl) Re(I) tricarbonyl complex derivatives by Gasser *et al.*[52] The rhenium(I) pyridocarbazole complexes are derivatives based on a metallopyridocarbazole complex by Meggers *et al.*[53] which is able to induce cell death upon irradiation at wavelengths of $\lambda \geq 505$ nm. Improvements in these structures include the ability to bring about apoptosis at longer wavelengths and

[51] Wähler, K.; Ludewig, A.; Szabo, P.; Harms, K.; Meggers, E., *Eur. J. Inorg. Chem.,* 2014, 807-811.
[52] Leonidova, A.; Pierroz, V.; Rubbiani, R.; Heier, J.; Ferrari, S.; Gasser, G., *Dalton Trans.*, 2014, 43, 4287-4294.
[53] Kastl, A. ; Dieckmann, S.; Wähler, K.; Völker, T.; Kastl, L.; Vultur, A.; Shannan, B.; Harms, K.; Ocker, M.; Parak, W. J.; Herlyn, M.; Meggers, E., *ChemMedChem.*, 2013, 8, 924-927.

increase the chemical stability.[51] These rhenium(I) pyridocarbazole complexes show promise for dual functionality as PDT agents along with target therapy, due to their ability to inhibit protein kinases.[51] Gasser *et al*.[52] attempted to probe two *N,N'*-bis(quinolinoyl) Re(I) tricarbonyl complexes as photosensitisers for PDT. Gasser[52] demonstrated that these complexes could induce DNA damage by efficient production of $^1O_2$ in lipophilic environments. Although the irradiation wavelengths studied by this group were not ideal. This study does attract interest to metal containing PDT photosensitisers. These unfortunately display similar limitations to porphyrin-based PDT agents since these rhenium-based phototoxic agents produce singlet O_2 to induce cell death. Development of such complexes that display an unconforming mechanism of action by Marker *et al.*[49] may possibly contribute to new therapeutic modalities. These complexes by Marker *et al*.[49] consist of several rhenium(I) tricarbonyl complexes containing various *N,N'* bidentate ligands (Figure 2.8). They posses potent UVA (365 nm) light-activated toxicity toward multiple cancer cell lines. As mentioned by Marker *et al*.[49] for *in vivo* applications this penetration depth is too shallow. However, these complexes provide the basis for future rhenium-based PDT agent development.

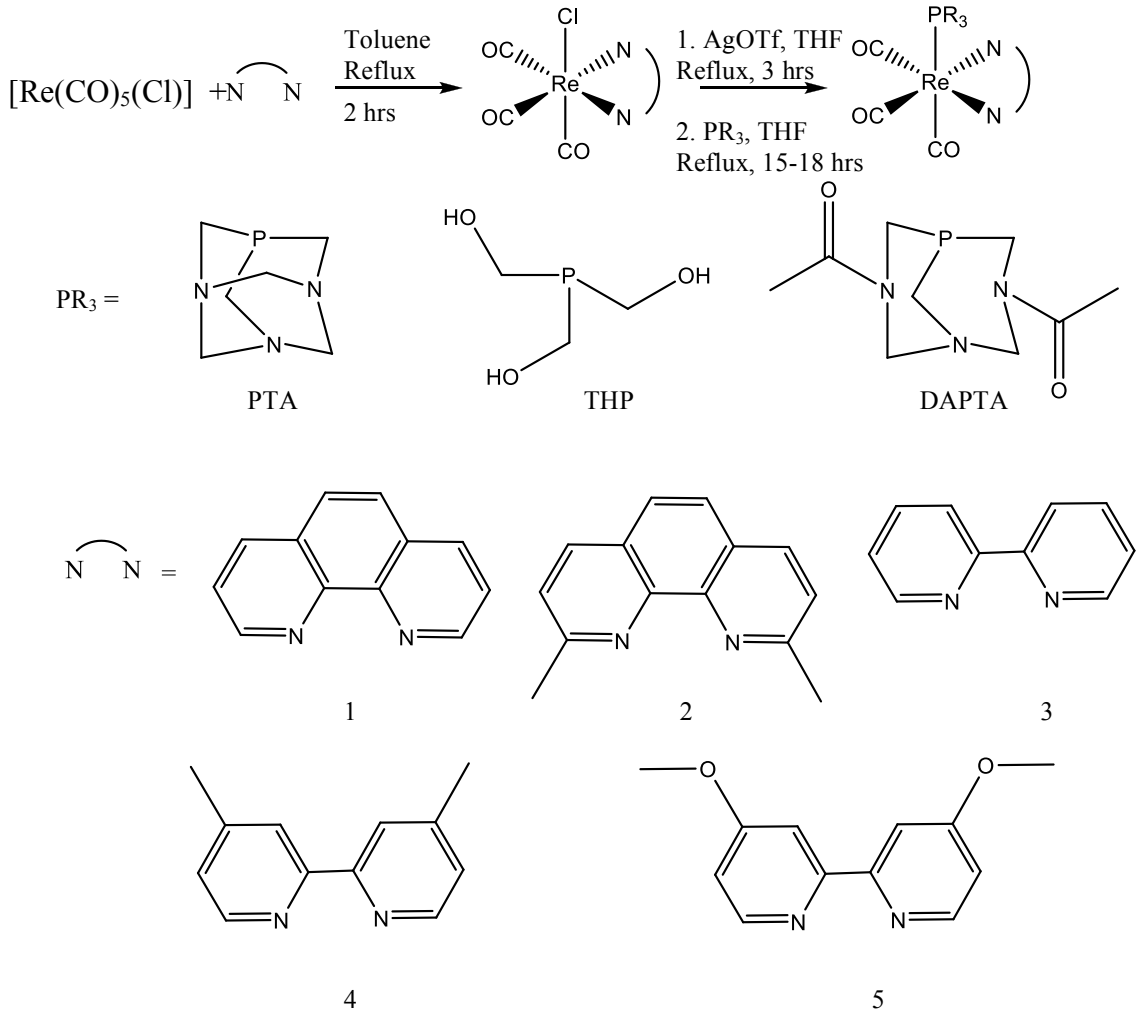

Figure 2.8: Synthetic scheme for the preparation of the $[Re(CO)_3(N,N')(PR_3)]^+$ complexes.[49]

1) 1,10-Phenanthroline

2) 2,9-dimethyl-1,10-Phenanthroline

3) 2,2'-bipyridine

4) 4,4'-dimethyl-2,2'-dipyridyl

5) 4,4'-dimethoxy-2,2'-bipyridine

2.4.2 Rhenium and Technetium as Chemotherapeutic Agents

When radiopharmaceuticals are used for therapeutic purposes, a suitable radioisotope is required which must show specificity at the tumour site, display the necessary pharmokinetics, as well as have physical characteristics such as the correct type of energy and optimal half-life.[54] Rhenium and technetium have been extensively researched as possible radionuclides in radiopharmaceuticals.[55] These group 7 transition metals are highly versatile and possess a rich coordination chemistry and

[54] Neves, M.; Kling, A.; Lambrecht, R. M., *Appl. Rad. Isotop.*, 2002, 57, 657-664.
[55] Abram, U.; Alberto, R., *J. Braz. Chem. Soc.*, 2006, 17, 1486-1500.

can range in oxidation state from -1 to +7.[56] The d^6 electron configuration of the +1 oxidation state and the d^2 electron configuration of the +5 oxidation state[57] are stable, while the d^1 configuration of the +6 oxidation state causes it to be unstable.[58, 59]

Rhenium-188 and rhenium-186 are the radionuclides commonly used in rhenium radiopharmaceuticals. Both ^{188}Re and ^{186}Re are β- and γ-emitting. ^{188}Re is produced from a ^{188}W generator while ^{186}Re is produced within a nuclear reactor. Lyra *et al.*[60] reported that rhenium-188 holds important advantages over many radioisotopes and is thus widely used in clinical application. These advantages include, although they are not limited to, the ease of access in hospitals from the tungsten-188 generator as well as the half-life of rhenium-188 which is favourable for therapeutic applications. Rhenium-188 is appealing for treatment of bone metastases and Re-188 HEDP palliative treatment is often administered to patients who still have bone pain after chemotherapy and those who have a short and uncomfortable life expectancy.[61]

The ^{99m}Tc radionuclide is used in diagnostic imaging applications. ^{99m}Tc is obtained from a ^{99}Mo generator, thus allowing it to be easily accessible in hospitals. The half-life of ^{99m}Tc (6.02 hours) allows sufficient time for diagnostic imaging without long-term radioation exposure to the patient. Kim *et al.*[62] reported that the product formed when chelating ^{99m}Tc with galactosyl-methylated chitosan, ^{99m}Tc-Galactosylated Chitosan (^{99m}Tc-GMS), displays uptake into the liver within minutes of administration. The activity of ^{99m}Tc-GMS within the liver gradually increased for two hours. ^{99m}Tc-GMS was found to be highly active within the kidney. Results of fluorescence studies of the Kupffer cells within the liver suggest that mediation by ASGP-R protein receptors lead to the accumulation of GMC in the liver.[62] Ghfir and

[56] Alberto, R., *Comprehensive Coordination Chemistry II,* in J. A. McCleverty, T. J. Meyer (Eds.), 5, Elsevier, Oxford, 2004, p. 127.
[57] Cotton, F. A.; Wilkinson, G.; Murillo, C. A.; Bochmann, M., *Advanced Inorganic Chemistry,* 6th Edition, J. Wiley Interscience, New York, 1999.
[58] Canlier, A.; Kawasaki, T.; Chowdhury, S.; Ikeda, Y., *Inorg. Chim. Acta.*, 2010, 363, 1-7.
[59] Das, S., *Inorg. Chim. Acta.*, 2008, 361, 2815-2820.
[60] Argyrou, M.; Valassi, A.; Andreou, M.; Lyra, M., *Int. Mol. Imag*. 2013, 1-7.
[61] Bodei, L.; Lam, M.; Chiesa, C., *Eur. J. Nucl. Med. Mol. Imag.*, 2008, 35, 1934-1940.
[62] Kim, E.; Jeong, H.; Park, I.; Cho, C.; Kim, C.; Bom, H., *J. Nucl. Med.*, 2005, 46, 141-145.

Raïs[63] reported ^{99m}Tc-HMDP whole body scintigraphy for the detection of primary lung cancer. ^{99m}Tc-MIBI was initially developed for the detection of myocardial perfusions[64] but has since been welcomed as a successful imaging agent for cancerous tumours. [65,66,67] A comparison of ^{99m}Tc-MIBI and ^{99m}Tc-HMDP by Wakasugi *et al.*[68] showed that the sensitivity toward detection of bone metastases of ^{99m}Tc-MIBI was superior to that of ^{99m}Tc-HMDP. This group reported that ^{99m}TC-HMDP scans showed 39 false positive findings on lesions while ^{99m}Tc-MIBI only showed two false positive findings. ^{99m}Tc-MIBI scintimammography is used for the detection of tumours in the breast and display good visualisation while ^{99m}TC-MDP scintigraphy is used in the staging of bone metastases related to breast cancer.

Rhenium-186 hydroxyethylidene diphosphonate (^{186}Re-HEDP) is known for its use as palliative treatment for bone metastases. De Klerk *et al.*[69] studied the dose effect of ^{186}Re-HEDP on 24 patients diagnosed with hormone-resistant prostate cancer. De Klerk *et al.*[69] found that the tolerated dose of ^{186}Re-HEDP for this type of cancer is 2960 MBz. In another study, De Klerk *et al.*[70] studied the dose effect of rhenium-186-HEDP on twelve patients with breast cancer-related bone metastases.[70] They found that the tolerated dose of ^{186}Re-HEDP for this type of cancer is 2405 MBq (65 mCi) and observed changes in alkaline phosphatase levels which suggest that ^{186}Re-HEDP has anti-tumour effects.

---

[63] Ghfir, I.; Raïs, N., *Internet J. Nucl. Med.*, 2006, 3, 1-4.
[64] Jones, A. G.; Abrams, M. J.; Davison, A.;Brodack, J.W.; Toothaker, A. K.; Adelstein, S. J.; Kassis, A. I., *Int. J. Nucl. Med. Biol.*, 1984, 11, 225-234.
[65] Aktolun, C.; Bayhan, H.; Kir, M., *Clin. Nucl. Med*., 1992, 17, 171-176.
[66] Caner, B.; Kitapol, M.; Unlu, M.; Erbengi, G.; Calikoglu, T.; Bekdik; Coskun, B. *J. Nucl. Med.*, 1992, 33, 319-324.
[67] Delmon-Moingeon, L. I.; Piwnica-Worms, A. D.; Van den Abbeele. B; Holman, L; Davison, A.; Jones, A. G., *Cancer Res.*, 1990, 50, 2198-2202.
[68] Wakasugi, S.; Noguti, A.; Katuda, T.; Hashizume, T.; Hasegawa, Y., *J. Nucl. Med.*, 2002, 43, 596-602.
[69] De Klerk, J. M. H.; Zonnenberg, B. A.; Van het Schip, A. D.; van Dijk, A.; Han, S. H.; Quirijnen, J. M. S. P.; Blijham, G. H.; Van Rijk, P. P., *Eur. J. Nucl. Med.*, 1994, 21, 1114-1120.
[70] De Klerk, J. M.H.; Van het Schip, A. D.; Zonnenberg, B. A.; van Dijk, A.; Quirijnen, J. M. S. P.; Blijham, G. H.; Van Rijk, P. P., *J Nucl. Med.*, 1996, 37, 244-249.

2.5 Platinum Medicinal Applications

Although metals have been used in cancer treatment since the sixteenth century,[71] it was not until the discovery of cisplatin (Figure 2.9)[72] that the value of metal complexes for the treatment of cancer was realised. Almost 50 % of oncology treatments are platinum-based.[73] Cisplatin has been used to treat various cancers which include testicular, ovarian, and lung cancers.[74] The apoptosis brought about by cisplatin may be attributed to the formation of cisplatin adducts that become positively charged upon entry to the tumour cell and irreversibly bind to DNA nucleobases.[74,75] The limitations of cisplatin include drug resistance and toxic side effects. Carboplatin (Figure 2.9) is known as the second generation analogue of cisplatin. The labile chlorido ligands of cisplatin are replaced with 1,2-cyclobutanedicarboxylate in carboplatin in an attempt to improve the toxicity of the platinum complex. Carboplatin is more stable than cisplatin and is mainly used in ovarian cancer treatment. The replacement of the non-leaving amine ligands by a (1*R*, 2*R*)-diaminocyclohexane moiety resulted in the formation of oxaliplatin (Figure 2.9). The *O,O'*-bidentate leaving group of oxaliplatin also differs from that of carboplatin. Oxaliplatin is used in colorectal cancer treatment because patients with colorectal cancer have been known to overexpress organic cation transporters (OCTs) and oxaliplatin has the ability to act as a substrate for OCTs.[74, 76]

[71] Desoize, B., *Anticancer Res.* 2004, 24, 1529-1544.
[72] Rosenberg, B.; Vancamp, L.; Krigas, T., *Nature*, 1965, 205, 698-699.
[73] Johnstone, T. C.; Suntharalingam, K.; Lippard, S. J., *Philos. Trans. A Math. Phys. Eng. Sci.*, 2015, 373
[74] Johnstone, T. C.; Suntharalingam, K.; Lippard, S. J., *Chem. Rev.*, 2016, 116, 3436-3486.
[75] Kelland, L., *Nat. Rev. Cancer*, 2007, 7, 573-584.
[76] Zhang, S.; Lovejoy, K. S.; Shima, J. E.; Lagpacan, L. L.; Shu, Y.; Lapuk, A.; Chen Y.; Komori, T.; Gray, J. W.; Chen, X.; Lippard, S. J.; Giacomini, K. M., *Cancer Res.*, 2006, 66, 8847-8857.

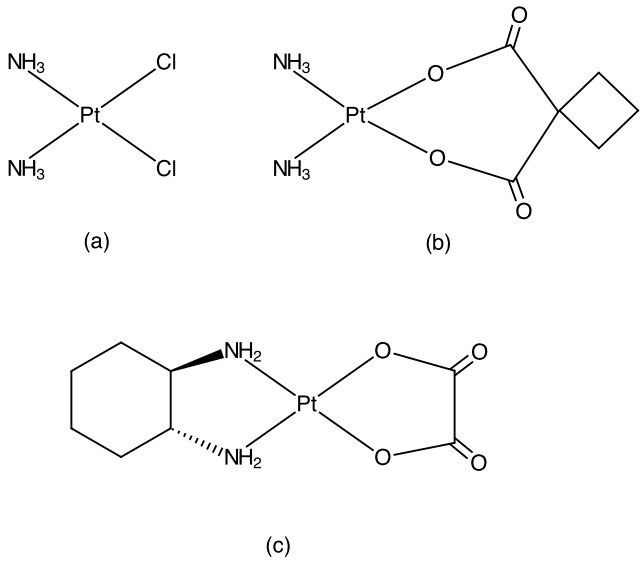

Figure 2.9: Chemical structures of cisplatin (a), carboplatin (b), and oxaliplatin (c).

2.6 Palladium Medicinal Applications

The discovery of the anti-tumour properties of cisplatin sparked off an interest into the development of more efficient, less toxic complexes in which other platinum group metals were used. Palladium(II) analogues to cisplatin were some of the first complexes to be explored and used in clinical trials.[77] This is due to Pd(II) and Pt(II) having similar chemistry to one another. Both Pd(II) and Pt(II) rarely form trigonal bipyrimidal complexes and more frequently form square planar complexes. Pt(II) complexes have been found to be both more kinetically and thermodynamically stable than their Pd(II) counterparts. Yet Pd(II) complexes undergo ligand exchange and aquation 10^5 times faster than Pt(II), resulting in lower anti-tumour activity.[78] This lower anti-tumour activity is attributed to the leaving groups being hydrolyzed. Borle *et al*.[79] studied the selectivity of the palladium-bacteriopheophorbide photosensitiser, TOOKAD® (Figure 2.10), for photodynamic therapy. The response of TOOKAD® in PDT applications was measured in the cheek pounch of a Syrian hamster. Borle *et al*.[79] found that TOOKAD® exhibits fast decay of PDT with regard to drug-light interval and therefore fits the profile of a photosensitiser by exhibiting vascular

[77] Maitlis, P., *The Organic Chemistry of Palladium in Organometallic Chemistry, A Series of monographs*, Maitlis, P., Stone, F., West. R., Eds: Academic Press Inc.: New York, 1971, Vol. 1.
[78] Garoufis, A.; Hadjikakou, S. K.; Hadjiliadis, N., *Coord. Chem. Rev.*, 2009, 253, 1384-1397.
[79] Borle, F.; Radu, A.; Fontolliet, C.; Van den Bergh, H.; Monnier, P.; Wagnières, G., *Br. J. Cancer,* 2003, 89, 2320-2326.

effects. Azzouzi *et al*.[80] reported that Palediporfin vascular-targeted photodynamic therapy is safe and effective in the treatment of localised, lower-risk prostate cancer.

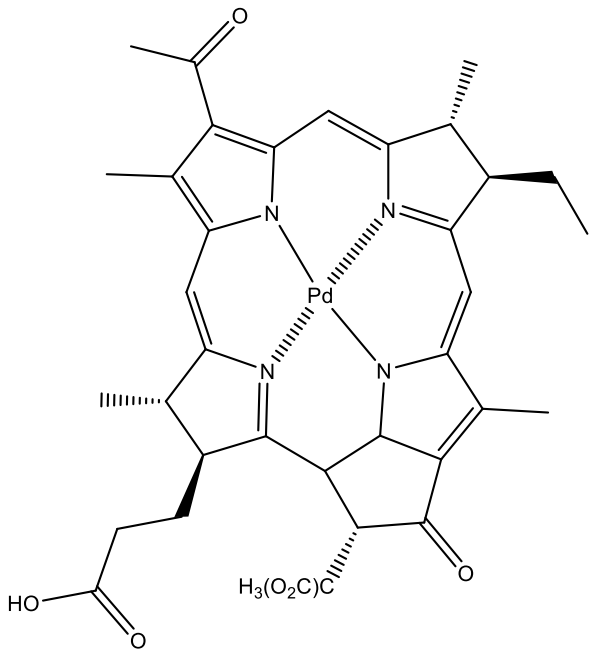

Figure 2.10: Chemical structure of the palladium-metalated bacteriopheophorbide, Tookad®

2.7 Photoluminescence

2.7.1 Background on Photoluminescence

One of the most powerful tools in medicinal science and modern biology is fluorescence cell imaging. Various luminescence cell imaging techniques allow visualization of cell compartments and the ability to observe and detect cellular uptake and activity. Organometallic transition metal complexes are attractive in novel luminescent probes since they generally overcome limitations that fluorescent organic probes are frequently unable to overcome.[81,82,83,84,85] In sum, the advantage of using

[80] Azzouzi, A.; Vincendeau, S.; Barret, E.; Cicco, A.; Kleinclauss, F.; Van der Poel, H. G.; Stief, C. G.; Rassweiler, J.; Salomon, G.; Solsona, E.; Alcaraz, A.; Tammela, T. T.; Rosario, D. J.; Gomez-Veiga, F.; Ahlgren, G.; Benzaghou, F.; Gaillac, B.; Amzal, B.; Debruyne, F. M. J.; Fromont, G.; Gratzke, C.; Emberton, M., *Lancet Oncol.*, 2017, 18, 181-191.
[81] Baggaley, E.; Weinstein, J. A.; Williams, J. A. G., *Coord. Chem. Rev.,* 2012, 256, 1762-1785.
[82] Haas, K. L.; Franz, K. J., *Chem. Rev.,* 2009, 109, 4921-4960.
[83] Patra, M.; Gasser, G., *ChemBioChem.*, 2012, 13, 1232-1252.
[84] Zhao, Q.; Huang, C.; Li, F., *Chem. Soc. Rev.*, 2011, 40, 2508-2524.

transition-metal complexes may be accredited to their photophysical properties.[86] Processes of fast intersystem-crossing are a result of metal-induced strong spin-orbit coupling (SOC).[87,88] This intersystem-crossing initially preceeds from the photoexcited singlet state (S_0) to the triplet state (T_1) and it is sometimes from T_1 to S_0. Yersin *et al.*[89], Evans *et al*.[90], and Xiang *et al*.[91] reported various transition metals that form complexes with appropriate organic ligands and have shown intense phosphorescence at room temperature. Hirata *et al.*[92] reported that for a metal-based luminophore the emission lifetime is longer than that of purely organic material by some order of magnitude; it is shorter than the expected lifetime of an organic emitter. The result is, when using time-gated detection, emissions from a transition metal-based probe are easy to distinguish.[93,94]

In vivo fluorescence imaging makes use of a highly sensitive camera which has the ability to detect the fluorescence emission from fluorophores in small living animals. Fluorophores require long emission at the near-infrared region (NIR) to prevent photon attenuation in living tissues.[95] Advances made in imaging strategies and *in vivo* fluorescence imaging reporter techniques, pertain to improvements in the probe affinity, specificity and the modulation and amplification of the signal at target sites affording improved sensitivity.[95]

---

[85] Thorp-Greenwood, F. L., *Organometallics*, 2012, 31, 5686-5692.
[86] Kowalski, K.; Szczupak, L.; Bernas, T.; Czerwieniec, R., *J. Organomet. Chem.*, 2015, 782, 124-130.
[87] Rausch, A. F.;. Homeier, H. H. H; Yersin, H., *Top. Organomet. Chem.*, 29, 2010, 193-235.
[88] Bakova, R.; Chergui, M.; Daniel, C.; Vlcek Jr., A.; Zalis, S., *Coord. Chem. Rev.*, 2011, 255, 975-989.
[89] Yersin, H.; Rausch, A. F.; Czerwieniec, R.; Hofbeck, T.; Fischer, T., *Coord. Chem. Rev.*, 2011, 255, 2622-2652.
[90] Evans, R. C.; Douglas, P.; Winscom, C. J., *Coord. Chem. Rev.*, 2006, 250, 2093-2126.
[91] Xiang, H.; Cheng, J.; Ma, X.; Zhou, X.; Chruma, J. J., *Chem. Soc. Rev.*, 2013, 42, 6128-6185.
[92] Hirata, S.; Totani, K.; Zhang, J.; Yamashita, T.; Kaji, H.; Marder, S. R.; Wantanabe, T.; Adachi, C., *Adv. Funct. Mater.*, 2013, 23, 3386-3397.
[93] Botchway, S. W.; Charnley, M.; Haycock, J. W.; Parker, A. W.; Rochester, D. L.; Weinstein, J. A.; Williams, J. A. G., *Proc. Natl. Acad. Sci. U. S. A.*, 105, 2008, 16071-16076.
[94] Murphy, L.; Congreve, A.; Palsson, L. O.; Williams, J. A. G., *Chem. Commun.*, 2010, 46, 8743-8745.
[95] Rao, J.; Dragulescu-Andrasi, A.; Yao, A., *Curr. Opin. Biotech.,* 2007, 18, 17-25.

A resemblance may be observed between fluorescence microscopy and *in vivo* fluorescence imaging in that both these techniques make use of a low-light camera and appropriate filters for fluorescence emission collection. These techniques do, however, differ in their operation at macroscopic level. In *in vivo* fluorescence imaging, the objects that are viewed are whole-body small animals, whereas for fluorescence microscopy, the viewed objects are cells on slides or in culture dishes.[95] Although this whole-body imaging allows intact visualization of biology, this may be challenging. Two limitations of *in vivo* fluorescence imaging are the additional demands placed on the imaging probe or contrast agent and the fact that the dense animal tissue can absorb and scatter photons, thereby creating autofluorescence, and thus obscuring quantification and signal collection.[96]

2.7.2 Rhenium as Photodynamic or Photoactivated Therapeutic Agent.

In recent years there has been great interest in organometallic complexes and their lower cytotoxic effects in respect of numerous cancer cell lines.[97,98,99,100] Among these organometallic complexes with low cytotoxic effects are rhenium complexes, which, when compared to cisplatin, exhibit superior anti-proliferative activity.[101,102,103,104,105,106,107] According to Dhar and Lippard[108], high cytotoxicity is

[96] Cheong, W. F.; Prahl, S. A.; Welch, A. J., *J. Quantum Electron*, 1990, 26, 2166-2195.
[97] Gasser, G.; Ott, I.; Metzler-Nolte, N., *J. Med. Chem*., 2010, 54, 3-25.
[98] Hartinger, C. G.; Metzler-Nolte, N.; Dyson, P. J., *Organometallics*, 2012, 31, 5677-5685.
[99] Gasser, G.; Metzler-Nolte, N., *Curr. Opin. Chem. Biol.*, 2012, 16, 84-91.
[100] Hartinger, C. G.; Dyson, P. J., *Chem. Soc. Rev.*, 2009, 38, 391-401.
[101] Zhang, J.; Vittal, J. J.; Henderson, W.; Wheaton, J. R.; Hall, I. H.; Hor T. S. A.; Yan, Y. K., *J. Organomet. Chem.,* 2002, 650, 123-132.
[102] Wang, W.; Yan, Y. K.; Hor, T. S. A.; Vittal, J. J.; Wheaton, J. R.; Hall, I. H., *Polyhedron*, 2002, 21, 1991-1999.
[103] Bartholoma, M. D.; Vortherms, A. R.; Hillier, S.; Ploier, B.; Joyal, J.; Babich, J.; Doyle, R. P.; Zubieta, J., *ChemMedChem*, 2010, 5, 1513-1529.
[104] Can, D.; Peindy N'Dongo, H. W.; Spingler, B.; Schmutz, P.; Raposinho, P.; Santos, I.; Alberto, R., *Chem. Biodiversity*, 2012, 9, 1849-1866.
[105] Choi, W.; Louie, M.; Li, S. P.; Liu, H.; Chan, B. T.; Lam, T. C.; Lin, A. C.; Cheng, S.; Lo, K. K, *Inorg. Chem.*, 2012, 51, 13289-13302.
[106] Louie, M.; Choi, A. W.; Liu, H.; Chan, B. T.; Lo, K. K., *Organometallics*, 2012, 31, 5844-5855.

not the only characteristic necessary to overcome severe side-effects of chemotherapy. Improved selectivity of the treatment in respect of specific cancer cells is desirable and necessary to ensure maximum uptake at the tumour site, thereby lowering the concentration of the treatment in healthy tissue.

Gasser *et al.*[109,110], Viola-Villegas *et al.* [111,112], Stephenson *et al.*,[113] and Schaffer *et al.*[114] reported the synthesis of Re(I) tricarbonyl *N,N'*-bis(quinolinoyl) derivatives that are coordinated to targeting vectors. These complexes allow for targets specific to cancer cells and thus may lead to improved selectivity. On account of their large stokes shifts, polarized emission and long luminescent lifetimes, the initial developmental use of organometallic rhenium complexes was as luminescent probes.[115,116,117,118,119] These probes have proven useful not only in imaging studies of bioconjugates in cells, such as derivatives of the β-breaker peptide[113] and peptide nucleic acids[109,110] but they have also exhibited potential for therapeutic properties. Stephenson *et al.*[113] reported that the Re-β breaker peptides may possibly be used to treat Alzheimer's disease by inhibiting the formation of amyloid plaque.

---

[107] Ho, J.; Lee, W. Y.; Koh, K. J. T.; Lee, P. P. F.; Yan, Y., *J. Inorg. Biochem.*, 2013, 119, 10-20.
[108] Dhar, S.; Lippard, S. J.; in *Bioinorganic Medicinal Chemistry*, ed. E. Alessio, Wiley-VCH Verlag GmnH & Co. K`gaA, Weinheim, 2011, pp. 79-95.
[109] Gasser, G.; Pinto, A.; Neumann, S.; Sosniak, A. M.; Seitz, M.; Merz, K.; Heumann, R.; Metzler-Nolte, N., *Dalton Trans.,* 2012, 41, 2304-2313.
[110] Gasser, G.; Neumann, S.; Ott, I.; Seitz, M.; Heumann, R.; Metzler-Nolte, N., *Eur. J. Inorg. Chem*., 2011, 36, 5471-5478.
[111] Viola-Villegas, N.; Rabideau, A. E.; Bartholoma, M.; Zubieta, J.; Doyle, R. P., *J . Med. Chem.*, 2009, 52, 5253-5261.
[112] Viola-Villegas, N.; Rabideau, A. E.; Cesnavicious, J.; Zubieta, J.; Doyle, R. P., *ChemMedChem.,* 2008, 3, 1387-1394.
[113] Stephenson, K. A.; Reid, L. C.; Zubieta, J.; Babich, J. W.; Kung, M.; Kung, H. F.; Valliant, J. F., *Bioconjugate Chem.*, 2008, 19, 1087-1094.
[114] Schaffer, P.; Gleave, J. A.; Lemon, J. A.; Reid, L. C.; Pacey, L. K. K.; Farncombe, T. H.; Boreham, D. R.; Zubieta, J.; Babich, J. W.; Doering, L. C.; Valliant, J. F., *Nucl. Med. Biol.*, 2008, 35, 159-169.
[115] Amoroso, A. J.; Coogan, M. P.; dunne, J. E.; Fernandez-Moreira, V.; Hess, J. B.; Hayes, A. J.; Lloyd, D.; Millet, C.; Pope, S. J. A.; Williams, C., *Chem. Commun*., 2007, 3066-3068.
[116] Lo, K. K.; Zhang, K. Y.; Li, S. P., *Eur. J. Inorg. Chem.*, 2011, 3551-3568.
[117] Lo, K. K.; Choi, A. W.; Law, W. H., *Dalton Trans.*, 2012, 41, 6021-6047.
[118] Patra, M.; Gasser, G., *ChemBioChem.*, 2012, 13, 1232-1252.
[119] Thorp-Greenwood, F. L.; Balasingham, R. G.; Coogan, M. P., *J. Organomet. Chem.*, 2012, 714, 12-21.

As mentioned in paragraph 2.2 above, photodynamic therapy (PDT) relies on photosensitisers to generate reactive singlet oxygen upon irradiation with an external light source. Gao *et al.*[120], Liu *et al.*[121] and Abdel-Shafi *et al.*[122] reported that since rhenium complexes are efficient triplet photosensitisers, they were therefore used in photocatalysis. As far as the author is able to ascertain, Meggers *et al.*[123] was the first group to use a rhenium(I) complex as a photosensitiser for PDT. They reported that once this metallopyridocarbazole complex (Figure 2.11) was irradiated at wavelengths of $\lambda \geq 505$ nm, it led to DNA damage.

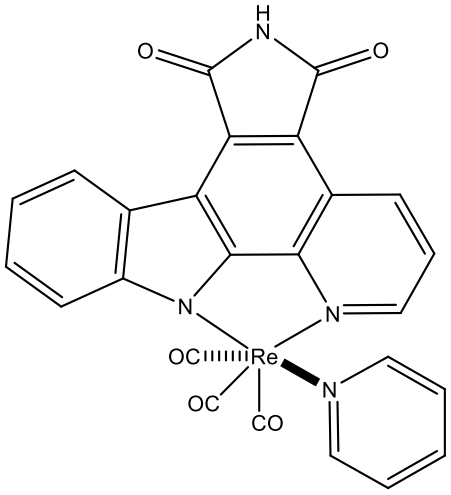

Figure 2.11: Illustration of the metallopyridocarbazole complex.[123]

Later, Meggers and co-workers[124] reported a derivative of the metallopyridocarbazole scaffold improving the chemical stability and red-shifted visible-light-induced anti-cancer activity. Gasser[125] soon followed, reporting that Re(I) tricarbonyl *N,N'*-bis-(quinolinoyl) complexes (Figure 2.12) were efficient in singlet oxygen production in lipophilic environments, thus causing apoptosis.[125] They managed to control the

[120] Gao, Y.; Sun, S.; Han, K., *Spectrochim. Acta, Pt A*, 2009, 71, 2016-2022.
[121] Liu, J.; Jiang, W., *Dalton Trans.*, 2012, 41, 9700-9707.
[122] Abdel-Shafi, A. A.; Bourdelandeb, J. L.; Ali, S. S., *Dalton Trans.*, 2007, 2510-2516.
[123] Kastl, A.; Dieckmann, S.; Wähler, K.; Völker, T.; Kastl, L.; Merkel, A. L.; Vultur, A.; Shannan, B.; Harms, K.; Ocker, M.; Parak, W. J.; Herlyn, M.; Meggers, E., *ChemMedChem.*, 2013, 8, 924-927.
[124] Wähler, K.; Ludewig, A.; Szabo, P.; Harms, K.; Meggers, E., *Eur. J. Inorg. Chem.,* 2014, 807-811.
[125] Leonidova, A.; Pierroz, V.; Rubbiani, R.; Heier, J.; Ferrari, S.; Gasser, G., *Dalton Trans.*, 2014, 43, 4287-4294.

cellular uptake of the rhenium organometallic complexes by attaching targeting molecules.

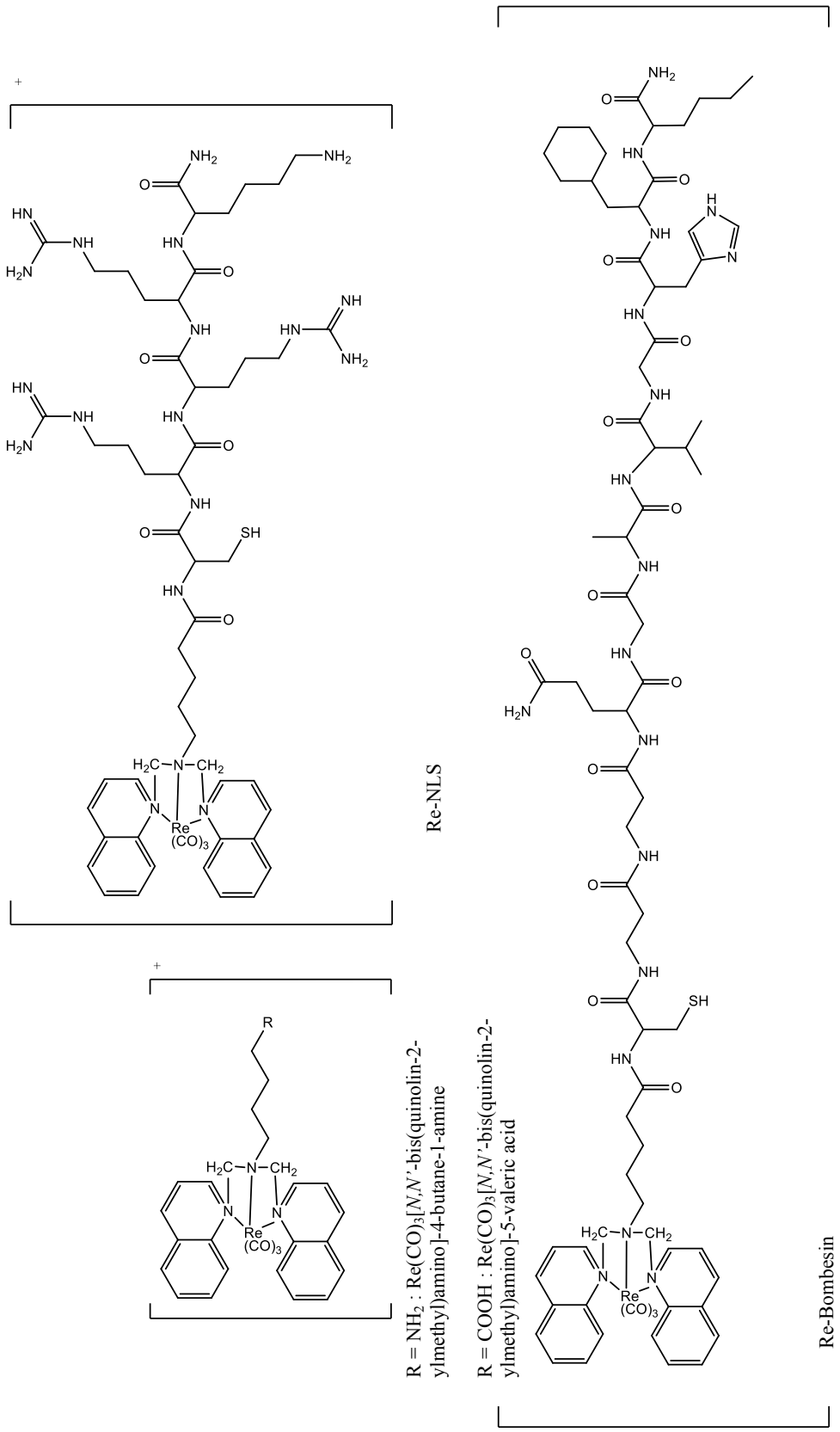

Figure 2.12: Re(I) tricarbonyl *N,N'*-bis-(quinolinoyl) complexes. Re-NLS and Re-Bombesin are bioconjugates of Re-COOH[125]

2.8 Cytotoxicity and Bimetallic Complexes

Ma *et al.*[126] reported the cytotoxic effects of $[Pt(terpy)(C\equiv(Ar)]^+$ compared to $[Pt(terpyCl]^+$ (Figure 2.13). $[Pt(terpy)(C\equiv(Ar)]^+$ was found to display cytotoxicity 100 × superior to cisplatin.[126] This finding supports the idea that the addition of an alkynyl ligand to a metal complex may increase its cytotoxic activity.

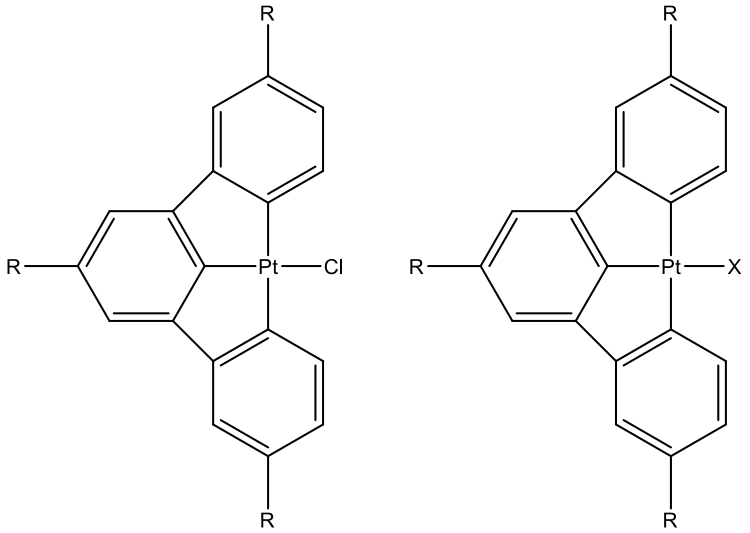

(a) (b)

Figure 2.13: Chemical structure of $[Pt(terpy)(Cl)]^+$ and $[Pt(terpy)(C\equiv(Ar)]^+$. R = Bu^t, X = glucosylated arylacetylide.

Fernández-Moreira *et al.*,[127] however, reported the synthesis and cytotoxic studies of luminescent *fac*-$[Re(bpy)(CO)_3(L)]^+$ and *fac*-$[Re(bpy)(CO)_3(L\text{-}AuPPh_3)]^+$ (L=Alkynyl-pyridine, imidazole, or alkynyl-imidazole). The cytotoxicity studies were performed in human A549 lung cancer cells. They found that the bimetallic Au(I)/Re(I) complex displayed IC_{50} values more than ten times less than the corresponding Re(I) complex. However, a comparison of these three bimetallic complexes containing an alkynyl species to a similar bimetallic complex without an alkynyl species showed that the presence of the alkynyl group significantly increases the toxicity. The results of the fluorescence cell imaging by Fernández-Moreira *et al.*[127] lead one to the conclusion that the rhenium complexes follow typical mitochondrial localization, while the bimetallic Au(I)/Re(I) complexes showed more

[126] Ma, D. L.; Shum, T. Y. T.; Zhang, F.; Che, C. M.; Yang, M., *Chem. Commun.*, 2005, 4675.
[127] Fernández-Moreira, V.; Marzo, I.; Gimeno, M. C., *Chem Sci.*, 2014, 5, 4434-4446.

intense luminescence; thus the higher uptake into the target cell. The exact mechanism of the Au(I)/Re(I) complexes is still unclear but they suggest that a high uptake level may be due to disruptions of the cell membrane resulting in accumulation in the nucleus.

François *et al.*[128] reported the synthesis of a ^{99m}Tc/Re(I) bimetallic compound that proved promising for both a pre- and intra-operative diagnostic probe.[128] Figure 2.14 shows the complex before the ^{99m}Tc-radiolabelling step as well as the ^{99m}Tc/Re(I) complex.

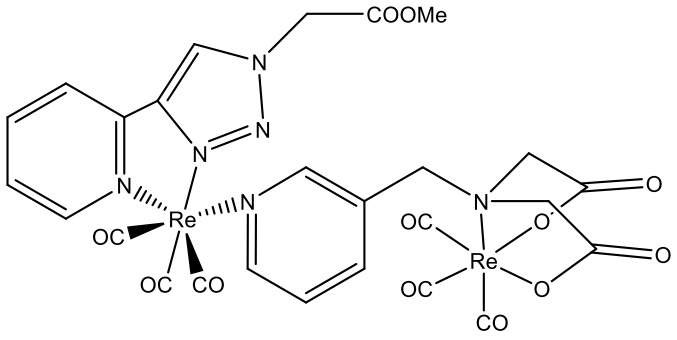

(a)

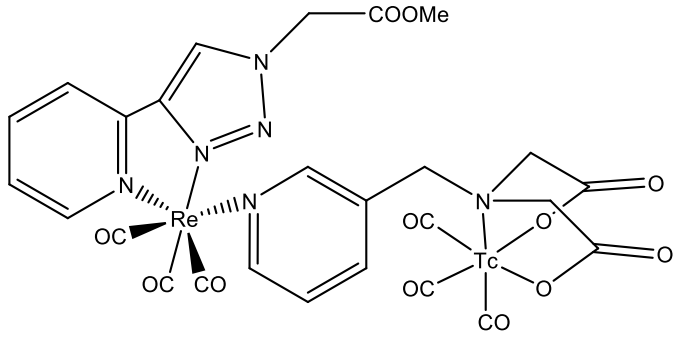

(b)

Figure 2.14: (a) Re(I)/Re(I) bimetallic complex. (b) ^{99m}Tc/Re(I) bimetallic complex.

The cytotoxicity of the Re(I)/Re(I) complex revealed that it displayed very low cytotoxicity toward human breast MCF7, human lung A549, and human colon HT29 cancer cell lines. Since this complex was insufficiently soluble at > 300 μM concentration in PRMI medium with 1% DMSO, however, François *et al.*[128] was

[128] François, A.; Auzanneau, C.; Le Morvan, V.; Galaup, C.; Godfrey, H. S.; Marty, L.; Boulay, A.; Artigau, M.; Mestre-Voegtlé, B.; Leygue, N.; Picard, C.; Coulais, Y.; Robert, J.; Benoist, E., *Dalton Trans.*, 2014, 43, 439-450.

unable to determine the accurate IC_{50} values of this complex. However, François [128] reported that the IC_{50} values for the Re(I)/Re(I) complex were all higher than 300 μM, which is high when compared to other Re(I) complexes. This low cytotoxicity paired with the optimal luminescence properties of the Re(I)/Re(I) complex led them to evaluate this bimetallic complex as an imaging agent and model for the ^{99m}Tc/Re(I) complex. The ^{99m}Tc/Re(I) complex was found to be water soluble and stable in histidine. Moreover, the Re(I)/Re(I) complex was found to exhibit a quantum yield of 0.86% at 496 nm of bright green luminescence.

2.9 Conclusion

It is common cause that cancer cases are expected to increase over time. The increase in patients, along with the expensive and hazardous cancer treatment available, demand cost-effective, less toxic, and more easily administered treatments. Photodynamic therapy attracts researchers due to its ability to overcome toxicity issues related to the available cancer treatments. Both ruthenium and rhenium complexes show promising photophysical and toxicity characteristics, suggesting that these types of complexes are well suited to PDT. The use of bi-metallic complexes in PDT is appealing since the medical usage can be two-fold. One metal complex may possess diagnostic capabilities while the other may have therapeutic capabilities. The combination of these complexes may lead to more cost-effective treatment.

For a complex to be suitable for photodynamic therapy, the following characteristics are required; it must:

1. be non-toxic in the absence of an external light source,
2. possess strong molar absorptivity values at long wavelengths,
3. be hydrophilic,
4. possess a high photophysical quantum yield (QY),
5. show prolonged retention in target tissue, and
6. show expeditious clearance from the body.

The synthesis, characterisation, and luminescence studies of Re(I) complexes and bi-metallic complexes will provide further insight into these complexes as photosensitisers for PDT.

3 SYNTHESIS AND CHARACTERISATION OF LIGANDS AND METAL COMPLEXES

3.1 Introduction

1,10-Phenanthroline (phen) is a heterocyclic organic compound which due to its ability to form strong coordination bonds to metal ions, is often used as a ligand in coordination chemistry. 2,2'-Bipyridine (bpy) displays similarities in coordination properties to 1,10-phenanthroline. Both 2,2'-bipyridine and 1,10-phenanthroline have shown their importance as chelating ligands in coordination chemistry due to their high binding affinity towards transition metal ions.[1] 1,10-Phenanthroline-5,6-dione ($phenO_2$) is a derivative of 1,10-phenanthroline. The structural difference between phen and $phenO_2$ is the addition of two carboxyl groups at positions 1 and 2 in $phenO_2$ (Figure 3.1).

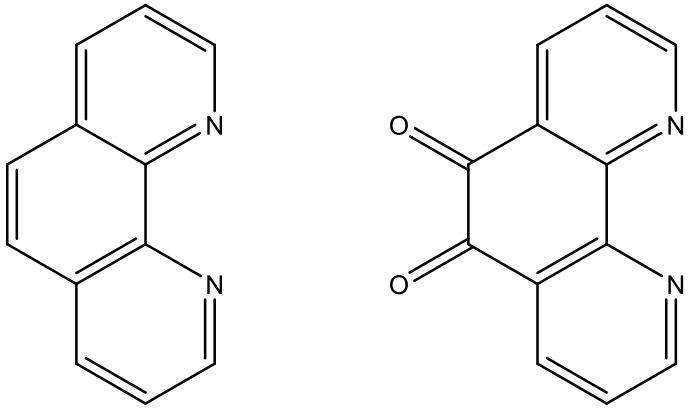

(a) (b)

Figure 3.1: Schematic representation of (a) 1,10-phenanthroline and (b) 1,10-phenanthroline-5,6-dione.

As seen in Figure 3.2 below, $phenO_2$ possesses two coordination functionalities; the Lewis base diiminic functionality and the redox reactive quinoid functionality. This

[1] Keniley, L. K.; Ray, L.; Konvir, K.; Dellinger, L. A.; Hoyt, J. M.; Shatruk, M., *Inorg. Chem*., 2010, 49, 1307-1309.

chelate ligand can therefore interact with a metal centre and compounds *via* the di-imine or quinonoid functionality.[2] Stable compounds are formed, and even multiple metal centres can be incorporated. With the exception of the hydrogen atoms, all of the atoms of phenO_2 are sp^2-hybridised, and due to the o-quinone moiety this ligand is electrochemically active.

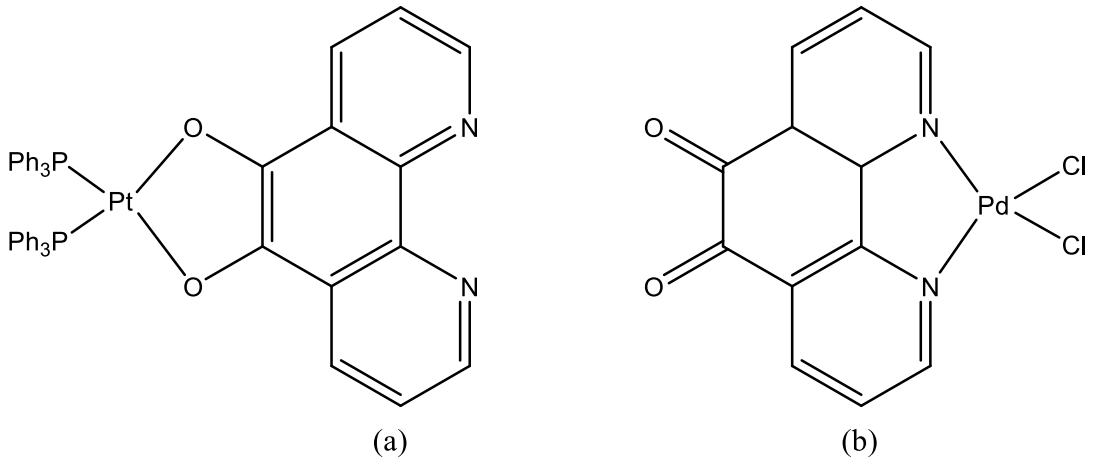

Figure 3.2: Illustration of how 1,10-phenanthroline-5,6-dione can coordinate *via* (a) the quinonoid or (b) the diiminic functionality.[3]

2,2'-Bipyridine (bpy) is a bidentate chelating ligand known for its complex formation with various transition metal ions. The bpy ligand coordinates to ruthenium and platinum, and exhibits intense luminescence in the visible spectrum; this has practical applications in photodynamic therapy (PDT).[4,5] $RuCl_2(bpy)_2$ has proved to be a useful precursor in mixed ligand complexes.

Phosphines are useful as nucleophiles, ligands, and reductants. Phosphines display similarities in basic properties and structure to amines but do, however, exhibit a range of differences. These differences include, but are not limited to, electronegativity, delocalisation of the positive charge, and energy needed for bond

[2] Calderazzo, F.; Marchetti, F.; Pampaloni, G.; Passarelli, V., *J. Chem. Soc. Dalton Trans.*, 1999, 4389-4396.
[3] Girgis, A. Y.; Sohn, Y. S.; Balch, A. L., *Inorg. Chem*., 1975, 14, 2327-2331.
[4] Yang, G. W.; Zhang, X.; Li, G. M.; Yang, J.; Shen, L.; Chen, D. Y.; Li, Q. Y.; Zou, D. F., *New J. Chem.*, 2018, 42, 5395-5402.
[5] Garner, R. N.; Goulucci, J. C.; Dunbar, K. R.; Turro, C., *Inorg. Chem.*, 2011, 50, 9213-9215.

formation. The large size and empty 3d orbitals of a phosphorus atom allow improved delocalisation, while nitrogen atoms have a higher electronegativity.[6] The phosphine ligands used in this study are 1,3,5-triaza-7-phosphaadamantane (PTA) and triphenylphosphine (PPh_3) (Figure 3.3). PTA displays both lipophilic and hydrophilic properties. PTA is an air-stable, neutral ligand and is soluble in aqueous media as well as a range of organic solvents.[7] Mascharak *et al.*[8] are of opinion that the aqueous solubility of this ligand is due to the hydrogen bonding of the tertiary amine N atoms. PTA-based metal complexes have been studied for homogeneous catalysis[9] and as potential anti-cancer agents.[10]

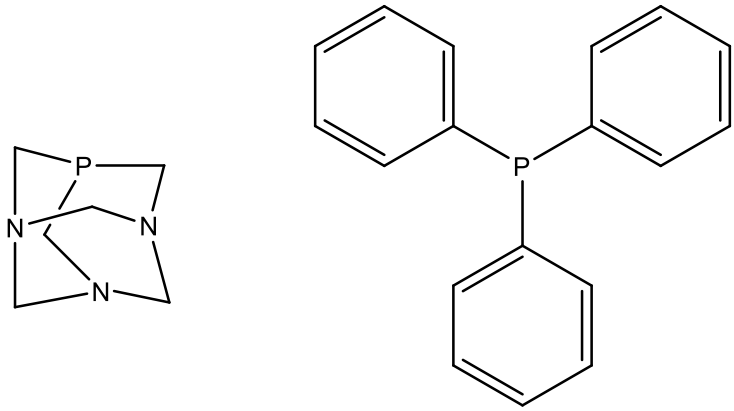

(a) (b)

Figure 3.3: Schematic representation of (a) 1,3,5-triaza-7-phosphaadamantane (PTA) and (b) triphenylphosphine (PPh_3).

Two amino acids are competitors of the bidentate ligand which is coordinated to the ^{99m}Tc metal core, in the body: cysteine is a human amino acid which is of importance to protein synthesis,[11] and histidine is a human amino acid responsible for growth and

[6] Haav, K.; Saame, J.; Kütt, A.; Leito, I., *Eur. J. Org. Chem.* 2012, 2167-2172.
[7] Daigle, D. J.; Pepperman, A. B.; Vail, S. L., *J. Hetrocycl. Chem.* 1974, 11, 407-408.
[8] Chakraborty, I.; Carrington, S. J.; Roseman, G.; Mascharak, P. K., *Inorg. Chem.* 2017, 56, 1534-1545.
[9] Crochet, P.; Cadierno, V., *Dalton. Trans.* 2014, 43, 12447-12462.
[10] Clavel, C. M.; Paunescu, E.; Nowak-Sliwinska, P.; Grifficen, A. W.; Scopelliti, R.; Dyson, P. J., *J. Med. Chem.* 2015, 58, 3356-3365.
[11] https://pubchem.ncbi.nlm.nih.gov/compound/L-cysteine (Date accessed 2019/01/14).

tissue repair.[12] In order to ensure successful labelling, it is imperative that the ^{99m}Tc complex does not decompose by conjugation to these amino acids.[13] Therefore, stability studies are done in cysteine and histidine at 37.0 °C to mimic the environment the ^{99m}Tc complex will be exposed to upon uptake in the body. Lipophilicity is defined by Smith and Cucurull-Sanchez[14] as a physiochemical parameter that links the membrane permeability and solubility and thus the drug distribution, absorption, and rate of clearance from the body.

3.2 Apparatus and Chemicals used

Unless stated otherwise, the reagents used in the preparation and characterisation are commercial grade, purchased from Merck SA or Sigma Aldrich. Rhenium pentacarbonyl bromide was purchased from Strem Chemicals, Newburyport, USA. These reagents were used without further purification. pH adjustments were made using HNO_3 while inert environments were achieved by using N_2 gas.

^{1}H and ^{13}C NMR spectra were collected on Bruker 300 MHz, Bruker 400 MHz, or Bruker 600 MHz NMR spectrometers and ^{31}P NMR spectra were collected on a Bruker 400 MHz spectrometer. The various deuterated solvents that were used are indicated in each case. NMR chemical shifts (δ) were determined relative to internal TMS and recorded in ppm.

The bidentate ligands employed in this study are 2,2'-bipyridine (bpy) and 1,10-phenanthroline-5,6-dione (phenO_2) as N,N-donor ligands in metal coordination reactions. The ligand 1,10-phenanthroline-5,6-dione has been synthesised. The monodentate ligands employed in this study are 1,3,5-triaza-7-phosphaadamantane (PTA) and triphenylphosphine (PPh_3). The metal complexes employed as starting materials are potassium tetrachloroplatinate ($K_2[PtCl_4]$), palladium(II) chloride ($PdCl_2$), and ReAA (*fac*-$[NEt_4]_2$ $[Re(CO)_3(Br)_3]$).

[12] https://pubchem.ncbi.nlm.nih.gov/compound/L-histidine#section=Top (Date accessed 2019/01/24).
[13] Steffens, M. G.; Oosterwijk, E.; Kranenborg, M. H. G. C.; manders, J. M. B.; Debruyne, F. M. J.; Corstens, F. H. M.; Boerman, O. C., *J. Nucl. Med.*, 1999, 40, 829-836.
[14] Smith, D. A.; Cucurull-Sanchez, L., *Comp. Med. Chem.*, 2007, 5, 957-969.

The following ligand and ruthenium complexes were synthesised in this study:

- 1,10-Phenanthroline-5,6-dione
- *cis*-$(bpy)_2RuCl_2 \cdot 2\ H_2O$
- $[Ru(bpy)_2(phenO_2)][PF_6]_2 \cdot 2\ H_2O$

The following rhenium(I) tricarbonyl complexes were synthesised in this study:

- *fac*-$[NEt_4]_2[Re(CO)_3(Br)_3]$ (ReAA)
- *fac*-$[Re(CO)_3(bpy)(CH_3OH)][NO_3]$
- *fac*-$[Re(CO)_3(bpy)(Br)]$
- *fac*-$[Re(CO)_3(bpy)(PPh_3)][Br]$
- *fac*-$[Re(CO)_3(bpy)(PTA)][NO_3]$
- *fac*-$[Re(CO)_3(phenO_2)(Br)]$
- *fac*-$[Re(CO)_3(phenO_2)(PPh_3)][Br]$
- *fac*-$[Re(CO)_3(phenO_2)(PTA)][NO_3]$

The following rhenium(I) dicarbonyl complexes were synthesised in this study:

- *cis-trans*-$[Re(CO)_2(bpy)(PPh_3)_2][NO_3]$
- *cis-trans*-$[Re(CO)_2(bpy)(PTA)_2][NO_3]$
- *cis-trans*-$[Re(CO)_2(phenO_2)(PPh_3)_2][Br]$
- *cis-trans*-$[Re(CO)_2(phenO_2)(PTA)_2][Br]$

The following precursors were synthesised in this study:

- *cis*-$[Pt(DMSO)_2Cl_2]$
- *cis*-$[Pd(DMSO)_2Cl_2]$

The following bimetallic complexes were synthesised in this study:

- $[(Cl_2)Pt(O,O'\text{-}phenO_2\text{-}N,N')\text{-}Re(CO)_3(Br)]$
- $[(Cl_2)Pd(O,O'\text{-}phenO_2\text{-}N,N')\text{-}Re(CO)_3(Br)]$
- $[(Cl_2)Pt(O,O'\text{-}phenO_2\text{-}N,N')\text{-}Ru(bpy)_2][PF_6]_2 \cdot 2\ H_2O]$
- $[(Cl_2)Pd(O,O'\text{-}phenO_2\text{-}N,N')\text{-}Ru(bpy)_2][PF_6]_2 \cdot 2\ H_2O]$

The following ^{99m}technetium dicarbonyl complexes were synthesised in this study:

- *cis-trans*-$[^{99m}Tc(CO)_2(bpy)(PPh_3)_2]^+$

- *cis-trans*-[^{99m}Tc(CO)$_2$(bpy)(PTA)$_2$]$^+$

3.3 Handling of Radioactive Isotopes

Unstable and radioactive forms of rhenium and technetium are required for diagnostic and therapeutic nuclear medicine studies. Research pertaining to these unstable, radioactive metals require various safety precautions during the handling of these reagents. ^{185}Re (37.4%) is a stable naturally occurring isotope of rhenium and may safely be used for 'cold' chemistry in all laboratories because it can be handled without extensive safety precautions. There are no known stable naturally occurring technetium isotopes, therefore radiation safety procedures are imperative when working with technetium. ^{99m}Tc has a half-life of six hours and emits low energy ϒ-rays (0.143 MeV). ^{99m}Tc chemicals employed during this study were handled with prescribed tools and were stored behind a lead tower shield. [^{99m}Tc]$NaTcO_4$ was purchased in saline as a commercial ^{99}Mo/^{99m}Tc generator eluate. The ^{99m}Tc labelling studies were performed in the certified radiation laboratory at the National Centre for Scientific Research "Demokritos" in Athens, Greece. Radioactive waste was disposed of according to prescribed protocols and protective clothing was worn during all experiments.

3.4 Ligand Synthesis

3.4.1. 1,10-Phenanthroline-5,6-dione[2,15]

1,10-Phenanthroline (1.0031 g, 4.772 mol) and KBr (6.8044 g, 0.05718 mol) were added to previously cooled (liquid nitrogen) sulphuric acid (23 mL, 98 %). The mixture was allowed to warm up to room temperature and a thick orange paste was obtained. Concentrated nitric acid (12 mL) was added dropwise to the orange paste resulting in a red solution. The solution was stirred at 90 °C for 3 hours. The solution was then added to water (280 mL) and neutralized using Na_2CO_3. The product was extracted with DCM, the extract was dried on $MgSO_4$ and the solvent was removed *in vacuo*. The yellow solid was recrystallized using toluene.

Yield: 0.5952 g (50.9 %). IR (KBr, cm^{-1}): ν_{co} = 1685, $\nu_{C=C}$ = 1560. EA: Calculated: C: 68.57 %, H: 2.87 %, N: 13.33 %; Found: C: 68.56 %, H: 2.84 %, N: 13.35 %. ^{1}H NMR (600 MHz, acetone-d^6): δ 9.1 (dd, *J* = 5, 2 Hz, 2H), 8.5 (dd, *J* = 8, 2 Hz, 2H), 7.7 (dd, *J* = 8, 5 Hz, 2H), ppm. ^{13}C NMR (600 MHz, acetone d^6): δ 180, 156.1, 137, 126.1, ppm. UV/Vis: λ_{max} = 293 nm, ε = 7656 M^{-1} cm^{-1}.

3.5 Ruthenium Complexes

3.5.1 *Cis*-$(bpy)_2RuCl_2 \cdot 2H_2O$[16]

$RuCl_3 \cdot 3H_2O$ (0.6171 g, 0.003 mol), 2,2'-bipyridine (0.9388 g, 0.006 mol), and LiCl (0.8446 g, 0.2 mol) were dissolved in DMF (5 mL) and refluxed at 90 °C for 8 hours. The mixture was allowed to cool to room temperature and acetone (25 mL) was added. The solution was allowed to stand overnight at 0 °C. Filtering yielded a red/ red-violet solution and a dark green/black crystalline product. The product was washed with 3 portions of water and 3 portions of diethyl ether and dried by suction. Yield: 0.2506 g (17.2 %). IR (ATR, cm^{-1}): $\nu_{C=C}$ = 1678, 1601, 1497. EA: Calculated: C: 49.18 %, H: 4.12 %, N: 11.47 %; Found: C: 49.21 %, H: 4.16 %, N: 11.45 %. UV/Vis: λ_{max} = 292 nm, ε = 11 339 M^{-1} cm^{-1}.

[15] Ocakogly, K.; Zafer, C.; Cetinkaya, B.; Icli, S., *Dyes and Pigments*, 2007, 75, 385-394.
[16] Sullivan, B. P.; Salmon, D. J.; Meyer, T. J., *Inorg. Chem.*, 1978, 17, 3334-3341.

3.5.2 $[Ru(bpy)_2(phenO_2)][PF_6]_2 \cdot 2H_2O$ [17, 18]

cis-$(bpy)_2RuCl_2 \cdot 2H_2O$ (0.9961 g, 1.914 mmol) and 1,10-phenanthroline-5,6-dione (0.4033 g, 1.919 mmol) were dissolved in ethanol (20 cm^3) and refluxed for 3 hours at 70 °C. An ethanolic solution of NH_4PF_6 was added to the solution which resulted in the precipitation of the product. The product was recrystallised by vapour diffusion of diethyl ether and acetonitrile.

Yield: 0.5272 g (27 %). IR (ATR, cm^{-1}): ν_{CO} = 1701, $\nu_{C=C}$ = 1610, 1569. EA: Calculated: C: 40.48 %, H: 2.76 %, N: 8.85 %; Found: C: 40.46 %, H: 2.72 %, N: 8.84 %. ^1H NMR (600 MHz, DMSO-d_6): δ 9.6 (1H); 9.2 (2H); 9.0 (2H); 8.72 (2H); 8.70 (2H); 8.5 (1H); 8.4 (2H); 8.3 (1H); 8.2 (2H); 8.0 (2H); 7.9 (1H); 7.5 (1H); 7.2 (2H); 6.4 (1H) ppm. UV/Vis: λ_{max} = 381 nm, ε = 27 847 M^{-1} cm^{-1}.

3.6 Rhenium Tricarbonyl Complexes

3.6.1 *fac*-$[NEt_4]_2[Re(CO)_3(Br)_3]$ (ReAA)[19]

Tetraethylammonium bromide (NEt_4Br) (5.25 g, 25 mmol) was finely ground and dried. 2,5,8-Trioxane diglyme (150 mL) was added to NEt_4Br under nitrogen conditions and stirred for 30 minutes at 80 °C. The system was evacuated and purged throughout according to Schlenck conditions. $[Re(CO)_5Br]$ (5.0 g, 12.3 mmol) was added and the mixture was stirred for 15 hours at 115 °C. The reaction mixture was allowed to cool to room temperature and was filtered and dried to yield a white solid. The solid was washed with cold ethanol and DCM and was dried.

Yield: 8.139 g, (85.9 %). IR (KBr, cm^{-1}): ν_{co} = 1998, 1864. EA: Calculated: C: 29.62 %, H: 5.23 %, N: 3.64 %; Found: C: 29.59 %, H: 5.19 %, N: 3.65 %. UV/Vis: λ_{max} = 279 nm, ε = 10 906 M^{-1} cm^{-1}.

[17] Keniley, L. K.; Ray, L.; Konvir, K.; Dellinger, L. A.; Hoyt, J. M.; Shatruk, M., *Inorg. Chem*., 2010, 49, 1307-1309.
[18] Fletcher, N. C.; Rebinson, T. C.; Behrendt, A.; Jeffrey, J. C.; Reeves, Z. R.; Ward, M. D., *J. Chem. Soc.*, *Dalton Trans.*, 1999, 2999-3006.
[19] Schutte, M. PhD Thesis, "*Novel Radiopharmaceuticals Characterization, Substitution Kinetics and Biological Evaluation of Tricarbonyl Complexes of Rhenium(I).*", 2011, University of the Free State.

3.6.2 *fac*-$Re(CO)_3(bpy)(CH_3OH)][NO_3]$[20]

ReAA (0.1007 g, 0.141 mmol) was subjected to 3 eq. of $AgNO_3$ (0.0720 g, 0.424 mmol) in water for 24 hours at pH 2, resulting in a grey/white precipitate (AgBr). To the filtrate, 2,2'-bipyridine (0.0312 g, 0.2 mmol) dissolved in methanol, was added. The solution was stirred overnight. The dark yellow precipitate was filtered off and dried *in vacuo*. The dark yellow precipitate was dissolved in methanol (20 mL) and stirred for 8 hours. Upon evaporation a bright yellow crystalline product was obtained.

Yield: 0.05261 g, (77.3 %). IR (KBr, cm^{-1}): ν_{CO} = 2026, 1940, 1900, 1892. EA: Calculated: C: 32.31 %, H: 1.93 %, N: 8.07 %; Found: C: 32.34 %, H: 1.90 %, N: 8.09 %. ^{1}H NMR (300 MHz, acetone-d_6): δ 8.8 (d, J = 4 Hz, 2H), 8.5 (d, J = 8 Hz, 2H), 8.1 (td, J = 8, 2 Hz, 2H), 7.6 (dd, J = 5, 2 Hz, 2H) ppm. ^{13}C NMR (300 MHz, acetone-d_6): δ 198.8, 198. 5, 198.3, 131.2, 117.9, 114.7 ppm. UV/Vis: λ_{max} = 282 nm, ε = 10 607 M^{-1} cm^{-1}.

3.6.3 *fac*-$[Re(CO)_3(bpy)(Br)]$[22]

ReAA (0.1002 g, 0.1300 mmol) was dissolved in water (20 mL) and added to 2,2'-bipyridine (bpy) (0.0229 g, 0.1466 mmol) dissolved in ethanol (3 mL). The solution was stirred for 2 days and the solvent was filtered off. The yellow solid was washed with water, cold ethanol and petroleum ether and allowed to air-dry. Crystals suitable for single crystal X-ray diffraction were obtained.

Yield: 0.0495 g (75.2 %). EA: calculated: C: 30.84 %, H: 1.59 %, N: 5.53 %; found: C: 30.87 %, H: 1.62 %, N: 5.55 %. IR (ATR, cm^{-1}): ν_{CO}= 2010, 1902, 1871. ^{1}H NMR (400 MHz, chloroform-d_1): δ 9.1 (dd, J = 6, 1 Hz, 2H), 8.2 (dd, J = 8, 1 Hz, 2H), 8.1 (ddd, J = 8, 8, 2 Hz, 2H), 7.6 (ddd, J = 7, 6, 2 Hz, 2H) ppm. ^{13}C NMR (400 MHz, chloroform-d_1): δ 153.4, 138.9, 134.2, 127.1, 123.1 ppm. UV/Vis: λ_{max} = 292 nm, ε = 18 395 M^{-1} cm^{-1}.

3.6.4 *fac*-$[Re(CO)_3(bpy)(PPh_3)][Br]$[21]

fac-$[Re(CO)_3(bpy)(Br)]$ (0.2456 g, 0.485 mmol) was dissolved in methanol (20 mL) and PPh_3 (0.0915 g, 0.585 mmol) was added. The solution was stirred at room

[20] Schutte, M; Kemp, G; Visser, H. G.; Roodt, A., *Inorg. Chem.* 2011, 50, 12486-12498.

temperature for 24 hours. The solvent was removed *in vacuo* and the product was purified by recrystallisation using methanol.

Yield: 0.05818 g, (74 %). IR (ATR, cm^{-1}): ν_{CO}= 2011, 1912, 1875. EA: Calculated: C: 48.44 %, H: 3.01 %, N: 3.64 %; Found: C: 48.47 %, H: 3.05 %, N: 3.66 %. ^{1}H NMR (400 MHz, acetone-d_6): δ 9.1 (dq, J = 6, 2, 1 Hz, 2H), 8.8 (d, J = 8, 2H), 8.4 (ddd, J = 7, 6, 1 Hz, 2H), 7.4 (m, 15H) ppm. ^{13}C NMR (600 MHz, acetone-d_6): δ 205.2, 155.8, 153.2, 139.8, 137.4, 133.6, 131.8, 128. 8, 127.5, 124 ppm. UV/Vis: λ_{max} = 291 nm, ε = 8 423 M^{-1} cm^{-1}.

3.6.5 *fac*-[Re(CO)$_3$(bpy)(PTA)][NO$_3$][21]

fac-[Re(CO)$_3$(bpy)(CH$_3$OH)][NO$_3$] (0.2537 g, 0.485 mmol) was dissolved in methanol (20 mL) and PTA (0.0915 g, 0.585 mmol), dissolved in water, was added. The solution was stirred at room temperature for 24 hours. The solvent was removed *in vacuo* and the product was purified by recrystallisation using methanol.

Yield: 0.2209 g (70.2 %). IR (ATR, cm^{-1}): ν_{CO}= 2019, 1877, 1715. EA: Calculated: C: 35.35 %, H: 3.12 %, N: 13.02 %; Found: C: 35.35 %, H: 3.16 %, N: 13.04 %. ^{1}H NMR (400 MHz, water-d_2): δ 9.1 (d, J = 5 Hz, 2H); 8.6 (d, J = 8 Hz, 2H); 8.3 (t, J = 16, 8 Hz, 2H); 7.8 (dd, J = 7, 6, 1 Hz, 2H); 4.4 (m, 6H); 4.0 (d, J = 10 Hz, 6H) ppm. ^{13}C NMR (600 MHz, DMSO-d_6): δ 183.0; 153.4; 140.8; 128.9; 128.4; 124.8; 70.4; 52.8 ppm. UV/Vis: λ_{max} = 319 nm, ε = 9 572 M^{-1} cm^{-1}.

3.6.6 *fac*-[Re(CO)$_3$(phenO$_2$)(Br)][22]

ReAA (0.4999 g, 0.6498 mmol) was dissolved in water (20 mL) and added to 1,10-phenanthroline-5,6-dione (0.1629 g, 0.7750 mmol) dissolved in ethanol (3 mL). The solution was stirred for 2 days and the solvent filtered off. The orange solid was washed with water, cold ethanol and petroleum ether and allowed to air dry. Crystals suitable for X-ray diffraction were obtained but the quality of the data obtained was not suitable for further refinement. Recrystallisation will be attempted.

Yield: 0.2961 g, (81.4 %). IR (ATR, cm^{-1}): ν_{co} = 2024, 1937, 1879. EA: Calculated: C: 32.15 %, H: 1.08 %, N: 4.99 %; Found: C: 32.18 %, H: 1.06 %, N: 5.01 %.

[21] Manicum, A., PhD Thesis, "*A Solid State and Mechanistic Study of Carbonyl Activation in Rhenium(I) Complexes as Radiopharmaceutical Models*.", 2017, University of the Free State.

[22] Kurz, R.; Spingler, B.; Alberto, R., *Eur. J. Inorg. Chem.* 2006, 2966-2974.

^{1}H NMR (400 MHz, acetone-d_6): δ 9.4 (dd, *J* = 5, 1 Hz, 2H), 8.8 (dd, *J* = 8, 2 Hz, 2H), 8.1 (dd, *J* = 8, 5 Hz, 2H) ppm. ^{13}C NMR (400 MHz, acetone-d_6): δ 153.2, 152.8, 141, 134, 127.7 ppm. UV/Vis: λ_{max} = 305 nm, ε = 31 681 M^{-1} cm^{-1}.

3.6.7 *fac*-[$Re(CO)_3(phenO_2)(PPh_3)$][Br][21]

fac-[$Re(CO)_3(phenO_2)(Br)$] (0.1001 g, 0.1786 mmol) was dissolved in methanol (2 mL) and added to PPh_3 (0.0469 g, 0.1785 mmol) dissolved in methanol (3 mL). The solution was stirred overnight and filtered.

Yield: 0.0560 g (38.1 %). IR (ATR, cm^{-1}): ν_{CO}= 2014, 1941, 1881. EA: Calculated: C: 48.18 %, H: 2.57 %, N: 3.41 %; Found: C: 48.20 %, H: 2.56 %, N: 3.39 %. ^{1}H NMR: (400 MHz, methanol-d_4): δ 9.2 (dd, *J* = 5, 1 Hz, 2H); 8.9 (dd, *J* = 8, 1 Hz, 2H); 7.9 (dd, *J* = 8, 5 Hz, 2H); 7.7 (m, 10H); 7.6 (m, 5H) ppm. ^{13}C NMR (600 MHz, methanol-d_4): δ 153.8, 151.7, 137.4, 133.8, 133.6, 133.1, 133, 132.3, 130, 129.9, 126.2 ppm. ^{31}P NMR (400 MHz, methanol-d_4): δ 32.4 (s) ppm. UV/Vis: λ_{max} = 292 nm, ε = 48 153 M^{-1} cm^{-1}.

3.6.8 *fac*-$Re(CO)_3(phenO_2)(PTA)][NO_3]$[21]

fac-[$Re(CO)_3(phenO_2)(Br)$] (0.1006 g, 0.1795 mmol) was dissolved in methanol (2 mL) and added to PTA (0.0281g, 0.1788 mmol)) dissolved in methanol (3 mL). The solution was stirred overnight and filtered.

Yield: 0.08759 g (69.7 %). IR (ATR, cm^{-1}): ν_{CO}= 2026, 1942, 1912. EA: Calculated: C: 32.58 %, H: 2.73 %, N: 12.67 %; Found: C: 32.59 %, H: 2.77 %, N: 12.66 %. ^{1}H NMR (600 MHz, acetone-d_6): δ 9.4 (dd, *J* = 5, 1 Hz, 2H); 8.9 (dd, *J* = 8, 1 Hz, 2H); 8.1 (dd, *J* = 8, 5 Hz, 2 H); 4.4 (d, *J* = 13 Hz, 6 H); 4.3 (d, *J* = 13 Hz, 6H) ppm. ^{13}C NMR (400 MHz, acetone-d_6): δ 174.5, 157.7, 155.2, 138.8, 131.1 129.1, 71.0, 53.9 ppm. ^{31}P NMR (400 MHz, methanol-d_4): δ -13.2 (s) ppm. UV/Vis: λ_{max} = 249 nm, ε = 20 438 M^{-1} cm^{-1}.

3.7 Rhenium Dicarbonyl Complexes

3.7.1 *cis-trans*-[$Re(CO)_2(bpy)(PPh_3)_2$][NO_3][23]

fac-[$Re(CO)_3(bpy)(CH_3OH)$] (0.4077 g, 0.787 mmol) and PPh_3 (0.4970g, 1.892 mmol) were dissolved in o-dichlorobenzene (8 mL). The solution was purged for 20 minutes with nitrogen and refluxed under nitrogen conditions for 5 hours. The orange solution was allowed to cool to room temperature, hexane was added and a precipitate formed. The mixture was filtered and washed with hexane and diethyl ether and air-dried.

Yield: 0.1832 g (23.7 %). IR (KBr, cm^{-1}): ν_{CO}= 2020, 1930, 1889, 1847. EA: Calculated: C: 58.30 %, H: 4.04 %, N: 4.43 %; Found: C: 58.27 %, H: 4.03 %, N: 4.45 %. ^{1}H NMR (300 MHz, methanol-d_4): δ 9.1 (dd, *J* = 27, 6 Hz, 2H), 8.7 (d, *J* = 8.03 Hz, 2H), 8.3 (dd, *J* = 17, 8 Hz, 2H), 7.9 (d, *J* = 4 Hz, 2H), 7.6 (m, 30H) ppm. ^{13}C NMR (600 MHz, methanol-d_4): δ 158.3, 154.2, 141.1, 134, 133.9, 131.4, 129.8, 129.8, 128.7 ppm. ^{31}P NMR (400 MHz, methanol-d_4): δ 21.9 ppm. UV/Vis: λ_{max} = 320 nm, ε = 14 894 M^{-1} cm^{-1}.

3.7.2 *cis-trans*-[$Re(CO)_2(bpy)(PTA)_2$][NO_3][23]

fac-[$Re(CO)_3(bpy)(CH_3OH)$] (0.244 g, 0.389 mmol) and PTA (0.1486 g, 0.946 mmol) were dissolved in o-dichlorobenzene (8 mL). The solution was purged for 20 minutes with nitrogen and refluxed under nitrogen conditions for 5 hours. The orange solution was allowed to cool to room temperature, hexane was added and a precipitate formed. The mixture was filtered and washed with hexane and diethyl ether and air-dried. Yield: 0.0213 g (80.3 %). IR (KBr, cm^{-1}): ν_{CO}= 1935, 1862. EA: Calculated: C: 41.08 %, H: 4.59 %, N: 11.98 %; Found: C: 41.07 %, H: 4.62 %, N: 11.97 %. ^{1}H NMR (300 MHz, methanol-d_4): δ 9.1 (d, *J* = 4 Hz, 2H); 8.7 (d, *J* = 8 Hz, 2H); 8.3 (d, *J* = 8 Hz, 2H); 7.7 (d, *J* = 8 Hz, 2H); 4.5 (m, 20H); 4.0 (d, *J* = 10 Hz, 4 H), ppm. UV/Vis: λmax = 245 nm, ε = 14 506 M^{-1} cm^{-1}.

[23] Smithback, J. L.; Helms, J. B.; Schutte, E.; Woessner, S. M.; Sullivan, B. P., *Inorg. Chem.*, 2006, 45, 2163-2174.

3.7.3 *cis-trans*-[$Re(CO)_2(phenO_2)(PPh_3)_2$][Br][23]

fac-[$Re(CO)_3(phenO_2)(Br)$] (0.0223 g, 0.03980 mmol) and PPh_3 (0.02481g, 0.09459 mmol) were dissolved in o-dichlorobenzene (8 mL). The solution was purged for 20 minutes with nitrogen and refluxed under nitrogen conditions for 5 hours. The dark orange solution was allowed to cool to room temperature, hexane was added and a precipitate formed. The mixture was filtered and washed with hexane and diethyl ether and air-dried.

Yield: 0.0054 g (12.8 %). IR (ATR, cm^{-1}): ν_{CO} = 2021, 1889. EA: Calculated: C: 58.54 %, H:3.53 %, N: 2.73 %; Found: C: 58.57 %, H: 3.55 %, N: 2.72 %. ^1H NMR (600 MHz, Benzene-d_6): δ 8.7 (dd, *J* = 5, 1 Hz, 2H); 8.3 (d, *J* = 8 Hz, 2H); 7.6 (dd, *J* = 12, 8 Hz, 10 H); 7.3 (m, 4 H); 7.0 (m, 6H); 6.9 (ddd, *J* = 15, 8, 3 Hz, 10 H); 6.5 (dd, *J* = 8, 5 Hz, 2H) ppm. ^{13}C NMR (600 MHz, Benzene-d_6): δ 203.4, 156.3, 136.2, 132.1, 132.0, 131.7 ppm. ^{31}P NMR (400 MHz, Benzene-d_6): δ 29.1 ppm. UV/Vis: λ_{max} = 289 nm, ε = 24 064 M^{-1} cm^{-1}.

3.7.4 *cis-trans*-[$Re(CO)_2(phenO_2)(PTA)_2$][Br][23]

fac-[$Re(CO)_3(phenO_2)(Br)$] (0.0223 g, 0.03980 mmol) and PTA (0.0150 g, 0.09545 mmol) were dissolved in o-dichlorobenzene (8 mL). The solution was purged for 20 minutes with nitrogen and refluxed under nitrogen conditions for 5 hours. The orange solution was allowed to cool to room temperature, hexane was added and a precipitate formed. The mixture was filtered and washed with hexane and diethyl ether and air-dried.

Yield: 0.0248 g (73.6 %). IR (ATR, cm^{-1}): ν_{CO} = 2019, 1916, 1876. EA: Calculated: C: 40.37 %, H: 3.90 %, N: 9.05 %; Found: C: 40.39 %, H: 3.88 %, N: 9.04 %. ^1H NMR (600 MHz, DMSO-d_6): δ 9.3 (d, *J* = 4 Hz, 2H); 8.9 (d, *J* = 7 Hz, 1H); 8.7 (d, *J* = 8 Hz, 1H); 8.0 (dd, *J* = 8, 5 Hz, 1H); 7.9 (dd, *J* = 8, 6 Hz, 1H); 4.2 (d, *J* = 12 Hz, 6H); 4.1 (d, *J* = 12 Hz, 6 H); 3.8 (d, *J* = 10 Hz, 6 H). ^{31}P NMR (400 MHz, DMSO-d_6): δ -11.9 ppm. UV/Vis: λmax = 294 nm, ε = 19 904 M^{-1} cm^{-1}.

3.8 Precursor complexes

3.8.1 *cis*-[Pt(DMSO)$_2$(Cl)$_2$][24]

Dimethylsulfoxide (0.06392 mL, 9 mmol) was added to a 10 mL aqueous solution of $K_2[PtCl_4]$ (1.245 g, 3 mmol). The red solution was allowed to stand at room temperature. After 2 hours, white/yellow crystals precipitated. These were washed with water, ethanol, and ether. The complex was then dried *in vacuo*.

Yield: 1.1334 g (89.45 %). IR(ATR, cm^{-1}): ν_{SO}= 1152, 1130. EA: calculated: C: 11.38 %, H: 2.86 %, S: 15.18 %; found: C: 11.40 %, H: 2.85 %, S: 15.28 %. ICP-OES: Calculated: Pt: 46.20 %, Found: Pt: 46.21 %.

3.8.2 *cis*-[Pd(DMSO)$_2$Cl$_2$][24]

$PdCl_2$ (0.2498 g, 1.410 mmol) was dissolved in dimethylsulfoxide (5 mL) and heated to 50 °C. The solution was allowed to cool to room temperature and anhydrous diethyl ether was added to precipitate the product as an orange solid.

Yield: 0.2760 g (58.74%). IR(KBr, cm^{-1}): ν_{SO}= 1661, 1296. EA: Calculated: C: 14.40 %, H: 3.622 %; Found: C: 14.38 %, H: 3.60 %. ICP-OES: Calculated: Pd: 31.90 %, Found: Pd: 31.87 %.

3.9 Rhenium Bimetallic complexes

3.9.1 [(Cl$_2$)Pt(*O,O'*-phenO$_2$-*N,N'*)-Re(CO)$_3$(Br)][25]

$[PtCl_2(DMSO)_2]$ (0.1057 g, 0.25 mmol) was dissolved in warm water (60 °C, 5 mL) and *fac*-$[Re(CO)_3(phenO_2)(Br)]$ (0.1403 g, 0.25 mmol) dissolved in ethanol (5 mL) was added. The solution was stirred for 2 days at 100 °C. The solid that formed was filtered off.

Yield: 0.0232 g (10.66 %). IR (KBr, cm^{-1}): ν_{co} = 2025, 1915, 1879. EA: Calculated: C: 21.80 %, H: 0.73 %, N: 3.39 %; Found: C: 21.81 %, H: 0.76 %, N: 3.41 %. ICP-OES: Calculated: Pt: 23.61 %, Re: 22.53 %; Found: Pt: 23.58 %; Re: 22.54 %. ^{1}H NMR (600 MHz, DMSO-d_6): δ 9.1 (m, 2H); 8.8 (m, 2H); 7.9 (m, 2H) ppm. UV/Vis: λ_{max} = 381 nm, ε = 22 668 M^{-1} cm^{-1}.

---

[24] Price, J. H.; Williamson, A. N.; Schramm, R. F.; Wayland, B. B., *Inorg. Chem.,*1972, 11, 1280-1284.

[25] Do Couto Almeida, J.; Marzano, I. M.; Silva de Paula, F. C.; Pivatto, M.; Lopes, N. P.; de Souza, P. C.; Pavan, F. R.; Formiga, A. L. B.; Pereira-Maia, E. C.; Guerra, W., *J. Mol. Struct.*, 2014, 1075, 370-376.

3.9.2 [(Cl_2)Pd(*O,O'*-phenO_2-*N,N'*)-Re$(CO)_3$(Br)][25]

[$PdCl_2(DMSO)_2$] (0.0387 g, 0.1160 mmol) was dissolved in warm water (60 °C, 5 mL) and *fac*-[$Re(CO)_3$(phenO_2)(Br)] (0.0649 g, 0.1158 mmol) dissolved in methanol (5 mL) was added. The solution was stirred for 2 days at room temperature.

Yield: 0.0245 g (27.1 %). IR (ATR, cm^{-1}): ν_{CO}= 2026.06, 1936.93, 1886.36. EA: Calculated: C: 24.42 %, H: 0.82 %, N: 3.79 %; Found: C: 24.45 %, H: 0.84 %, N: 3.80 %. ICP-OES: Calculated: Pd: 14.43 %, Re: 25.24 %; Found: Pd: 14.44 %; Re 25.21 %. ^{1}H NMR (600 MHz, DMSO-d_6): δ 9.2 (s, 2H); 8.7 (s, 2H); 7.9 (s, 2H). UV/Vis: λ_{max} = 381 nm, ε = 17 718 M^{-1} cm^{-1}.

3.10 Ruthenium Bimetallic complex

3.10.1 [(Cl_2)Pt(*O,O'*-phenO_2-*N,N'*)-Ru$(bpy)_2$][PF_6]$_2$·2 H_2O[25]

[$PtCl_2(DMSO)_2$] (0.0112 g, 0.02651mmol) and [$Ru(bpy)_2$(phenO2][PF_6]$_2$.2H_2O (0.0248 g, 0.02611 mmol) were dissolved in DCM (10 mL). The solution was stirred at 50 °C for 2 days. The brown product was filtered and allowed to air-dry.

Yield: 0.0072 g (21.9 %). IR (ATR, cm^{-1}) : ν_{CO} = 1698, $\nu_{C=C}$ = 1617, 1569. EA: Calculated: C: 31.62 %, H: 2.15 %, N: 6.91 %; Found: C: 31.63 %, H: 2.14 %, N: 6.92 %. ICP-OES: Calculated: Pt: 16.05 %, Ru: 8.31 %; Found: Pt: 16.04 %; Ru 8.29 %. ^{1}H NMR (600 MHz, DMSO-d_6): δ 9 (dd, *J* = 5,2 Hz, 1H); 8.89 (d, *J* = 8 Hz, 1H); 8.86 (1H, m); 8.6 (ddd, *J* = 8, 4, 1 Hz, 2H); 8.5 (dd, *J* = 8,1 Hz, 1H); 8.4 (dd, *J* = 8,4 Hz, 1H); 8.2 (m, 2H); 8 (ddd, *J* = 12, 6, 1 Hz, 2 H); 7.8 (d, *J* = 5 Hz, 1H); 7.76 (m, 3H); 7.7 (dd, *J* = 8, 6 Hz, 1H); 7.67 (dd, *J* = 8, 5 Hz, 1H); 7.62 (ddd, *J* = 13, 6 Hz, 1H); 7.6 (m, 1H); 7.2 (s, 1H); 7.1 (s, 1H); 7.0 (s, 1H) ppm. UV/Vis: λ_{max} = 491 nm, ε = 20 508 M^{-1} cm^{-1}.

3.10.2 [(Cl_2)Pd(*O,O'*-phenO_2-*N,N'*)-Ru$(bpy)_2$][PF_6]$_2$·2 H_2O[25]

[$PdCl_2(DMSO)_2$] (0.0086 g, 0.02578 mmol) and [$Ru(bpy)_2$(phenO_2][PF_6]$_2$.2H_2O (0.0239 g, 0.0.02520 mmol) were dissolved in DCM (10 mL). The solution was stirred at 50 °C for 2 days. The brown/green product was filtered and allowed to air-dry.

Yield: 0.0134 g (45.52 %). IR (ATR, cm^{-1}) : $\nu_{C=C}$ = 1620, 1596, ν_{SO} = 1418, 1315. EA: Calculated: C: 34.11 %, H: 2.32 %, N: 7.46 %; Found: C: 34.09 %, H: 2.33 %, N: 7.45 %. ICP-OES: Calculated: Pd: 9.44 %, Ru: 8.97 %; Found: Pd: 9.46 %; Ru 8.94

%. ^{1}H NMR (600 MHz, DMSO-d_6): δ 9.3 (dd, *J* = 6,2 Hz, 2H); 9.2 (dd, *J* = 6, 2H); 8.8 (dd, *J* = 8,1 Hz, 4H); 8.4 (td, *J* = 14, 8 Hz, 4H); 8.1 (dd, *J* = 8,6 Hz, 4H); 8.0 (m, 2H); 7.8 (ddd, *J* = 13, 7 Hz, 4 H) ppm. UV/Vis: λ_{max} = 381 nm, ε = 21 295 M^{-1} cm^{-1}.

3.11 *In situ* Synthesis of ^{99m}Tc compounds

The two attempts at labelling were successful. The characterisation methods used for the ^{99m}Tc compounds were HPLC with gamma detection. *cis-trans*-[^{99m}Tc(CO)$_2$(bpy)(PPh$_3$)$_2$]$^+$ was successfully prepared although small amounts of *fac*-[^{99m}Tc(CO)$_3$(bpy)(PPh$_3$)]$^+$ were also detected. *cis-trans*-[^{99m}Tc(CO)$_2$(bpy)(PTA)$_2$]$^+$ was prepared, although from the HPLC chromatogram it was determined that *fac*-[^{99m}Tc(CO)$_3$(bpy)(PTA)]$^+$ was also formed and was indeed the major product.

3.11.1 *cis-trans*-[^{99m}Tc(CO)$_2$(bpy)(PPh$_3$)$_2$]$^+$[26]

Sodium tartrate (20 mg), sodium borohydrate (5 mg), disodium carbonate (4 mg), and ^{99m}Tc pertechnetate (from the ^{99}Mo/^{99m}Tc generator) were sealed in a vial and flushed with CO for 5 minutes. The solution was heated at 85 °C for 30 minutes. The precursor was confirmed by HPLC analysis with a 99.92 % reduction of [^{99m}TcO$_4$]$^-$ to *fac*-[^{99m}Tc(CO)$_3$(H$_2$O)$_3$]$^+$. In a second vial bpy (1 mg) was dissolved in methanol (500 μL). *fac*-[^{99m}Tc(CO)$_3$(H$_2$O)$_3$]$^+$ (500 μL) was added and the solution was flushed with N_2 for 1 minute and heated for 30 minutes at 70 °C. HPLC analysis confirmed the complexation with bpy (R_t = 12.411 min). PPh_3 (5 mg) dissolved in methanol (500 μL) was added. The solution was flushed with N_2 for 1 minute and heated for 30 minutes at 95 °C. After 30 minutes *fac*-[^{99m}Tc(CO)$_3$(bpy)(PPh$_3$)]$^+$ (R_t = 15.853 min) had formed in 71.22 % yield and *cis-trans*-[^{99m}Tc(CO)$_2$(bpy)(PPh$_3$)$_2$]$^+$ (R_t = 16.928 min) had formed in 26.41 % yield. After an additional heating of 30 minutes at 95 °C the percentage yield of *fac*-[^{99m}Tc(CO)$_3$(bpy)(PPh$_3$)]$^+$ was 6.64 % and *cis-trans*-[^{99m}Tc(CO)$_2$(bpy)(PPh$_3$)$_2$]$^+$ 61.6 % yield. *cis-trans*-[^{99m}Tc(CO)$_2$(bpy)(PPh$_3$)$_2$]$^+$ was isolated by collection at the correct retention time. Co-injection with *cis-trans*-[Re(CO)$_2$(bpy)(PPh$_3$)$_2$]$^+$, the rhenium analogue, confirmed that it was indeed the bisphosphine complex (R_t = 16.816 min). HPLC analysis was performed with a 85:15 (methanol:water) gradient.

[26] Alberto, R.; Schibli, R.; Egli, A.; Schubiger, A. P., *J. Am. Chem. Soc.,* 1998, 120, 7987-7988.

3.11.2 *cis-trans*-[^{99m}Tc(CO)$_2$(bpy)(PTA)$_2$]$^{+}$[26]

Sodium tartrate (20 mg), sodium borohydrate (5 mg), disodium carbonate (4 mg), and ^{99m}Tc pertechnetate (from the ^{99}Mo/^{99m}Tc generator) were sealed in a vial and flushed with CO for 5 minutes. The solution was heated at 85 °C for 30 minutes. The precursor was confirmed by HPLC analysis with a 99.92 % reduction of [^{99m}TcO$_4$]$^{-}$ to *fac*-[^{99m}Tc(CO)$_3$(H$_2$O)$_3$]$^{+}$. In a second vial bpy (1 mg) was dissolved in methanol (500 μL). *fac*-[^{99m}Tc(CO)$_3$(H$_2$O)$_3$]$^{+}$ (500 μL) was added and the solution was flushed with N_2 for 1 minute and heated for 30 minutes at 70 °C. HPLC analysis confirmed the complexation with bpy (R_t = 12.411 min). PTA (5 mg) dissolved in methanol (500 μL) was added. The solution was flushed with N_2 for 1 minute and heated for 30 minutes at 95 °C. The percentage yield of *fac*-[^{99m}Tc(CO)$_3$(bpy)(PTA)]$^{+}$ (R_t = 14.768 min) was 82.65 % and *cis-trans*-[^{99m}Tc(CO)$_2$(bpy)(PTA)$_2$]$^{+}$ (R_t = 11.385 min) was 15.1 % after 30 minutes. After additional heating for 30 minutes at 95 °C the percentage yield of *fac*-[^{99m}Tc(CO)$_3$(bpy)(PTA)]$^{+}$ was 51.72 % and *cis-trans*-[^{99m}Tc(CO)$_2$(bpy)(PTA)$_2$]$^{+}$ was 42.89 %. *cis-trans*-[^{99m}Tc(CO)$_2$(bpy)(PTA)$_2$]$^{+}$ was isolated by collection at the correct retention time. Co-injection with *cis-trans*-[Re(CO)$_2$(bpy)(PTA)$_2$]$^{+}$, the rhenium analogue, confirmed that this was indeed the bisphosphine complex at R_t = 11.100 min. HPLC analysis was performed with a 70:30 (methanol:water) gradient.

3.12 Stability and Lipophilicity studies

3.12.1 *cis-trans*-[^{99m}Tc(CO)$_2$(bpy)(PPh$_3$)$_2$]$^{+}$ [26]

The isolated *cis-trans*-[^{99m}Tc(CO)$_2$(bpy)(PPh$_3$)$_2$]$^{+}$ was added to cysteine and histidine respectively and these were incubated at 37.0 °C. HPLC analyses were performed on these samples at 1 hour, and 6 hours of incubation. *cis-trans*-[^{99m}Tc(CO)$_2$(bpy)(PPh$_3$)$_2$]$^{+}$ was found to be stable in both cysteine and histidine after 1 hour and 6 hours as seen in Figure 3.4.

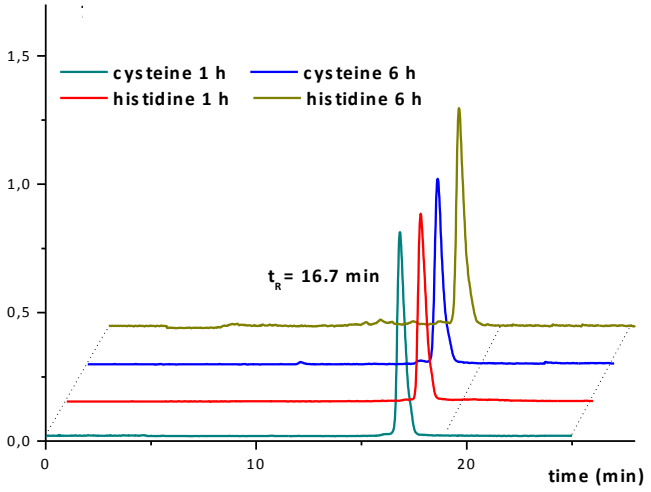

Figure 3.4: Chromatogram illustrating the stability of *cis-trans*-[^{99m}Tc(CO)$_2$(bpy)(PPh$_3$)$_2$]$^+$ in both cysteine and histidine at 37 °C after 1 hour and 6 hours (R_t = 16.928 min).

The partition coefficient of *cis-trans*-[^{99m}Tc(CO)$_2$(bpy)(PPh$_3$)$_2$]$^+$ was determined by adding the ^{99m}Tc complex (0.1 mL) to a phosphate buffer (0.2 mL, 0.125 M, pH 7.4) and 1-octanol (0.2 mL) in a centrifuge tube. The mixture was agitated on a Vortex mixer and centrifuged at 5000 rpm for 5 minutes. Both the 1-octanol and phosphate buffer layers were counted on a γ-counter. This experiment was repeated 3 times. The partition coefficient was reported as log P = 2.85 and calculated as the mean of each cpm/mL of octanol layer, divided by that of the buffer.

The stable nature of *cis-trans*-[^{99m}Tc(CO)$_2$(bpy)(PPh$_3$)$_2$]$^+$ in cysteine and histidine suggests that this complex may be considered as a potential labelling substrate since it does not dissociate in conditions similar to those found in the human body. The partition coefficient of *cis-trans*-[^{99m}Tc(CO)$_2$(bpy)(PPh$_3$)$_2$]$^+$ of 2.85 suggests high lipophilicity which satisfies a fundamental prerequisite for blood-brain barrier penetration[27,28] and thus be a possible candidate for further tests as a ^{99m}Tc brain imaging agent.

[27] Holman, B. L.; Devous, M. D., *J. Nucl. Med.*, 1992, 33, 1888-1904.
[28] Moretti, J. L.; Caglar, M.; Weinmann, P., *J. Nucl. Med.*, 1995, 36, 359-363.

3.12.2 *cis-trans*-[^{99m}Tc(CO)$_2$(bpy)(PTA)$_2$]$^+$ [26]

The isolated *cis-trans*-[^{99m}Tc(CO)$_2$(bpy)(PTA)$_2$]$^+$ was added to cysteine and histidine respectively and these were incubated at 37.0 °C. HPLC analyses were performed on these samples at 1 hour, and 6 hours of incubation. *cis-trans*-[^{99m}Tc(CO)$_2$(bpy)(PTA)$_2$]$^+$ was found to be stable in both cysteine and histidine after 1 hour and 6 hours as seen in Figure 3.5.

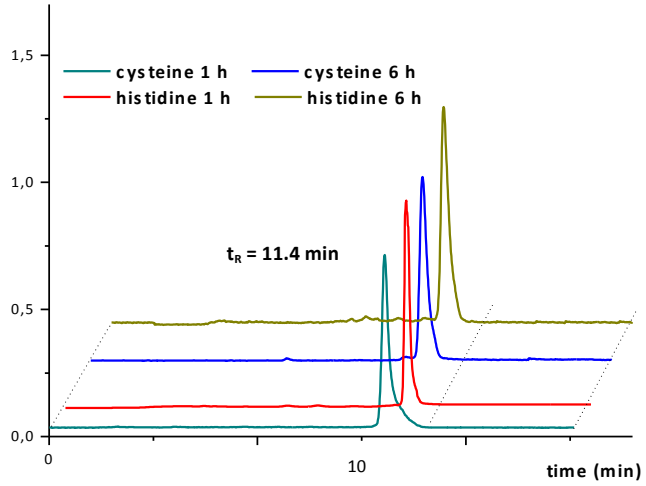

Figure 3.5: Chromatogram illustrating the stability of *cis-trans*-[^{99m}Tc(CO)$_2$(bpy)(PTA)$_2$]$^+$ in both cysteine and histidine at 37 °C after 1 hour and 6 hours (R_t = 11.385 minutes).

The partition coefficient of *cis-trans*-[^{99m}Tc(CO)$_2$(bpy)(PPh$_3$)$_2$]$^+$ was determined by adding the ^{99m}Tc complex (0.1 mL) to a phosphate buffer (0.2 mL, 0.125 M, pH 7.4) and 1-octanol (0.2 mL) in a centrifuge tube. The mixture was agitated on a Vortex mixer and centrifuged at 5000 rpm for 5 minutes. Both the 1-octanol and phosphate buffer layers were counted on a γ-counter. This experiment was repeated 3 times. The partition coefficient was reported as log P = -2.57 and was calculated as the mean of each cpm/mL of octanol layer divided by that of the buffer.

The stable nature of *cis-trans*-[^{99m}Tc(CO)$_2$(bpy)(PTA)$_2$]$^+$ in cysteine and histidine suggests that this complex may be considered as a potential labelling substrate since it does not dissociate in conditions similar to those found in the human body. The negative value of the partition coefficient of *cis-trans*-[^{99m}Tc(CO)$_2$(bpy)(PTA)$_2$]$^+$ of -2.57 suggests that this complex is hydrophilic with a high lipophilicity which satisfies a fundamental prerequisite for blood-brain barrier penetration.[27,28] and thus be a possible candidate for further tests as a ^{99m}Tc brain-imaging agent. The

hydrophilic nature of *cis-trans*-[^{99m}Tc(CO)$_2$(bpy)(PTA)$_2$]$^+$ causes this complex to be more favorable than *cis-trans*-[^{99m}Tc(CO)$_2$(bpy)(PPh$_3$)$_2$]$^+$ as a potential imaging agent.

3.13 Discussion

In this chapter, the synthesis of 1,10-phenanthroline-5,6-dione, two ruthenium complexes, nine *fac*-[Re(CO)$_3$]$^+$ type complexes, four *cis-trans*-[Re(CO)$_2$]$^+$ type complexes, [Pt(DMSO)$_2$(Cl)$_2$], [Pd(DMSO)$_2$(Cl)$_2$], four bimetallic complexes, and two cis-*trans*-[^{99m}Tc(CO)$_2$]$^+$ type complexes are reported. One aim of this study was to synthesise water soluble complexes suitable for use in photodynamic cancer therapy and the comparison of two bidentate ligands, bipyridine and 1,10-phenanthroline-5,6-dione, in a Re(I) complex for the above purpose.

The ^{1}H NMR of *fac*-[Re(CO)$_3$(PhenO$_2$)(Br)], showed double peaks for the aromatic protons when prepared in deuterated methanol. When the experiment was repeated on the same instrument using the same acquisition parameters, in deuterated acetone, the double peaks disappeared and just one set of peaks integrating for the correct amount of protons was observed. Methanol is a coordinating solvent which can substitute the bromido ligand: this would explain the observed double peaks. However, acetone is also a coordinating solvent, but this doubling of peaks is not seen in the experiment employing deuterated acetone.

Due to the long relaxation times of tricarbonyl carbons, these tricarbonyl carbon peaks, for most rhenium(I) complexes are not visible. This has serious economic implications for this type of characterisation, thus more economical methods, especially infrared spectroscopy, could determine the presence of the tricarbonyl carbon atoms. [Ru(bpy)$_2$(PhenO$_2$)][PF$_6$]$_2$·2H$_2$O, *cis-trans*-[Re(CO)$_2$(bpy)(PTA)$_2$][NO$_3$], *cis-trans*-[Re(CO)$_2$(PhenO2)(PTA)$_2$][Br] as well as all the bimetallic complexes showed no ^{13}C NMR peaks after 18 000 scans. Because of the economic implications of such a large number of scans per complex, other characterisation methods were used and no further ^{13}C NMR experiments were conducted on these complexes.

Table 3.1: CO stretching frequencies of Re(I) di- and tricarbonyl complexes in this study

Complex	ν_{CO} (cm^{-1})
fac-$[NEt_4]_2[Re(CO)_3(Br)_3]$	1864, 1998
fac-$Re(CO)_3(bpy)(CH_3OH)][NO_3]$	2026, 1940, 1892
fac-$[Re(CO)_3(bpy)(Br)]$	2010, 1902, 1871
fac-$[Re(CO)_3(bpy)(PPh_3)][Br]$	2011, 1912, 1875
fac-$[Re(CO)_3(bpy)(PTA)][NO_3]$	2019, 1877, 1715
fac-$[Re(CO)_3(phenO_2)(Br)]$	2024, 1937, 1879
fac-$[Re(CO)_3(phenO_2)(PPh_3)][Br]$	2014, 1941, 1881
fac-$Re(CO)_3(phenO_2)(PTA)][NO_3]$	2026, 1942, 1912
cis-trans-$[Re(CO)_2(bpy)(PPh_3)_2][NO_3]$	1930, 1889, 1847
cis-trans-$[Re(CO)_2(bpy)(PTA)_2][NO_3]$	1935, 1862
cis-trans-$[Re(CO)_2(phenO_2)(PPh_3)_2][Br]$	1909, 1889
cis-trans-$[Re(CO)_2(phenO_2)(PTA)_2][Br]$	1916, 1876

The IR stretching frequencies of the rhenium(I) tricarbonyl complexes (Table 3.1) display CO stretching frequencies that range from 2026 to 1715 cm^{-1}. Electron-donating ligands increase the electron density on the metal core and so increase the back-bonding from the CO ligands that results in lower IR frequencies. In bpy containing complexes lower CO frequencies are expected compared to the $phenO_2$ containing complexes. A weak donating phosphine ligand may reduce this electron density of the rhenium centre which can result in weaker π-back donation and ultimately increased CO stretching frequency values. This may account for the PTA containing complexes of both bpy and $phenO_2$ having the largest CO-stretching frequencies compared to their stronger donating PPh_3 and Br counterparts and the $phenO_2$ containing complexes having larger CO-stretching frequencies than the bpy containing complexes.

The rhenium(I) dicarbonyl complexes display two strong bands that range from 1935 to 1862 cm^{-1} for the bpy Re(I) dicarbonyl bisphosphine complexes and 1916 to 1862 cm^{-1} for the $phenO_2$ Re(I) dicarbonyl bisphosphine complexes. The IR stretching frequencies of the dicarbonyl complexes are much lower than their tricarbonyl counterparts which range from 1715-2019 cm^{-1} for bpy tricarbonyl complexes and 1881-2026 cm^{-1} for the $phenO_2$ tricarbonyl complexes. This may be due to an increase in electron density on the rhenium centre because of the phosphine ligand resulting in a weaker carbon to oxygen bond.

Lower valent metals are associated with stronger π-back-bonding and thus more readily delocalise electron density to the ligand. Low valent metals are therefore associated with stable carbonyl bonds. Because of this intense delocalisation of electrons from the metal core to the ligand, electronic transitions that involve these electrons require substantial changes in bonding. This intense delocalisation explains the relatively harsh conditions required during the removal of a carbonyl ligand during the synthesis of the Re(I) dicarbonyl moieties.

The successful synthesis of *cis-trans*-$[Re(CO)_2(bpy)(PPh_3)_2]^+$ and *cis*-$[Re(CO)_2(bpy)(PTA)_2]^+$ and their ^{99m}Tc analogues, *cis-trans*-$[^{99m}Tc(CO)_2(bpy)(PPh_3)_2]^+$ and *cis-trans*-$[^{99m}Tc(CO)_2(bpy)(PTA)_2]^+$, support the presumption that rhenium and technetium follow similar chemistry. Both ^{99m}Tc complexes display stability at 1 and 6 hours in both cysteine and histidine. Pirmettis *et al*.[29] reported a range of potential ^{99m}Tc brain-imaging agents with partition coefficients ranging from 2.38 to 2.99, thus, supporting the presumption that *cis-trans*-$[^{99m}Tc(CO)_2(bpy)(PPh_3)_2]^+$ and *cis-trans*-$[^{99m}Tc(CO)_2(bpy)(PTA)_2]^+$ may be potential ^{99m}Tc brain-imaging agents. *cis-trans*-$[^{99m}Tc(CO)_2(bpy)(PTA)_2]^+$ is also hydrophilic engendering the potential of clinical application.

[29] Pirmettis, I, C.; Papadopoulos, M. S.; Chiotellis, E, *J. Med. Chem.*, 1997, 40, 2539-2546.

4 CRYSTALLOGRAPHIC STUDY of *fac*-[Re(CO)$_3$(bpy)(Br)]

4.1 Introduction

This chapter reports the crystal structure of the rhenium (I) tricarbonyl complex, *fac*-[Re(CO)$_3$(bpy)(Br)] (**1**) (bpy = 2,2'-bipyridine).

Scheme 4.1 illustrates the synthetic procedure of **1** as reported in Chapter 3 while the crystallographic data of **1** is summarised in Table 4.1.

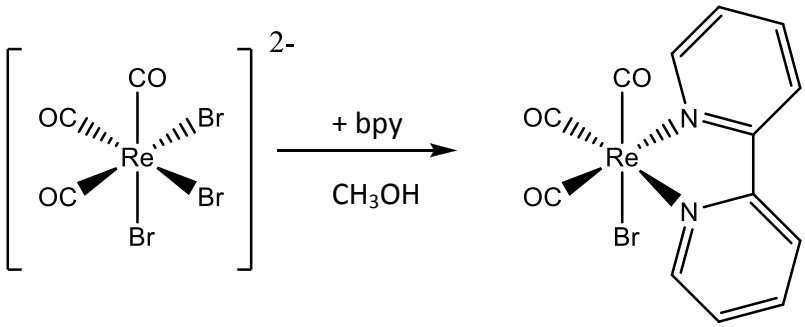

Scheme 4.1: Synthetic procedure of *fac*-[Re(CO)$_3$(bpy)(Br)].

4.2 Experimental

A Bruker X8 Apex Π 4K diffractometer was used for the collection of the structural data. This apparatus is equipped with graphite monochromated Mo kα radiation and has a wavelength of 0.71073 Å, and φ- and ω-scans at 100 K. The cell refinements were carried out using SAINT-Plus.[1] Data reduction was accomplished using SAINT-Plus and XPREP.[1] The multi-scan technique, as well as the SADABS[2] software package were used for the absorption corrections. SIR-97[3] was used to solve the

[1] Bruker, SAINT-Plus, Version 7.12 (including XPREP), Bruker AXS Inc., Madison, Wisconsin, USA, 2004.
[2] Bruker, SADABS, Version 2004/1, Bruker AXS Inc., Madison, Wisconsin, USA, 1998.
[3] Altomare, A.; Burla, M. C.; Camalli, M.; Cascarano, G. L.; Giacovazzo, C.; Guagliardi, A.; Moliterni, A. G. G.; Polidori, G.; Spagna, R., *J. Appl. Cryst.*, 1999, 32, 837-838.

structure, and the structure refinement was conducted, using SHELXL-97[4] and WINGX.[5] The molecular graphics were completed, using DIAMOND. All non-hydrogen atoms were anisotropically refined and all structures are shown with thermal ellipsoids drawn at 50 % probability level. Methyl as well as aromatic hydrogen atoms were positioned in ideal geometrical positions, C-H = 0.95 Å, and constrained to ride on their parent atoms $U_{iso}(H) = 1.2\ U_{eq}(C)$. Appendix A of the supplementary data contains the atomic coordinates, anisotropic displacement parameters, bond angles, and distances, torsion angles and hydrogen coordinates.

[4] Sheldrick G. M., SHALXL97, Program for the Refinement of Crystal Structures, University of Göttingen, Germany, 1997.
[5] Farrugia, L. J. *J. Appl. Cryst.*, 1999, 32, 837-838.

Table 4.1: Crystallographic data of *fac*-[Re(CO)$_3$(bpy)(Br)] (1).

Crystallographic data	**(1)**
Empirical formula	$C_{13}H_8BrN_2O_3Re$
Formula Weight (g.mol^{-1})	506.32
Crystal System	Monoclinic
Space Group	$P2_1/n$
a	6.920(5)
b	15.218(1)
c	13.478(1)
α (Å)	90
β (Å)	96.911(3)
ϒ (Å)	90
Volume (A^3)	1409.0(12)
Z	4
ρ_{calc} (g.cm^{-1})	2.387
Crystal Colour	Yellow
Crystal Morphology	Stout
Crystal Size (mm^3)	0.221×0.201×0.144
μ (mm^{-1})	11.466
F (000)	936
θ(°)	2.027 to 27.998
Index ranges	-9<=h<=9, -20<=k<=20, -12<=l<=17
Reflections Collected	25973
Unique Reflections	3371
Reflections with I>2σ(I)	2872
R_{int}	0.0424
Completeness to 2 theta (°, %)	99.6%
Data / restraints / parameters	3371/0/181
GooF	1.082
R[I >2σ(I)]	R_1=0.0264, wR_2=0.0600
R (all data)	R_1=0.0361 wR_2=0.0664
ρ_{max}, ρ_{min} (eA^{-3})	1.359, -1.108

bpy = 2,2'-bipyridine

4.3 Crystal Structure of *fac*-[Re(CO)$_3$(bpy)(Br)] (1)

fac-[Re(CO)$_3$(bpy)(Br)] (**1**) was synthesised according to the method described by Alberto *et al.*[6] Kia and Safari[7] reported a pale yellow crystal of this same complex grown in a 1:1 dichloromethane:hexane solution, and it was found that this complex crystallised in the monoclinic $P2_1/n$ space group. In this study, the yellow cuboidal crystals were grown in a 1:1 acetone:methanol solution to crystallise *fac*-[Re(CO)$_3$(bpy)(Br)] (**1**) in the monoclinic $P2_1/n$ space group. Kia and Safari[7] reported a substitutional disorder of the axial bromido ligand and the carbonyl ligand trans to it, with a refined site occupancy ratio of 0.759(3)/0.241(3) Å. This disorder of the axial bromido and carbonyl ligand was not observed in this study. The structure of *fac*-[Re(CO)$_3$(bpy)(Br)] indicated in Figure 4.1 consists of a rhenium atom octahedrally surrounded by a bidentate 2,2'-bipyridine ligand, a bromido ligand and three facially orientated carbonyl ligands. The equatorial plane in this chapter refers to the plane through O2-C2-Re1-C1-O1.

Figure 4.1: Molecular representation of the crystal structure of *fac*-[Re(CO)$_3$(bpy)(Br)] (1). Hydrogen atoms were omitted for clarity. Ellipsoids drawn at 50 % probability.

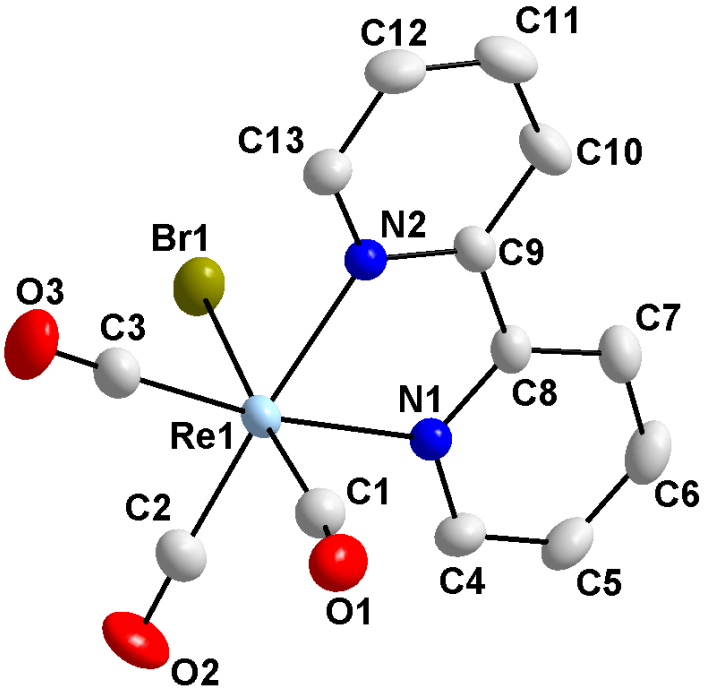

[6] Kurz, R.; Spingler, B.; Alberto, R.,*Eur. J. Inorg. Chem.* 2006. 2966-2974.
[7] Kia, R.; Safari, F., *Inorg. Chim. Acta*, 2016, 453, 357-368.

The general crystal data of **1** is summarised in Table 4.1 and the numbering of atoms is shown in Figure 4.1 (the hydrogen atoms are omitted for clarity). Table 4.2 gives a summary of some important bond angles and bond distances of **1**.

Table 4.2: Selected bond distances and angles of *fac*-[Re(CO)$_3$(bpy)(Br)] (1).

Selected bond distance (Å)		Selected bond angle (°)	
Re1-C3	1.912(6)	**N2-Re1-N1**	74.95(16)
Re1-C2	1.919(6)	**C3-Re1-C2**	89.2(2)
Re1-C1	2.008(7)	**C1-Re-N2**	93.77(17)
Re1-N2	2.170(4)	**C1-Re1-N1**	91.02(19)
Re1-N1	2.171(4)	**C3-Re1-Br1**	90.56(17)
Re1-Br1	2.6126(15)	**C2-Re1-Br1**	92.38(16)
		C1-Re1-Br1	176.16(15)
		N2-Re1-Br1	83.50(11)
		N1-Re1-Br1	85.66(11)

The rhenium to carbonyl carbon bond distances (C1, C2, C3) are in agreement with those seen in similar complexes.[8,9,10,11] The metal to bromido bond distance of 2.6126(15) Å agrees with those found in similar bromido complexes that range from 2.467(16) Å to 2.6334(9) Å.[12,13,14] Rhenium to nitrogen bond distances (Re1-N1, Re1-N2) of 2.171(4) Å and 2.170(4) Å, correspond with other rhenium complexes that possess the same *N,N'*-bidentate ligand and range from 2.143(6) Å to 2.203(12) Å.[8,9,10,11] *fac*-[Re(CO)$_3$(bpy)(Br)] has a small bite angle of 74.95(16)° which leads to a distortion of the octahedral coordination sphere. This is confirmed by the angle of 85.66(11)° for N1-Re1-Br1, 83.50(11)° for N2-Re1-Br1, and 176.16(15)° for C1-Re1-Br1.

[8] Hevia, E.; Pérez, J.; Riera, L.; Riera, V., *Organometallics,* 2002, 21, 1750-1752.
[9] Hevia, E.; Pérez, J.; Riera, V., *Inorg. Chem.*, 2002, 41, 4673-4679.
[10] Hightower, S. E.; Corcoran, R. C.; Sullivan, B. P., *Inorg. Chem.*, 2005, 44, 9601-9603.
[11] Domínguez, S. E.; Alborés, P.; Fagalde, F., *Polyhedron*, 2014, 67, 471-480.
[12] Schutte, M.; Visser, H. G.; Roodt, R., *Acta Cryst.*, 2009, E66, m859-m860.
[13] Schutte, M.; Visser, H. G.; Brink, A., *Acta Cryst.*, 2009, E65, m1575-m1576
[14] Schutte, M.; Visser, H. G.; Steyl, G., *Acta Cryst.*, 2007, E63, m3195-m3196

Kia and Safari[7] published the crystal structure of *fac*-[Re(CO)$_3$(bpy)(Br)] in 2016. The bond distances and angles reported by them are very similar to those reported here. They, however, reported a disorder of the bromido ligand and the carbonyl ligand *trans* to it but this disorder is not observed in **1** reported here.

A dihedral angle of 7.028(15) ° is calculated between the plane through the 2,2'-bipyridine system (N1, N2, C4-13) and the equatorial plane (O2-C2-Re1-C1-O1) and is illustrated in Figure 4.2. From Figure 4.2 it is clear that the 2,2'-bipyridine ligand bends out of the equatorial plane towards the bromido ligand.

Figure 4.2: Illustration of the plane through the 2,2'-bipyridine ligand ((N1, N2, C4-C13) - blue plane) and the equatorial plane ((O2-C2-Re1-C1-O1) - green plane), indicating the dihedral angle between the planes of *fac*-[Re(CO)$_3$(bpy)(Br)] (1).

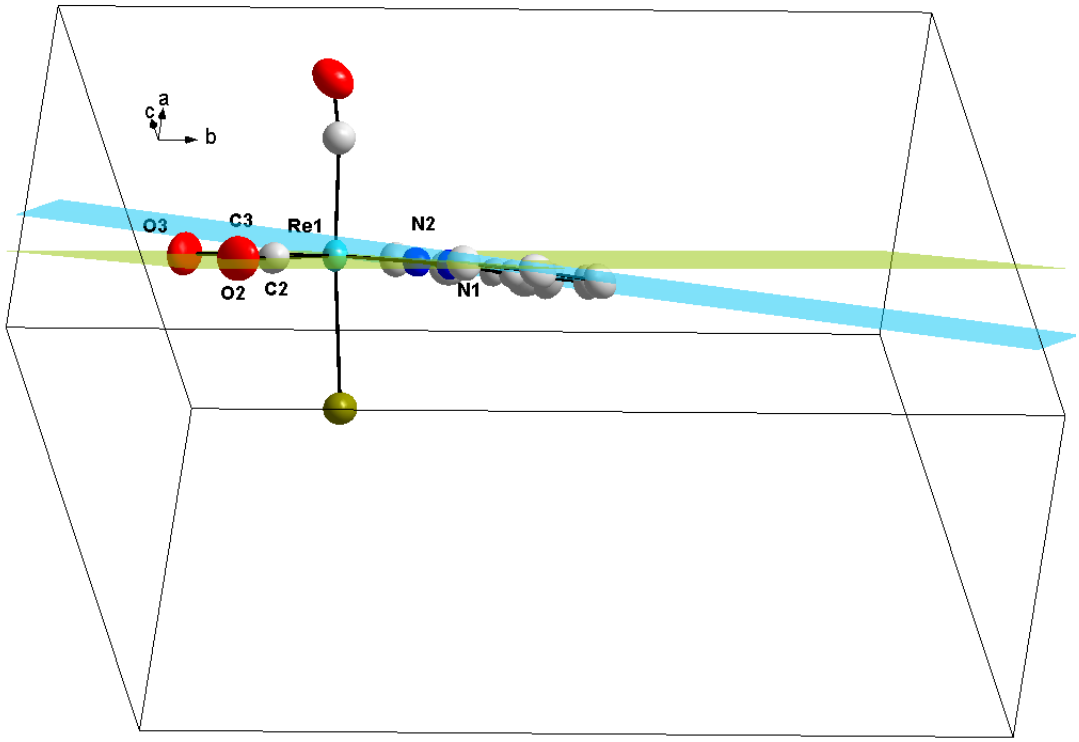

Only one hydrogen bonding interaction is observed (C6-H6···Br1). This is an intermolecular interaction between two neighbouring molecules in the unit cell. The hydrogen bonding interaction observed in **1** is illustrated in Figure 4.3. Table 4.3 summarises the hydrogen bonding interaction's distances, angles, and symmetry operators.

Figure 4.3: Hydrogen bonding interactions observed in *fac*-[Re(CO)$_3$(bpy)Br] (1) (Indicated in a green dashed line). Hydrogen atoms not taking part in the hydrogen bonding interaction are omitted for clarity.

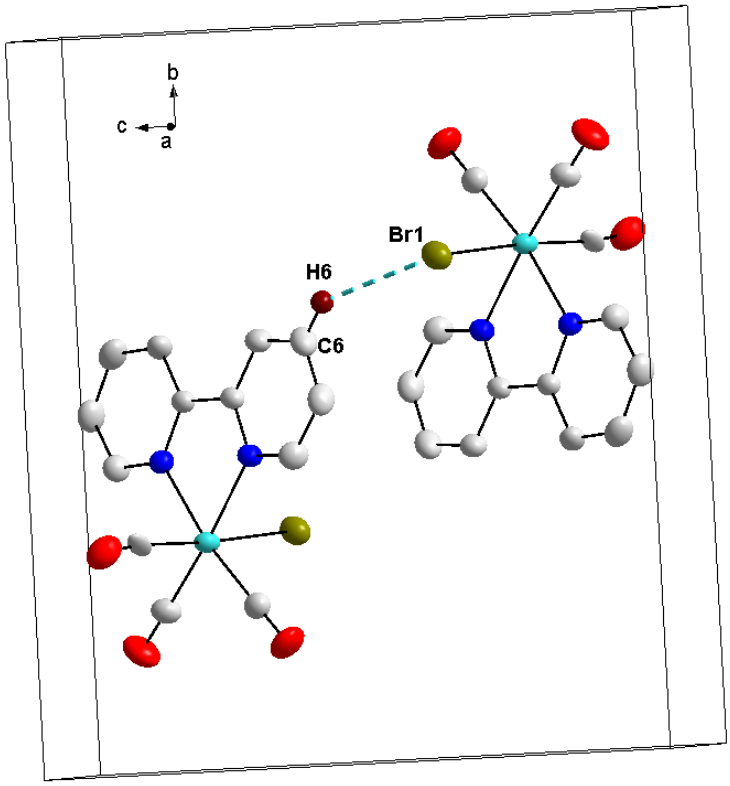

Table 4.3: Summary of the hydrogen bonding interaction's distances (Å) and angle (°) observed in 1.

D-H···A	d(D-H)	d(H···A)	d(D···A)	D-H···A angle
C6-H6 Br1[a]	0.95	2.93	3.707(6)	140.4

Symmetry transformations used to generate equivalent atoms:

[a] –x+1; -y+1; -z+1

Three π-interactions are observed in the structure of **1**. A strong intramolecular π-interaction is observed between the five membered centroid, Re1-N1-C8-C9-N2, and Br1 with a Br to centroid distance of 2.998 (3) Å. A strong intermolecular π-interaction is observed between the six membered centroid, N1-C4-C5-C7-C8 and the same centroid of the next molecule with a centroid to centroid distance of 3.710 Å and a weak intermolecular π-interaction is seen between the six membered centroid, N2-C9-C10-C11-C12-C13 and the same centroid of the next molecule with a centroid

to centroid distance of 3.819(4) Å. These three possible π-interactions are illustrated in Figure 4.4.

Figure 4.4: Illustration of the π-Interactions observed in 1. Hydrogen atoms are omitted for clarity. Pink dashed lines indicate the π interactions.

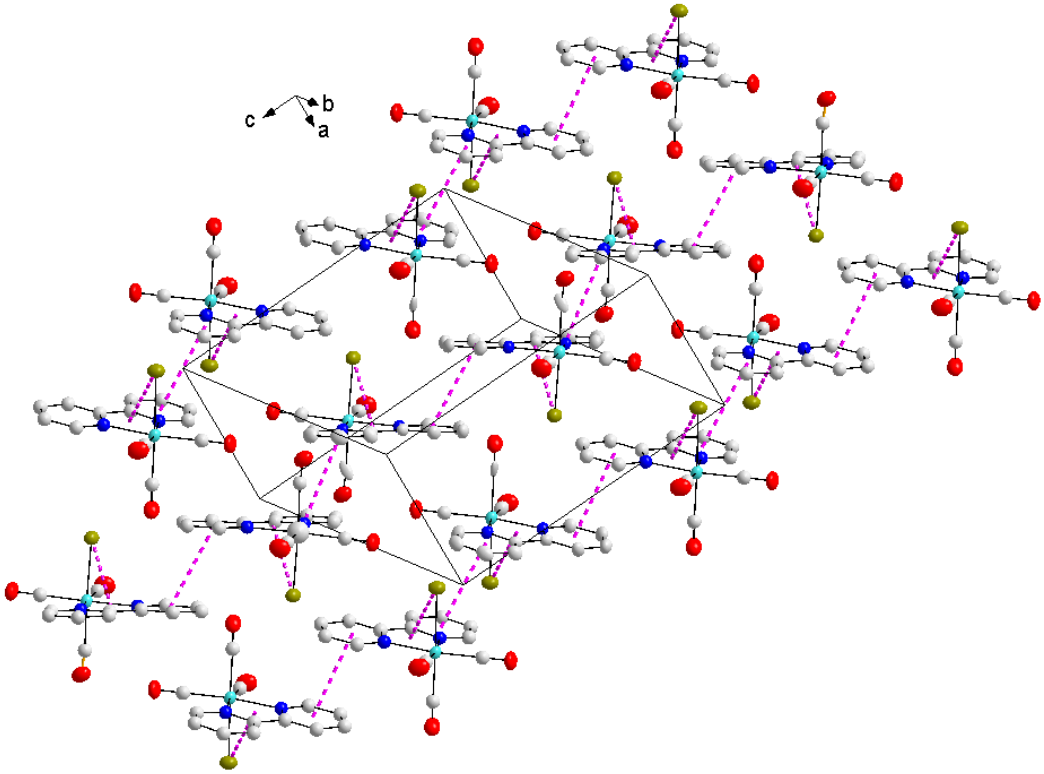

1 packs in a head-to-tail fashion in column-like structures between the a-axis when viewed along the b- and c-axis. The packing of **1** is illustrated in Figure 4.5.

Figure 4.5: Packing of 1, viewed along the a-axis. Hydrogen atoms omitted for clarity.

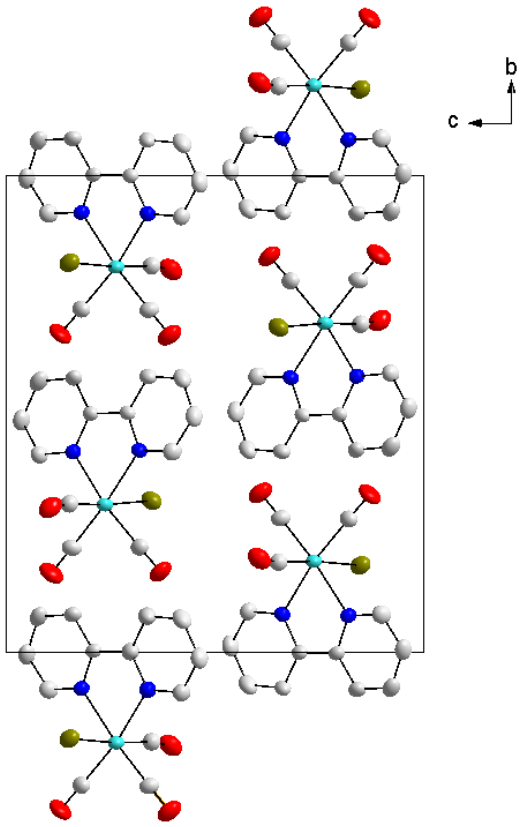

4.4 Discussion

In this chapter a single Re(I) tricarbonyl structure containing a *N,N'*-donor bidentate ligand was reported. The Re tricarbonyl bond distances are all within normal range. The rhenium to bidentate nitrogen bond distances of 2.171 (4) Å (Re1-N1) and 2.170 (4) Å (Re1-N2) and the rhenium to monodentate bromido bond distance of 2.6126 (15) Å agrees with similar bond distances reported in literature.[8,9,10,11,12,13,14] The small bite angle (N1-Re1-N2) of 74.95 (16) ° agrees with similar structures found in literature.[15] The crystal structure of *fac*-[Re(CO)$_3$(bpy)(Br)] has already been published[7] and all bond distances and angles correspond to bond distances and angles reported before. However, a disorder of the bromido ligand was reported by Kia and Safari[7] which was not seen in **1**. In this structure a definite bending of the ligand system from the equatorial plane is observed with a dihedral angle of 7.028(15) ° which is significantly higher than the dihedral angle of 4.306(297) ° reported by Kia

[15] Schutte, M., PhD Thesis, "*Novel Radiopharmaceuticals Characterization, Substitution Kinetics and Biological Evaluation of Tricarbonyl Complexes of Rhenium(I).*", 2011, University of the Free State.

and Safari[7]. Three π-interactions were observed; two were intermolecular interactions between the aromatic rings of the bpy ligand and the third π-interaction was an intramolecular interaction from the centroid formed between the metal centre and the bidentate ligand to the bromido ligand. Domínguez *et al.*[11] reported a neutral bpy Re(I) tricarbonyl complex with a nitro group in the 6th position. Hydrogen bonding was not reported for this structure while only a single strong π-interaction of 2.6115(43) Å was reported as C-H$\cdot\cdot\cdot$O-NO compared to the three π-interactions observed in **1**. The structure reported here unequivocally confirms the coordination of the bidentate and monodentate ligand to the metal centre.

5 PHOTOLUMINESCENCE STUDY OF RE(I) COMPLEXES

5.1 Introduction

The coordination of N-heterocyclic ligands, such as polypyridine ligands, has been successful in adjusting the luminescent properties of various metal complexes.[1,2,3,4] The structure of these N-heterocyclic compounds allows for ligand modifications, for instance, substitution or addition, which may have steric and electronic implications. The luminescent properties of copper (I) complexes were reported to be affected by additional ligands such as phosphines and halides.[5, 6]

Common polypyridine luminophores for metal complexes include 1,10-phenanthroline and 2,2'-bipyridine. Bosnich proved that the framework of 2,2'-bipyridine is polarised at the 5,5'-axis.[7] Thus the addition of aromatic substituents at these sites can result in increased polarisation and ultimately to the increase of luminescence abilities of the complex into a red-shift emission maximum.[8]

For d^n (n = 1 to 9) complexes, the expected absorptions for ligands including CO are mainly ligand field (LF) and charge-transfer (CT) transitions. However, for some ligands, intra-ligand excited states are possible.[9] Wrighton reviewed $M(CO)_n(L)_{6-n}$ complexes and found that these complexes exhibit intense transitions in the UV-visible region ($\varepsilon > 10^2$).[9] He associated these transitions with LF and M → L and L

[1] Armardi, N.; Accorsi, G.; Holler, M.; Moudam, O.; Nierengarten, J.; Zhou, Z.; Wegh, R. T.; Welter, R., *Adv. Mater*., 2006, 18, 1313-1316.
[2] Yam, V. W. W.; Lo, K. K. W., *Chem. Soc. Rev*., 1999, 28, 323-334.
[3] Zhang, Q.; Zhou, Q.; Cheng, Y.; Wang, L.; Ma, D.; Jing, X.; Wang, F., *Adv. Mater*., 2004, 16, 432-436.
[4] Nishikawa, M.; Nomoto, K.; Kume, S.; Inoue, K.; Sakai, M.; Fuji, M.; Nishihara, H., *J. Am. Chem. Soc*., 2010, 132, 9579-9581.
[5] Safin, D. A.; Babashkina, M. G.; Bolte, M.; Klein, A., *Inorg. Chim. Acta.*, 2010, 363, 1897-1901.
[6] Cuttell, D. G.; Kuang, S.; Fanwick, P. E.; McMillin, D. R.; Walton, R. A., *J. Am. Chem. Soc*., 2002, 124, 6-7.
[7] Bosnich, B., *Acc. Chem. Res.*, 1969, 2, 266-273.
[8] Loren, J. C.; Siegel, J. S., *Angew. Chem. Int. Ed.*, 2001, 40, 754-757.
[9] Wrighton, M., *Chem. Rev.*, 1974, 74, 401-430.

→ M CT absorptions. Wrighton[9] also found that in some cases intra-ligand absorptions may cause intense transitions.

The Stokes shift is an important parameter that provides information on the excited states. It represents the difference between the maximum of the first absorption band and the maximum of the fluorescence spectrum. This value is expressed in wave number.[10] Valeur states, "From a practical point of view, the detection of a fluorescent species is, of course, easier when the Stokes shift is larger."[10]

An increase in π-conjugation causes a red-shift of the absorption and fluorescence and thus an increase in the fluorescence quantum yield.[10] Aromatic compounds therefore are expected to be fluorescent due to the extent of their π-electron systems. Aromatic aldehydes and ketones, however, for instance, anthrone and benzophenone, exhibit low fluorescence quantum yields because they possess a low-lying n-π* excited state. These excited states characteristically possess molar absorption coefficients that are 10^2 times smaller than those having π-π* transitions. In accordance with the Strickler-Berg equation, the radiative lifetime (τ_r) of n-π* transitions is 100 × longer than that of π-π* transitions.[11] As a result, it is impossible for slow n-π* transitions to compete with non-radiative π-π* transitions. Compounds containing heterocyclic nitrogen atoms such as quinone and pyridine are known to possess low-lying n-π* transitions and thereby also express relatively low fluorescence quantum yields.

In this chapter the photoluminescent properties of eleven synthesised Re(I) tri- and dicarbonyl complexes are discussed. The photoluminescence studies were conducted in solution. All complexes were studied in methanol, and two complexes, *fac*-$[Re(CO)_3(bpy)(PTA)][NO_3]$ and *cis-trans*-$[Re(CO)_2(bpy)(PTA)_2][NO_3]$, were also studied in water to determine the solvent effect on the photoluminescent properties of these samples. Recently reported work on luminescent rhenium(I) complexes as

[10] Valeur, B.; 2001. *Molecular Fluorescence: Principles and Applications, Wiley-VCH Verlag*, New York, 54-61.
[11] Valeur, B.; 2001. *Molecular Fluorescence: Principles and Applications, Wiley-VCH Verlag*, New York, 42-44.

possible photosensitisers for photodynamic therapy,[12,13] leads to the expectation that the Re(I) complexes synthesised in this study will also show promising results. The Re(I) tri and dicarbonyl complexes that were analysed and discussed in this chapter are displayed in Figure 5.1.

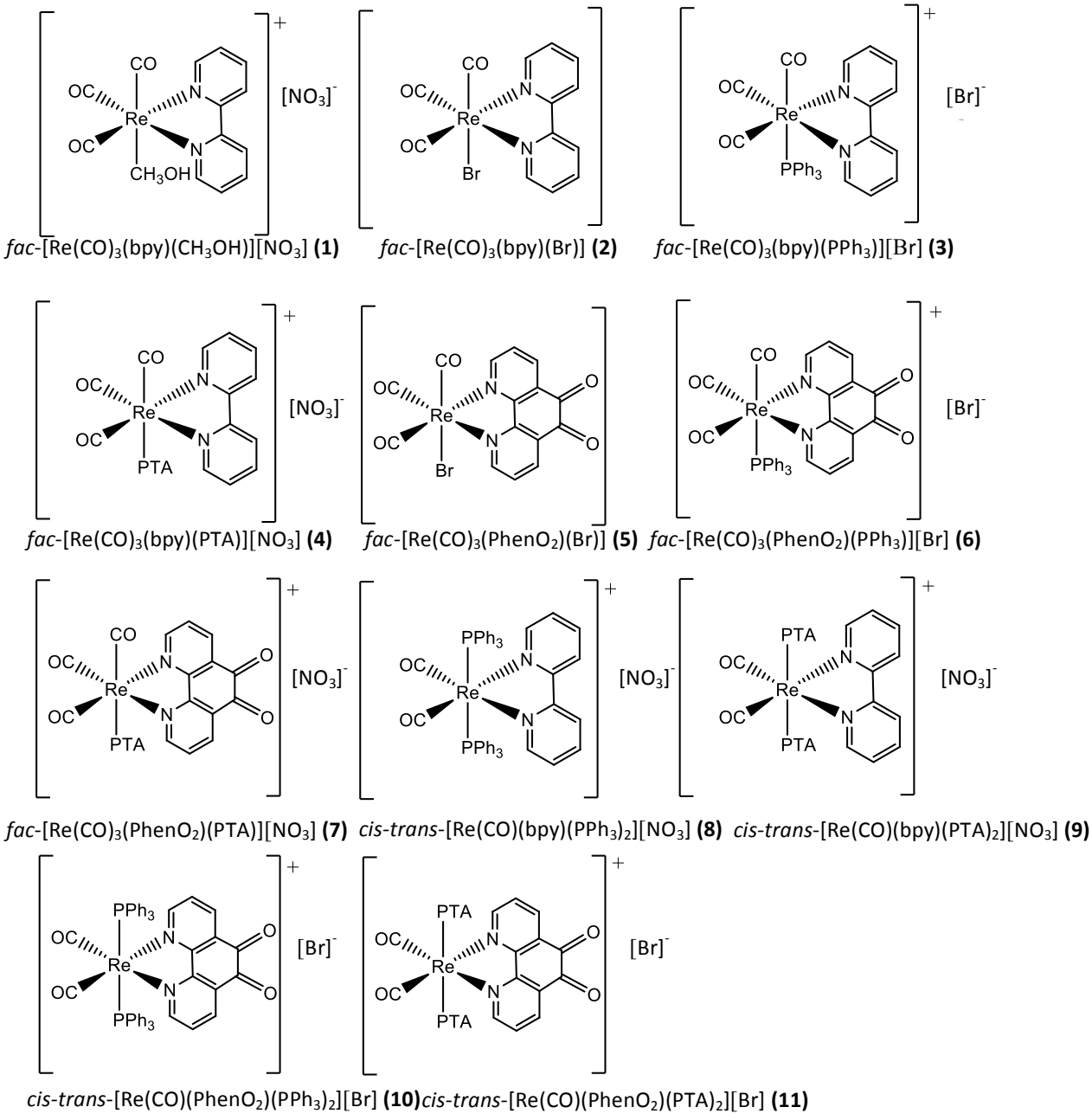

fac-[Re(CO)$_3$(bpy)(CH$_3$OH)][NO$_3$] **(1)** *fac*-[Re(CO)$_3$(bpy)(Br)] **(2)** *fac*-[Re(CO)$_3$(bpy)(PPh$_3$)][Br] **(3)**

fac-[Re(CO)$_3$(bpy)(PTA)][NO$_3$] **(4)** *fac*-[Re(CO)$_3$(PhenO$_2$)(Br)] **(5)** *fac*-[Re(CO)$_3$(PhenO$_2$)(PPh$_3$)][Br] **(6)**

fac-[Re(CO)$_3$(PhenO$_2$)(PTA)][NO$_3$] **(7)** *cis-trans*-[Re(CO)(bpy)(PPh$_3$)$_2$][NO$_3$] **(8)** *cis-trans*-[Re(CO)(bpy)(PTA)$_2$][NO$_3$] **(9)**

cis-trans-[Re(CO)(PhenO$_2$)(PPh$_3$)$_2$][Br] **(10)***cis-trans*-[Re(CO)(PhenO$_2$)(PTA)$_2$][Br] **(11)**

Figure 5.1: Re(I) tri- and dicarbonyl complexes studied in this chapter (PTA = 1,3,5-triaza-7-phosphaadamantane, PPh$_3$ = triphenylphosphine).

[12] Kastl, A. ; Dieckmann, S.; Wähler, K.; Völker, T.; Kastl, L.; Vultur, A.; Shannan, B.; Harms, K.; Ocker, M.; Parak, W. J.; Herlyn, M.; Meggers, E., *ChemMedChem.*, 2013, 8, 924-927.

[13] Leonidova, A.; Pierroz, V.; Rubbiani, R.; Heier, J.; Ferrari, S.; Gasser, G., *Dalton Trans.*, 2014, 43, 4287-4294.

5.2 Experimental

All solvents used were of analytical grade and purchased from Sigma-Aldrich and Merck. No further purification was necessary. Complexes were synthesised according to the methods discussed in Chapter 3. The instrument used for the UV/Vis measurements in this study was a Varian Cary 50 Conc. Spectrometer, equipped with a Julabo F12-mV temperature cell regulator accurate within 0.1 °C. The absorbance spectra measurements were conducted using a 1.000(1) cm tandem quartz cuvette. The solvent used for the bulk of the experiments were methanol altough in some cases water was used. Photoluminescence measurements were made while using an Edinburgh Instruments FLS980 series Fluorescence Spectrometer. The samples were excited with a continuous xenon lamp (Xe1) with a 450W arc lamp light source. The data acquisition technique was single photon counting. The luminescence was measured in solution while using a 1.000(1) cm quartz cuvette. Solvent correction scans were taken at each excitation wavelength. All samples were studied in methanol and two samples of water soluble complexes were measured in both methanol and water.

5.3 Results

5.3.1 Analysis of Re(I) tricarbonyl complexes

This section reports the emission and excitation spectra of the Re(I) tricarbonyl complexes synthesised in this study.

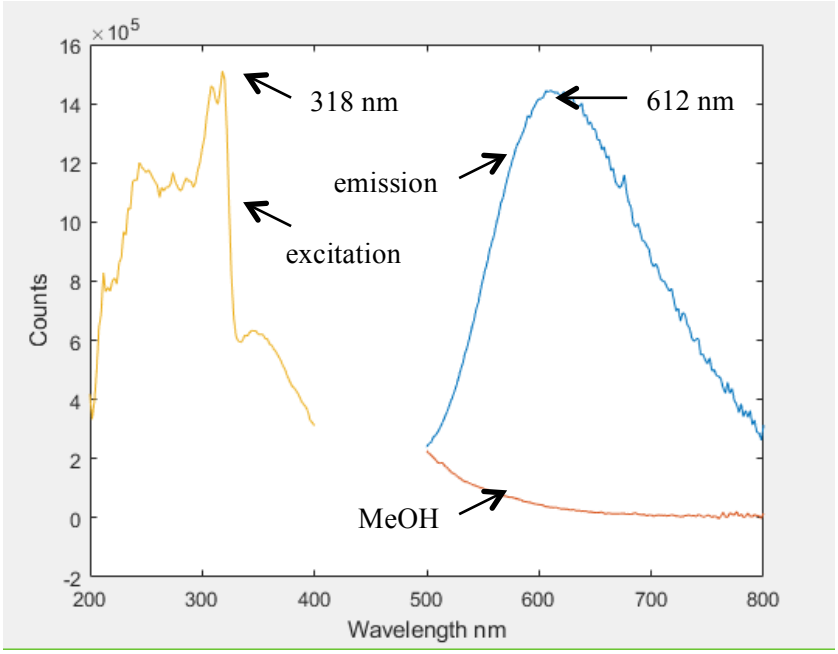

Figure 5.2: Excitation (yellow line) and emission (blue line) spectra of *fac*-[Re(CO)$_3$(bpy)(CH$_3$OH)][NO$_3$] (1) (1.7 × 10^{-5} M) in methanol solution.

1 is a multi-emitter, and so displays multiple excitation wavelengths in solution. The peak at 318 nm is the most prominent excitation peak and gives rise to a maximum emission at 612 nm as shown in Figure 5.2 The low lying emissions from 500 – 800 nm (orange plot) are those obtained for pure methanol. The emission peak at 612 nm appears to display a sharp peak on its right shoulder which may be attributed to noise.

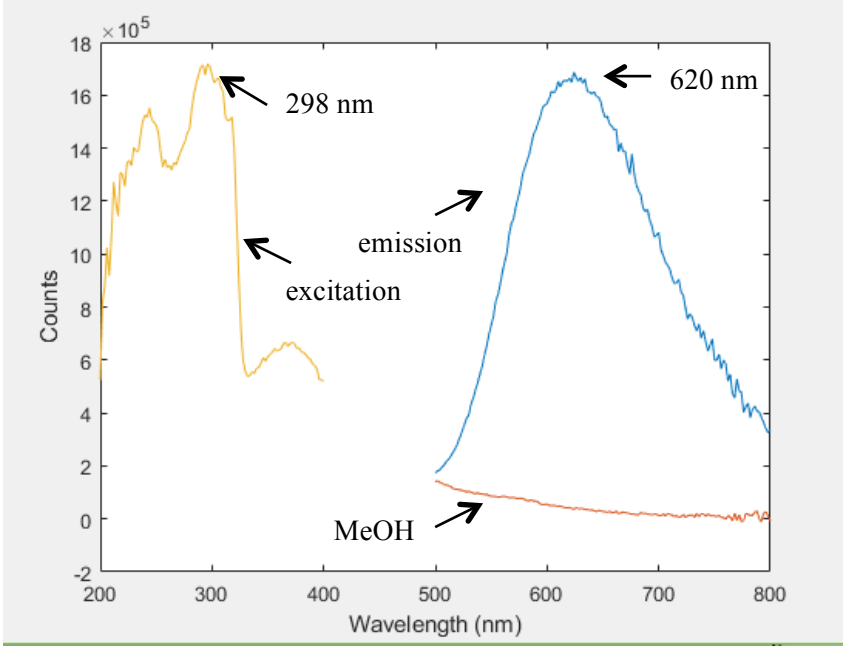

Figure 5.3: Excitation and emission spectra of *fac*-[Re(CO)$_3$(bpy)(Br)] (2) (2.4 × 10^{-5} M) in methanol solution.

2 shows excitation at 298 nm in methanol. Excitation at this wavelength gives rise to emission at 620 nm. **2** shows multiple excitations. However, 298 nm is the most prominent. This is illustrated in Figure 5.3.

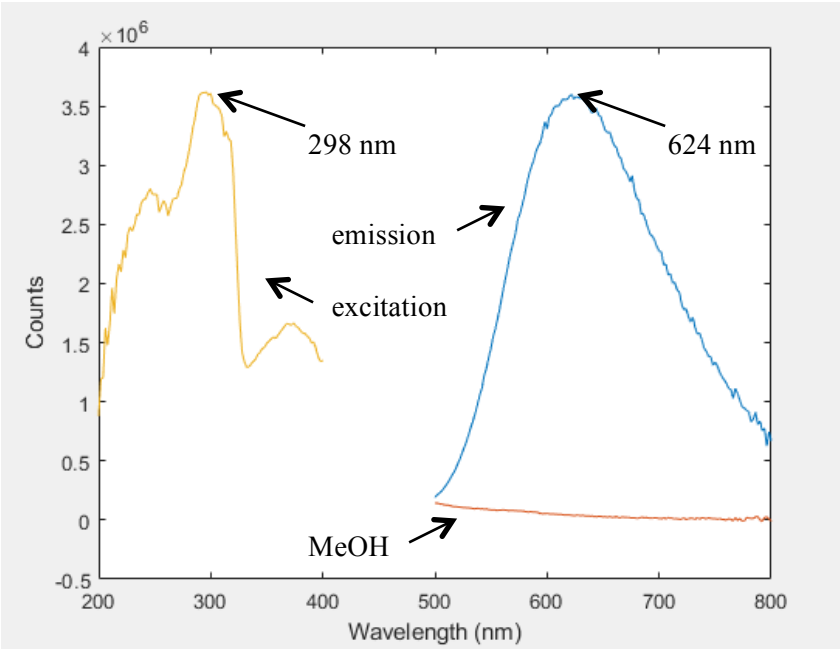

Figure 5.4: Excitation and emission spectra of *fac*-[Re(CO)$_3$(bpy)(PPh$_3$)][Br] (3) (1.3 × 10^{-5} M) in methanol solution.

3 shows excitation at 298 nm. Excitation at this wavelength results in emission at 624 nm. The excitation and emission of **3** are displayed in Figure 5.4.

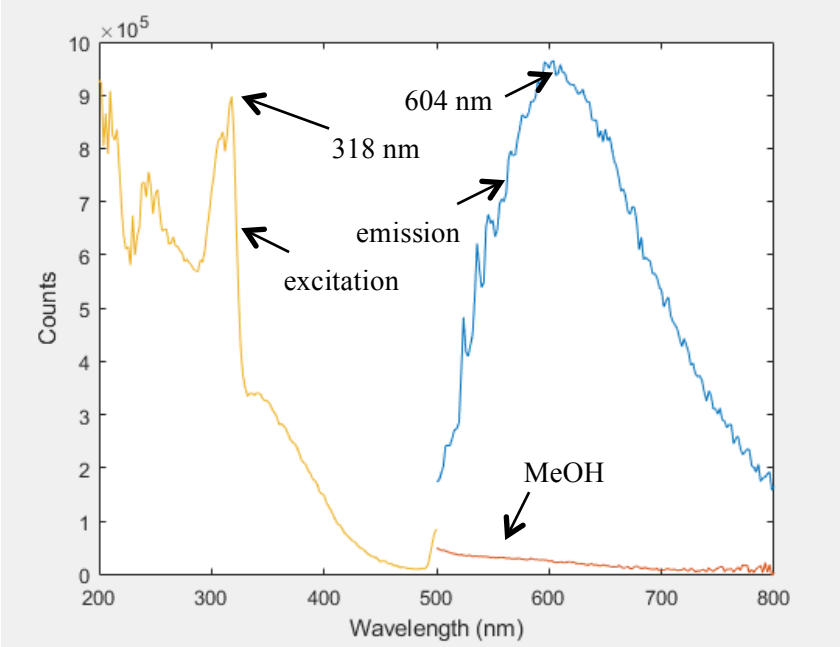

Figure 5.5: Excitation and emission spectra of *fac*-[Re(CO)$_3$(bpy)(PTA)][NO$_3$] (4) (1 × 10^{-5} M) in aqueous solution.

4 shows excitation at 318 nm in aqueous solution. Excitation at this wavelength gave rise to emission at 604 nm. Shoulder peaks to the left of the maximum emission may be attributed to noise (Figure 5.5).

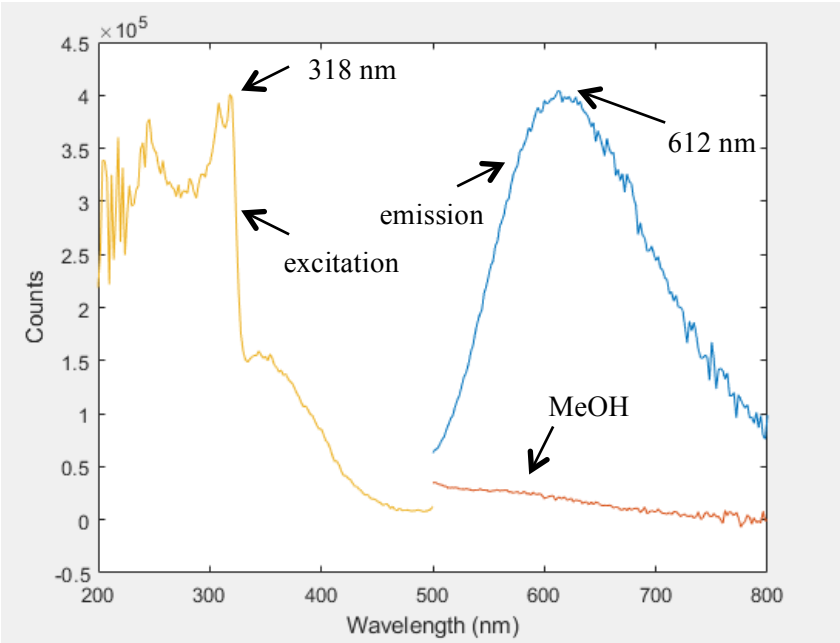

Figure 5.6: Excitation and emission spectra of *fac*-[Re(CO)$_3$(bpy)(PTA)][NO$_3$] (4) (1 × 10^{-5} M) in methanol solution.

4 in methanol showed excitation at 318 nm which is the same as that found for **4** in water. Excitation at this wavelength results in emission at 612 nm. The excitation and emission of **4** in methanol are illustrated in Figure 5.6. The emission of **4** is more red-shifted when in methanol solution compared to the emission of the same complex in aqueous solution.

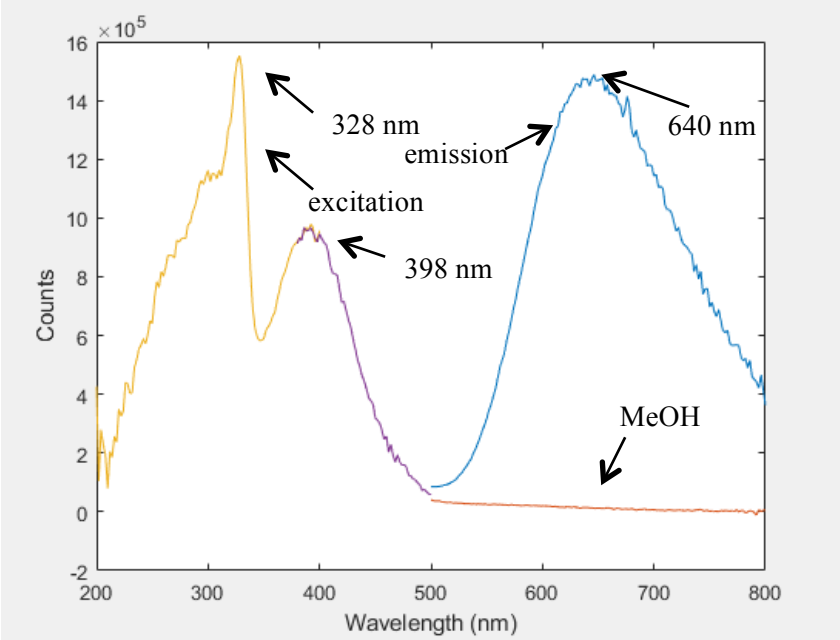

Figure 5.7: Excitation and emission spectra of *fac*-[Re(CO)$_3$(PhenO$_2$)(Br)] (5) (1.4 × 10^{-5} M) in methanol solution.

A second excitation scan was taken for **5** from 380 nm to 500 nm because the initial scan (200 – 400 nm) suggested the formation of a second peak. Hence, the wavelength range was increased. An excitation peak at 398 nm was obtained from this second scan. **5** also displays multiple excitation peaks. The main peak is found at 328 nm. Excitation at this wavelength gave rise to emission at 640 nm. The excitation and emission spectra of **5** in methanol are provided in Figure 5.7.

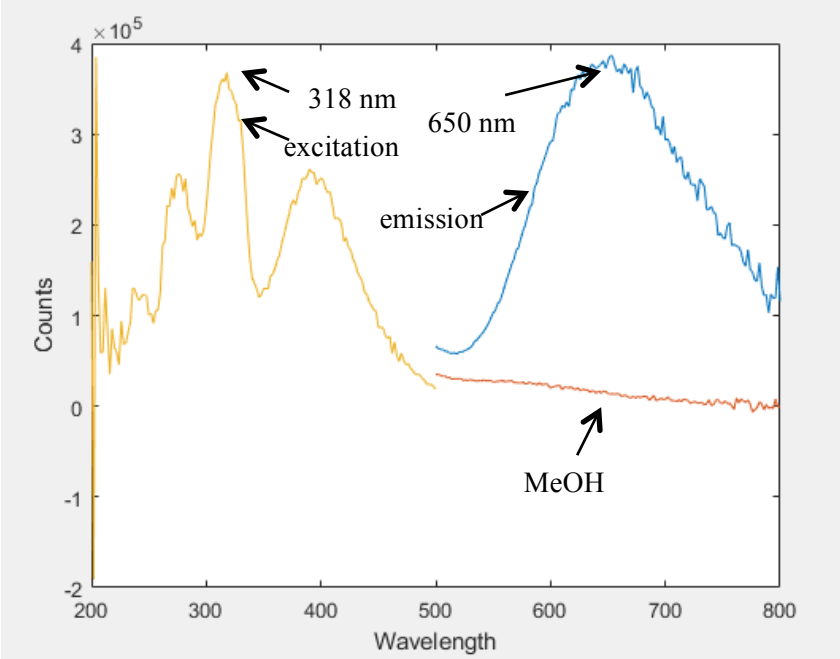

Figure 5.8: Excitation and emission spectra of *fac*-[Re(CO)$_3$(PhenO$_2$)(PPh$_3$)][Br] (6) (2.4 × 10^{-5} M) in methanol solution.

6 shows multiple excitation peaks. However, the main excitation peak is at 318 nm. Excitation at this wavelength results in emission at 650 nm. The excitation and emission spectra of **6** are reported in Figure 5.8.

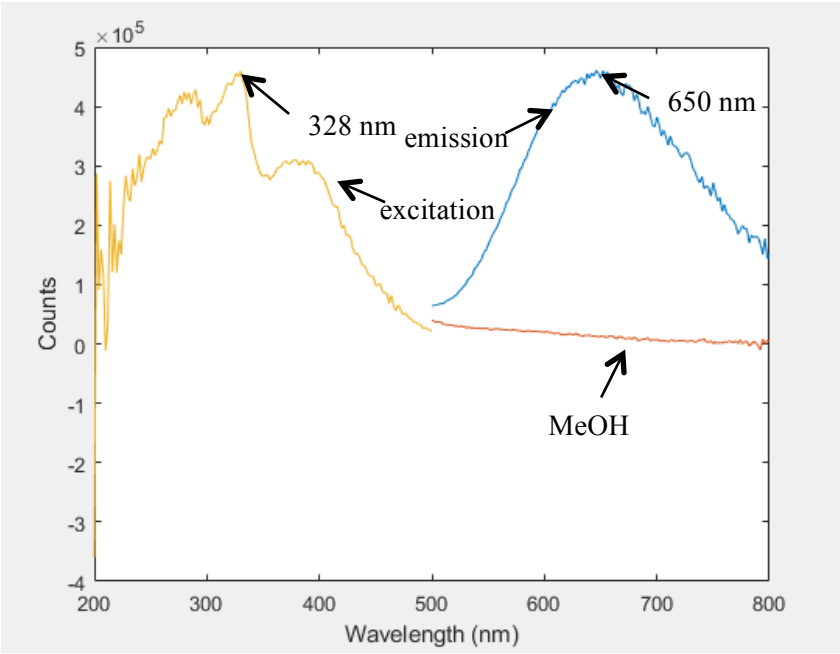

Figure 5.9: Excitation and emission spectra of *fac*-[Re(CO)$_3$(PhenO$_2$)(PTA)][NO$_3$] (7) (1.2 × 10^{-5} M) in methanol solution.

7 is excited at multiple wavelengths. However, 328 nm is the most prominent. Excitation at this wavelength results in emission at 650 nm. The excitation and emission spectra of **7** are reported in Figure 5.9.

5.3.2 Analysis of Re(I) dicarbonyl complexes.

This section reports the emission and excitation spectra of the Re(I) dicarbonyl complexes synthesised in this study.

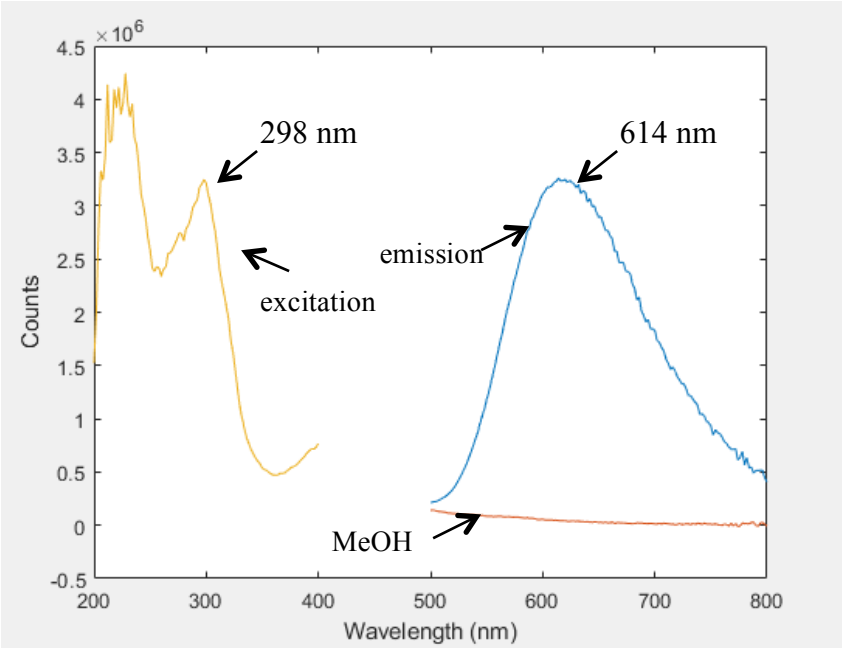

Figure 5.10: Excitation and emission spectra of *cis*-[Re(CO)$_2$(bpy)(PPh$_3$)$_2$][NO$_3$] (8) (1 × 10^{-5} M) in methanol solution.

8 shows prominent excitation in solution at 298 nm. Excitation at this wavelength gives rise to a maximum emission at 614 nm. The low-lying excitation values from 500 – 800 nm are obtained from methanol. The excitation and emission spectra of **8** are illustrated in Figure 5.10.

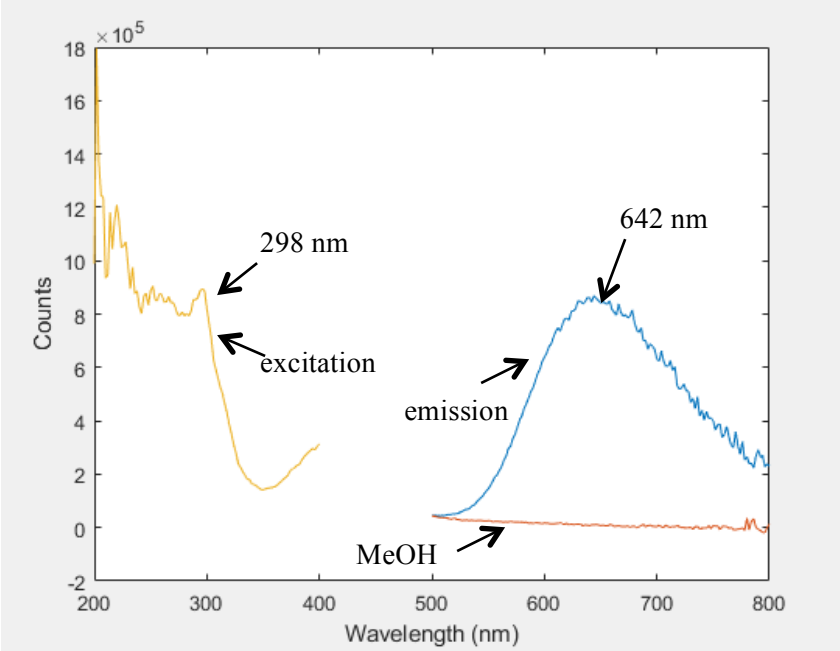

Figure 5.11: Excitation and emission spectra of *cis*-[Re(CO)$_2$(bpy)(PTA)$_2$][NO$_3$] (9) (9 × 10^{-6} M) in aqueous solution.

9 shows excitation at 298 nm in aqueous solution. Excitation at this wavelength results in emission at 642 nm. The low-lying excitation values from 500 – 800 nm are those obtained from distilled water (Figure 5.11).

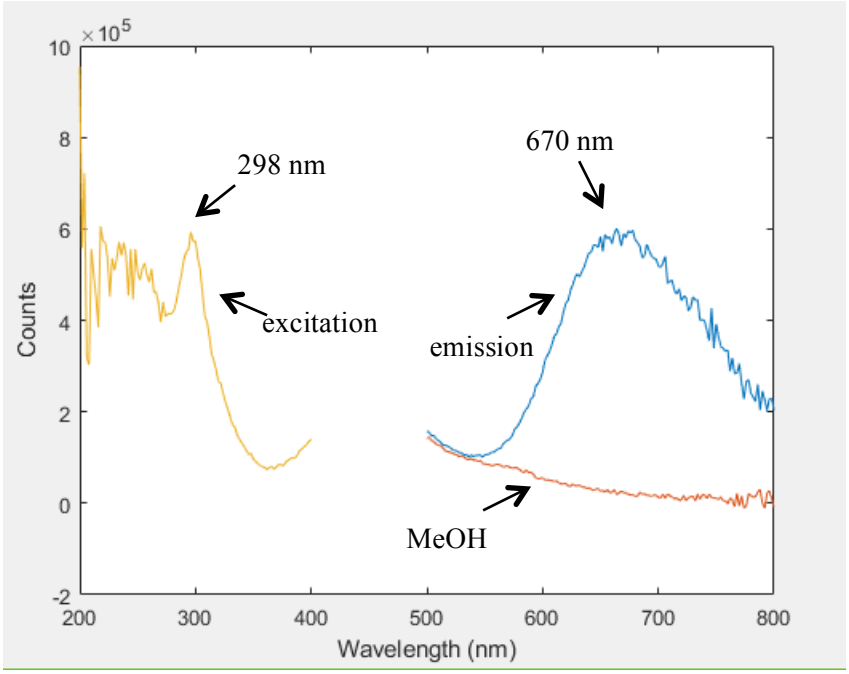

Figure 5.12: Excitaion and emission spectra of *cis*-[Re(CO)$_2$(bpy)(PTA)$_2$]NO$_3$ (9) (9 × 10^{-6} M) in methanol solution.

9 showed excitation at 298 nm in methanol (Figure 5.12) which is the same as its excitation in water. However, **9** has an emission peak at 670 nm which is significantly higher than that found for the same sample in water.

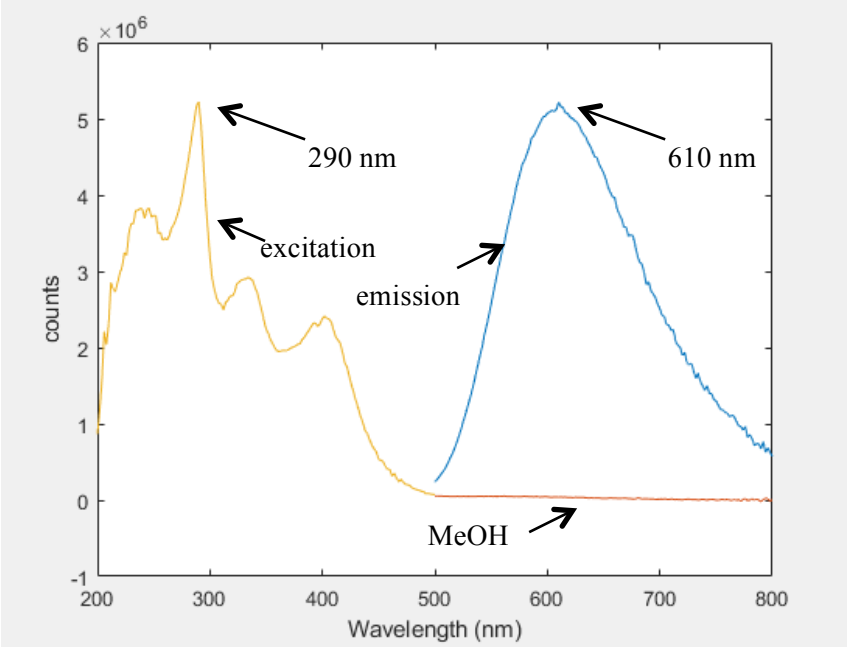

Figure 5.13: Excitation and emission spectra of *fac*-[Re(CO)$_2$(PhenO$_2$)(PPh$_3$)$_2$][Br] (10) (6.7 × 10^{-6} M) in methanol solution.

10 showed multiple excitation peaks. However, the maximum is at 290 nm. Excitation at this wavelength results in emission at 610 nm. The excitation and emission spectra of **10** are illustrated in Figure 5.13.

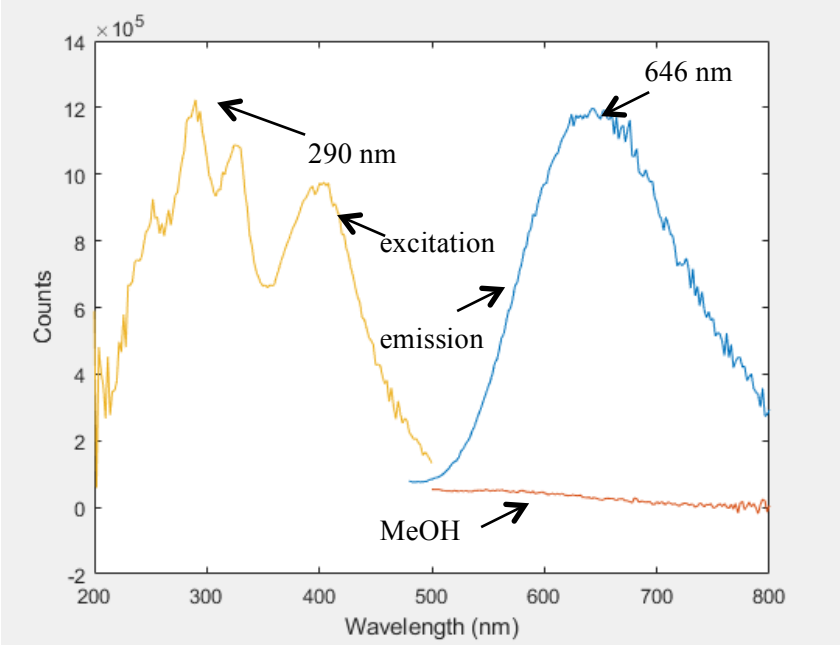

Figure 5.14: Excitation and emission spectra of *fac*-[Re(CO)$_2$(PhenO$_2$)(PTA)$_2$][Br] (11) (1.5 × 10^{-5} M) in methanol solution.

11 shows multiple excitation peaks. However, the main peak is at 290 nm. Excitation at this wavelength results in emission at 646 nm. The excitation and emission spectra of **11** are illustrated in Figure 5.14.

5.4 Discussion

Table 5.1 Summarises the absorbance, excitation and emission wavelengths of all Re(I) complexes discussed in this section.

Table 5.1: Absorbance, maximum excitation, and emission wavelengths of Re(I) tri- and dicarbonyl complexes.

Complex	Absorbance (nm)	Excitation (nm)	Emission (nm)
(1) *fac*-[$Re(CO)_3(bpy)(CH_3OH)][NO_3$]	282	318	612
(2) *fac*-[$Re(CO)_3(bpy)(Br)$]	292	298	620
(3) *fac*-[$Re(CO)_3(bpy)(PPh_3)][Br$]	291	298	624
(4) *fac*-[$Re(CO)_3(bpy)(PTA)][NO_3$] (Aq)	319	318	604
(4) *fac*-[$Re(CO)_3(bpy)(PTA)][NO_3$] (CH_3OH)	319	318	612
(5) *fac*-[$Re(CO)_3(PhenO_2)(Br)$]	305	328	640
(6) *fac*-[$Re(CO)_3(PhenO_2)(PPh_3)][Br$]	292	318	650
(7) *fac*-[$Re(CO)_3(PhenO_2)(PTA)][NO_3$]	249	328	650
(8) *cis*-[$Re(CO)_2(bpy)(PPh_3)_2][NO_3$]	320	298	614
(9) *cis*-[$Re(CO)_2(bpy)(PTA)_2][NO_3$] (Aq)	245	298	642
(9) *cis*-[$Re(CO)_2(bpy)(PTA)_2][NO_3$] ($CH_3OH$)	245	298	670
(10) *cis*-[$Re(CO)_2(PhenO_2)(PPh_3)_2][Br$]	289	290	610
(11) *cis*-[$Re(CO)_2(PhenO_2)(PTA)_2][Br$]	294	290	646

The substitution of the methanol ligand in the 6^{th} position in **1** with a bromido ligand in **2** would lead one to expect lower absorbance and fluorescence wavelengths, since methanol is an electron-donating ligand, which is known to increase molar absorption coefficients and thus red-shift absorbance and fluorescence.[10] The bromido ligand can cause an internal heavy-atom effect, increasing the possibility of intersystem crossing that may result in fluorescence quenching. This was not prominent in these results since the emission of **2** is red-shifted to 620 nm compared to the 612 nm of **1**.

8 and **9** are Re(I) dicarbonyl complexes, differing only in the monodentate phosphorous ligands, PPh_3 and PTA. In methanol solution, the emission of **9** is significantly red-shifted compared to that of **8**. This may be caused by the electron withdrawing nature of the PTA ligand (pKa = 2.52[14]), reducing the electron density on the rhenium centre causing a decrease in π-back bonding to the CO π* orbitals. **9**

[14] Phillips. A. D.; Gonsalvi, L.; Romerosa, A.; Vizza, F.; Peruzzini, M., *Coord. Chem, Rev.*, 2004, 248, 955-993.

was found to be hydrophilic. This characteristic along with a 642 nm emission in water solution promote **9** as a possible PDT agent.

In the monodentate phosphine containing tricarbonyl complexes it was observed that the complexes in possession of a $phenO_2$ bidentate ligand showed emission at a higher wavelength than their bpy counterparts, while in the monodentate bisphosphine containing dicarbonyl complexes the bpy complexes emit at higher wavelengths than the $phenO_2$ complexes. With exception to **3** and **4,** both the dicarbonyl and tricarbonyl PTA containing complexes (**7**, **9**, **11**) emit at higher wavelengths than the PPh_3 complexes (**6**, **8**, **10**). Marker *et al*.[15] assert that the energy of the MLCT transition, which is the state which is predominantly responsible for the photochemical properties of *fac*-$[Re(CO)_3]^+$ complexes, is basically independent of the nature of the phosphine. They also suggest that the nitrogen lone pairs on the PTA quench the MLCT, resulting in an absence of luminescence in the PTA complexes as reported by them. This suggests that the observation in our complexes may be due to the bpy ligand, which is less conjugated than $phenO_2$ and thus possesses higher energy π^* orbitals.

4 and **9** are water soluble. This is attributed to the water soluble PTA ligand present in both complexes. The substitution of the CO ligand with a PTA ligand in **9** caused a significant red-shift in emission values in both methanol and aqueous solution. The emission differences between both complexes in aqueous and methanol solution may be due to a solvent effect causing the energy bands to be closer to one another and thus resulting in a longer wavelength for the same sample in a different solvent solution.

In **5** and **6**, and in **2** and **3**, the substitution of the bromido ligand with a PPh_3 ligand did not result in a significant red-shift in emission values, perhaps because the electron-donating PPh_3 ligand and possible heavy-atom effect caused by the bromido ligand similarly inhibit fluorescence and therefore do not exhibit significant mutual differences.

[15] Marker, S. C.; MacMillan, S. N.; Zipfel, W. R.; Li, Z.; Ford, P. C.; Wilson, J. J., *Inorg. Chem.*, 2018, 57, 1311-1331.

3 has a PPh_3 ligand which contains three aromatic rings with large amounts of π-conjugation and a large cone angle of 145° [16], on the 6th posistion, while **4** has a PTA ligand with a small cone angle of 109° [17]. The emission of **3** is significantly red-shifted compared to **4**. This may be due to the nitrogen lone pairs of the PTA ligand quenching the MLCT, that could explain the lower emission wavelength of **4**.

The emission spectra of **6** and **11** were expected to follow the same trend as **4** and **9**. **6** and **11,** however, did not follow the trend of **4** and **9** and show little difference in emission wavelengths at similar excitation. This may be due to the higher electron density of the $phenO_2$ ligand compared to the bpy ligand.

On account of the very low intensity of light emitted, it was not possible to measure the quantum yields of these complexes accurately. An approximate estimation would suggest that the quantum yields would amount to being far below 1 %, thereby making these complexes unviable for use in photodynamic therapy.

[16] Tolman, C. A., *Chem. Rev.*, 1979, 77, 313-348.
[17] Britvin, S. N.; Lotnyl, A., *J. Am. Chem. Soc.,* 2015, 137, 5526-5535.

6 Critical Evaluation

6.1 Results obtained

This dissertation represents an endeavour to synthesise and characterise a range of rhenium(I) tricarbonyl and dicarbonyl complexes as well as several precursors, bimetallic complexes and ^{99m}Tc analogues of two rhenium dicarbonyl complexes. Also, to investigate the photoluminescent abilities of a range of rhenium(I) tricarbonyl and dicarbonyl complexes and determine the *in vitro* cytotoxicity of the bimetallic complexes for possible use as photosensitisers for photodynamic therapy.

One ligand was synthesised by an oxidation reaction of 1,10-phenanthroline. This ligand was fully characterised. The synthesis of several Re(I) complexes of the type *fac*-[Re(*N,N'*-bid)$(CO)_3(X)]^n$ and *cis-trans*-[Re(*N,N'*-bid)$(CO)_2(X)_2]^n$ (*N,N'*-bid = different *N,N'* donor bidentate ligands, n = 0, +1) (X = different phosphorous monodentate ligands) were successful. These complexes were fully characterised and were isolated in yields ranging from 38.10 to 85.90 % for rhenium(I) tricarbonyl complexes and 12.80 to 80.30 % for rhenium(I) dicarbonyl complexes.

Two *cis-trans*-[^{99m}Tc(*N,N'*-bid)$(CO)_2(X)_2]^n$ type complexes were successfully synthesised. *cis-trans*-[^{99m}Tc$(CO)_2$(bpy)$(PPh_3)_2]^+$ and *cis-trans*-[^{99m}Tc$(CO)_2$(bpy)$(PTA)_2]^+$ were fully characterised and yields of 61.6 % and 42.89 % respectively, were obtained. Both complexes were found to be stable up to six hours in cysteine and histidine respectively. Both these ^{99m}Tc(I) complexes displayed high partition coefficient values, and *cis-trans*-[^{99m}Tc$(CO)_2$(bpy)$(PTA)_2]^+$ was found to be hydrophillic. Due to limited time and financial contraints it was only possible to synthesise the ^{99m}Tc analogues of two rhenium complexes.

Four bimetallic complexes, [(Cl_2)Pt(*O,O'*-phenO_2-*N,N'*)-Re$(CO)_3$(Br)], [(Cl_2)Pd(*O,O'*-phenO_2-*N,N'*)-Re$(CO)_3$(Br)], [(Cl_2)Pt(*O,O'*-phenO_2-*N,N'*)-Ru$(bpy)_2][PF_6]_2 \cdot 2H_2O$, and [$(Cl_2)$Pd(*O,O'*-phen$O_2$-*N,N'*)-Ru$(bpy)_2][PF_6]_2 \cdot 2H_2O$ were synthesised and characterised. These complexes displayed yields ranging from 10.66 % to 45.52 %. Experience in *in vitro* cell studies was obtained in the laboratory of the Gasser Group at Paritech in Paris, France. These four compounds were sent for

in vitro screening, however, the results of these studies were not available at the time of submission, due to a contamination issue in their lab as well as NRF funding conditions.

The photoluminescent properties of the range of *fac*-[Re(*N,N'*-bid)$(CO)_3(X)]^n$ and *cis*-[Re(*N,N'*-bid)$(CO)_2(X)_2]^n$ complexes were successfully studied and reported in chapter 5. Regrettably, quantum yield determinations were not possible.

The key aim of this study was the synthesis and characterisation of a range of complexes and the investigation into their use as photosensitisers for photodynamic therapy with respect to the treatment of cancer. The overall results obtained indicate that the aims of this dissertation were achieved, subject, however, to three constraining factors. Firstly, the inability to obtain quantum yield determinations for the range of rhenium(I) tricarbonyl and dicarbonyl complexes. Secondly, the inability to synthesise the ^{99m}Tc analogues of all the rhenium complexes. Finally, the results of the *in vitro* cell studies of the four bimetallic complexes that were not available at the time of submission.

6.2 Future Research

The derivation of the 1,10-phenanthroline moiety is of great interest because of its possible luminescent abilities. The addition of electron-withdrawing substituents to this ligand should red-shift the emission of a complex coordinated to this ligand. Red-shift in emission and high quantum yield are of great importance in PDT and the enhancement of these characteristics is of great importance for future research.

A salient result of this study is the isolation and characterisation of the ^{99m}Tc dicarbonyl complex, *cis-trans*-$[^{99m}Tc(CO)_2(bpy)(PTA)_2]^+$, its hydrophillic partition coefficient, and stability. These characteristics engender possible medical application. Thus, the synthesis and isolation of more compounds of the type *cis*-[Re$(CO)_2$(*N,N'*-bid$)(X)_2]^+$ (*N,N'*-bid = derivatives of phenO_2) (X = various water soluble monodentate ligands) and their ^{99m}Tc analogues are an interesting scope for further studies.

The majority of commercial labelling kits are usually available in saline solution. It is therefore imperative to study the aqueous kinetics of the types of complexes referred to in this study in order to understand their mechanism of action and chemistry of these complexes. Finally, high pressure studies should be undertaken to determine the mechanism/s of action unequivocally.

Appendix

Appendix A

Table A.1: Atomic coordinates ($\times 10^4$) and equivalent isotropic displacement parameters ($Å^2 \times 10^3$) for *fac*-[Re(CO)$_3$(bpy)(Br)] (1). U(eq) is defined as one third of the trace of the orthogonalised U^{ij} tensor.

	x	y	z	U(eq)
Re(1)	5261(1)	3092(1)	7636(1)	26(1)
Br(1)	1905(1)	3179(1)	6521(1)	40(1)
O(1)	9120(7)	3038(3)	8939(4)	51(1)
O(2)	6807(7)	1686(3)	6302(4)	54(1)
O(3)	3686(7)	1657(3)	8914(4)	55(1)
N(1)	6046(6)	4236(3)	6809(3)	26(1)
N(2)	4138(6)	4207(3)	8392(3)	26(1)
C(1)	7853(10)	3113(3)	8484(4)	34(1)
C(2)	6204(8)	2204(4)	6805(4)	34(1)
C(3)	4290(8)	2188(4)	8428(4)	36(1)
C(4)	7070(7)	4212(4)	6020(4)	35(1)
C(5)	7484(8)	4951(4)	5499(4)	36(1)
C(6)	6836(8)	5746(4)	5784(4)	39(1)
C(7)	5793(8)	5786(3)	6597(4)	35(1)
C(8)	5412(7)	5025(3)	7093(4)	27(1)
C(9)	4351(7)	5009(3)	7978(4)	26(1)
C(10)	3588(8)	5756(3)	8376(4)	35(1)
C(11)	2628(8)	5689(4)	9210(4)	41(1)
C(12)	2435(8)	4872(4)	9628(4)	38(1)
C(13)	3198(7)	4147(4)	9200(4)	33(1)

Table A.2: Bond distances (Å) and angles (°) for *fac*-[Re(CO)$_3$(bpy)(Br)] (1).

Bond	Bond Distance	Bond Angle	Angle
Re(1)-C(3)	1.912(6)	C(3)-Re(1)-C(2)	89.2(2)
Re(1)-C(2)	1.919(6)	C(3)-Re(1)-C(1)	92.5(2)
Re(1)-C(1)	2.008(7)	C(2)-Re(1)-C(1)	90.0(2)
Re(1)-N(2)	2.170(4)	C(3)-Re(1)-N(2)	97.5(2)
Re(1)-N(1)	2.171(4)	C(2)-Re(1)-N(2)	172.15(19)
Re(1)-Br(1)	2.6126(15)	C(1)-Re(1)-N(2)	93.77(17)
O(1)-C(1)	1.015(7)	C(3)-Re(1)-N(1)	171.87(19)
O(2)-C(2)	1.150(7)	C(2)-Re(1)-N(1)	98.1(2)
O(3)-C(3)	1.151(7)	C(1)-Re(1)-N(1)	91.02(19)
N(1)-C(8)	1.349(6)	N(2)-Re(1)-N(1)	74.95(16)
N(1)-C(4)	1.347(6)	C(3)-Re(1)-Br(1)	90.56(17)
N(2)-C(13)	1.337(6)	C(2)-Re(1)-Br(1)	92.38(16)
N(2)-C(9)	1.358(6)	C(1)-Re(1)-Br(1)	176.16(15)
C(4)-C(5)	1.375(7)	N(2)-Re(1)-Br(1)	83.50(11)
C(4)-H(4)	0.9500	N(1)-Re(1)-Br(1)	85.66(11)
C(5)-C(6)	1.362(8)	C(8)-N(1)-C(4)	117.9(4)
C(5)-H(5)	0.9500	C(8)-N(1)-Re(1)	117.3(3)
C(6)-C(7)	1.383(8)	C(4)-N(1)-Re(1)	124.8(3)
C(6)-H(6)	0.9500	C(13)-N(2)-C(9)	118.9(4)
C(7)-C(8)	1.378(7)	C(13)-N(2)-Re(1)	124.5(3)
C(7)-H(7)	0.9500	C(9)-N(2)-Re(1)	116.6(3)
C(8)-C(9)	1.475(7)	O(1)-C(1)-Re(1)	172.1(6)
C(9)-C(10)	1.388(7)	O(2)-C(2)-Re(1)	178.3(5)
C(10)-C(11)	1.376(8)	O(3)-C(3)-Re(1)	178.6(5)
C(10)-H(10)	0.9500	N(1)-C(4)-C(5)	122.8(5)
C(11)-C(12)	1.379(8)	N(1)-C(4)-H(4)	118.6
C(11)-H(11)	0.9500	C(5)-C(4)-H(4)	118.6
C(12)-C(13)	1.379(7)	C(6)-C(5)-C(4)	119.1(5)
C(12)-H(12)	0.9500	C(6)-C(5)-H(5)	120.4
C(13)-H(13)	0.9500	C(4)-C(5)-H(5)	120.4
		C(5)-C(6)-C(7)	118.9(5)

	C(5)-C(6)-H(6)	120.5
	C(7)-C(6)-H(6)	120.5
	C(8)-C(7)-C(6)	119.7(5)
	C(8)-C(7)-H(7)	120.1
	C(6)-C(7)-H(7)	120.1
	N(1)-C(8)-C(7)	121.5(5)
	N(1)-C(8)-C(9)	115.2(4)
	C(7)-C(8)-C(9)	123.3(4)
	N(2)-C(9)-C(10)	120.8(5)
	N(2)-C(9)-C(8)	115.9(4)
	C(10)-C(9)-C(8)	123.3(4)
	C(11)-C(10)-C(9)	119.9(5)
	C(11)-C(10)-H(10)	120.1
	C(9)-C(10)-H(10)	120.1
	C(10)-C(11)-C(12)	118.7(5)
	C(10)-C(11)-H(11)	120.6
	C(12)-C(11)-H(11)	120.6
	C(11)-C(12)-C(13)	119.4(5)
	C(11)-C(12)-H(12)	120.3
	C(13)-C(12)-H(12)	120.3
	N(2)-C(13)-C(12)	122.3(5)
	N(2)-C(13)-H(13)	118.9
	C(12)-C(13)-H(13)	118.9

Table A.3: Anisotropic displacement parameters ($Å^2 \times 10^3$) for *fac*-[$Re(CO)_3(bpy)(Br)$] (1). The Anisotropic displacement factor exponent takes the form: $-2\pi^2(h2a^{*2}U^{11}+\ldots+2hka^*b^*U^{12})$.

	U11	U22	U33	U23	U13	U12
Re(1)	29(1)	20(1)	31(1)	1(1)	7(1)	1(1)
Br(1)	36(1)	39(1)	45(1)	7(1)	-2(1)	-3(1)
O(1)	44(2)	51(3)	58(3)	-14(2)	9(2)	-7(2)
O(2)	65(3)	45(2)	53(3)	-21(2)	9(2)	12(2)
O(3)	55(3)	48(3)	62(3)	22(2)	9(2)	-9(2)
N(1)	26(2)	24(2)	29(2)	2(2)	6(2)	1(2)
N(2)	24(2)	25(2)	28(2)	-1(2)	5(2)	0(2)
C(1)	59(4)	24(3)	22(2)	2(2)	14(3)	27(3)
C(2)	36(3)	32(3)	34(3)	-1(2)	-1(2)	2(2)
C(3)	36(3)	29(3)	43(3)	3(2)	6(2)	1(2)
C(4)	30(3)	37(3)	39(3)	-1(2)	12(2)	0(2)
C(5)	33(3)	47(3)	31(3)	1(2)	10(2)	-10(2)
C(6)	44(3)	40(3)	34(3)	7(2)	3(2)	-14(3)
C(7)	43(3)	26(3)	35(3)	1(2)	2(2)	-5(2)
C(8)	28(2)	23(2)	28(3)	2(2)	0(2)	-2(2)
C(9)	28(2)	23(2)	27(3)	1(2)	0(2)	1(2)
C(10)	47(3)	27(3)	30(3)	-1(2)	2(2)	9(2)
C(11)	42(3)	43(3)	39(3)	-10(3)	4(3)	13(3)
C(12)	35(3)	49(3)	32(3)	-3(2)	12(2)	5(2)
C(13)	32(3)	34(3)	33(3)	2(2)	10(2)	-1(2)

Table A.4: Hydrogen coordinates (× 10^4) and isotropic displacement parameters (Å^2 × 10^3) for *fac*-[Re(CO)$_3$(bpy)(Br)] (1).

	x	y	z	U(eq)
H(4)	7527	3660	5816	42
H(5)	8212	4908	4946	44
H(6)	7097	6265	5432	47
H(7)	5341	6335	6812	42
H(10)	3729	6313	8074	42
H(11)	2108	6196	9492	49
H(12)	1782	4808	10205	46
H(13)	3052	3585	9490	39

Table A.5: Torsion angles (°) for *fac*-[Re(CO)$_3$(bpy)(Br)] (1).

Torsion angle	Angle
C(8)-N(1)-C(4)-C(5)	-0.2(8)
Re(1)-N(1)-C(4)-C(5)	177.9(4)
N(1)-C(4)-C(5)-C(6)	-0.1(9)
C(4)-C(5)-C(6)-C(7)	0.5(8)
C(5)-C(6)-C(7)-C(8)	-0.7(8)
C(4)-N(1)-C(8)-C(7)	0.0(7)
Re(1)-N(1)-C(8)-C(7)	-178.2(4)
C(4)-N(1)-C(8)-C(9)	-178.3(4)
Re(1)-N(1)-C(8)-C(9)	3.4(6)
C(6)-C(7)-C(8)-N(1)	0.4(8)
C(6)-C(7)-C(8)-C(9)	178.6(5)
C(13)-N(2)-C(9)-C(10)	-0.8(7)
Re(1)-N(2)-C(9)-C(10)	176.5(4)
C(13)-N(2)-C(9)-C(8)	179.6(4)
Re(1)-N(2)-C(9)-C(8)	-3.0(5)
N(1)-C(8)-C(9)-N(2)	-0.2(7)
C(7)-C(8)-C(9)-N(2)	-178.5(5)
N(1)-C(8)-C(9)-C(10)	-179.8(5)

C(7)-C(8)-C(9)-C(10)	1.9(8)
N(2)-C(9)-C(10)-C(11)	1.0(8)
C(8)-C(9)-C(10)-C(11)	-179.5(5)
C(9)-C(10)-C(11)-C(12)	-0.5(8)
C(10)-C(11)-C(12)-C(13)	-0.2(9)
C(9)-N(2)-C(13)-C(12)	0.1(8)
Re(1)-N(2)-C(13)-C(12)	-177.0(4)
C(11)-C(12)-C(13)-N(2)	0.4(9)

Table A.6: Hydrogen bond distances (Å) and angles (°) for *fac*-[Re(CO)$_3$(bpy)(Br)] (1).

D-H···A	d(D-H)	d(H···A)	d(D···A)	D-H···A angle
C(6)-H(6)...Br(1)#1	0.95	2.93	3.707(6)	140.4

Symmetry transformations used to generate equivalent atoms:

#1: -x+1,-y+1,-z+1